NASA/CR—2014-218320

Development, Implementation, and Pilot Evaluation of a Model-Driven Envelope Protection System to Mitigate the Hazard of In-Flight Ice Contamination on a Twin-Engine Commuter Aircraft

Borja Martos, Richard Ranaudo, and Billy Norton
University of Tennessee Space Institute, Tullahoma, Tennessee

David Gingras and Billy Barnhart
Bihrle Applied Research Inc., Hampton, Virginia

October 2014

NASA STI Program . . . in Profile

Since its founding, NASA has been dedicated to the advancement of aeronautics and space science. The NASA Scientific and Technical Information (STI) program plays a key part in helping NASA maintain this important role.

The NASA STI Program operates under the auspices of the Agency Chief Information Officer. It collects, organizes, provides for archiving, and disseminates NASA's STI. The NASA STI program provides access to the NASA Aeronautics and Space Database and its public interface, the NASA Technical Reports Server, thus providing one of the largest collections of aeronautical and space science STI in the world. Results are published in both non-NASA channels and by NASA in the NASA STI Report Series, which includes the following report types:

- TECHNICAL PUBLICATION. Reports of completed research or a major significant phase of research that present the results of NASA programs and include extensive data or theoretical analysis. Includes compilations of significant scientific and technical data and information deemed to be of continuing reference value. NASA counterpart of peer-reviewed formal professional papers but has less stringent limitations on manuscript length and extent of graphic presentations.

- TECHNICAL MEMORANDUM. Scientific and technical findings that are preliminary or of specialized interest, e.g., quick release reports, working papers, and bibliographies that contain minimal annotation. Does not contain extensive analysis.

- CONTRACTOR REPORT. Scientific and technical findings by NASA-sponsored contractors and grantees.

- CONFERENCE PUBLICATION. Collected papers from scientific and technical conferences, symposia, seminars, or other meetings sponsored or cosponsored by NASA.

- SPECIAL PUBLICATION. Scientific, technical, or historical information from NASA programs, projects, and missions, often concerned with subjects having substantial public interest.

- TECHNICAL TRANSLATION. English-language translations of foreign scientific and technical material pertinent to NASA's mission.

Specialized services also include creating custom thesauri, building customized databases, organizing and publishing research results.

For more information about the NASA STI program, see the following:

- Access the NASA STI program home page at *http://www.sti.nasa.gov*

- E-mail your question to *help@sti.nasa.gov*

- Fax your question to the NASA STI Information Desk at 443–757–5803

- Phone the NASA STI Information Desk at 443–757–5802

- Write to:
  STI Information Desk
  NASA Center for AeroSpace Information
  7115 Standard Drive
  Hanover, MD 21076–1320

NASA/CR—2014-218320

Development, Implementation, and Pilot Evaluation of a Model-Driven Envelope Protection System to Mitigate the Hazard of In-Flight Ice Contamination on a Twin-Engine Commuter Aircraft

Borja Martos, Richard Ranaudo, and Billy Norton
University of Tennessee Space Institute, Tullahoma, Tennessee

David Gingras and Billy Barnhart
Bihrle Applied Research Inc., Hampton, Virginia

Prepared under Grant NNX07AD58A

National Aeronautics and
Space Administration

Glenn Research Center
Cleveland, Ohio 44135

October 2014

Acknowledgments

The development and testing of ICEPro was funded under a federal grant, which was a sponsored 3-year cooperative research effort with NASA under the NASA Research Announcement NNH06ZEA001N, Appendix B, of the Aviation Safety Program. The objectives of the NRA were defined under the Integrated Vehicle Health Management Project, topic IVHM 3.1, Environmental Hazards, which are caused by the "Effects of Icing on Aircraft State". The successful development, testing, and evaluation of ICEPro would not have been possible without the contributions of key individuals and organizations, which made up the research team. The author wishes to recognize Mr. Richard Ranaudo, University of Tennessee Space Institute, who was principal investigator of the original NRA and wrote all of the results thereof in this report. The author also wishes to recognize Mr. Thomas Ratvasky, NASA Glenn Research Center, and Dr. Eugene Morelli, NASA Langley Research Center for their guidance and support throughout this project. Mr. Ratvasky's experience and technical expertise with icing related problems were essential during the development and testing phases of ICEPro. Dr. Eugene Morelli provided critically important technical assistance during the integration and application of the Real Time Parameter Identification algorithm, which he and others from his organization had developed over a period of several years (see Refs. 13 to 15). In addition, Mr. David Gingras and Mr. Billy Barnhart, Bihrle Applied Research, who are experts in the field of modeling and simulation, successfully designed, developed, integrated and tested the ICEPro system in NASA's ICEFTD. Mr. Barnhart was directly involved during the test and evaluation phase of ICEPro, and along with Mr. Gingras, provided important simulation functionality, and solved numerous technical and integration problems necessary for a successful evaluation. Mr. Billy Norton, an engineering management doctoral candidate at UTSI developed and conducted the statistical data handling methods, which were essential to the analysis of pilot performance metrics. Lastly, the authors wish to express their sincere appreciation to the faculty and staff of the Embry Riddle Aeronautical University for their support of this testing at their Eagle Works facility in Daytona Beach, Florida. The additional 1-year extension to study the effects of atmospheric turbulence on ICEPro would not have been possible without the help of NASA's VSST project. The authors would like to thank Dr. Christine Belcastro and her team for this additional sponsorship and technical support.

Level of Review: This material has been technically reviewed by NASA technical management OR expert reviewer(s).

Available from

NASA Center for Aerospace Information
7115 Standard Drive
Hanover, MD 21076–1320

National Technical Information Service
5301 Shawnee Road
Alexandria, VA 22312

Available electronically at http://www.sti.nasa.gov

Contents

List of Tables

List of Figures

Development, Implementation, and Pilot Evaluation of a Model-Driven Envelope Protection System to Mitigate the Hazard of In-Flight Ice Contamination on a Twin-Engine Commuter Aircraft

Borja Martos, Richard Ranaudo, and Billy Norton
University of Tennessee Space Institute
Tullahoma, Tennessee 37388

David Gingras and Billy Barnhart
Bihrle Applied Research Inc.
Hampton, Virginia 23666

Abstract

Fatal loss-of-control accidents have been directly related to in-flight airframe icing. The prototype system presented in this report directly addresses the need for real-time onboard envelope protection in icing conditions. The combination of prior information and real-time aerodynamic parameter estimations are shown to provide sufficient information for determining safe limits of the flight envelope during in-flight icing encounters. The Icing Contamination Envelope Protection (ICEPro) system was designed and implemented to identify degradations in airplane performance and flying qualities resulting from ice contamination and provide safe flight-envelope cues to the pilot. The utility of the ICEPro system for mitigating a potentially hazardous icing condition was evaluated by 29 pilots using the NASA Ice Contamination Effects Flight Training Device. Results showed that real time assessment cues were effective in reducing the number of potentially hazardous upset events and in lessening exposure to loss of control following an incipient upset condition. Pilot workload with the added ICEPro displays was not measurably affected, but pilot opinion surveys showed that real time cueing greatly improved their awareness of a hazardous aircraft state. The performance of ICEPro system was further evaluated by various levels of sensor noise and atmospheric turbulence.

1.0 Introduction

Ice formations on aircraft can negatively affect performance, stability and control characteristics, and handling qualities. Accidents that have occurred due to these issues have been documented by the National Transportation Safety Board (NTSB) and the Federal Aviation Administration (FAA) over many years. In a recent study (Ref. 1) of aircraft icing accidents and incidents reported between 1978 and 2002, loss of control events were usually preceded by stall and more likely to occur during approach and landing. This is the busiest phase of flight where historically over 50 percent of all accidents occur, and where human error is responsible for approximately 75 percent of those accidents (Ref. 2). Ice contamination, on a critical airframe surface such as the wings and tail, which might be due to an Ice Protection System (IPS) failure, encountering an icing certification exceedance condition, or operator error can have a detrimental effect on aircraft performance, stability and control, and handling qualities. This situation is further exacerbated by the required changes in airspeed and configuration as the pilot slows and configures during the descent, approach, and landing phases.

One notable accident referenced above involved an ATR 72 that flew through SLD icing conditions near Roselawn, Indiana, on October 31, 1994. Even with the IPS operating normally, the aircraft experienced a roll control anomaly that led to the loss of control and impact into the ground. This accident and others since then have led to numerous safety recommendations from the National Transportation

Safety Board (NTSB) (Refs. 3 and 4) and the Commercial Aviation Safety Team (CAST) (Ref. 5) and motivated research activities within NASA and the FAA.

In its Tailplane Icing Program (TIP), NASA employed various artificial ice shapes, which were attached to the horizontal tail plane (Ref. 6) of a research aircraft. Numerous test maneuvers were conducted where wing flap settings, engine power, and flight speed were varied. The results showed a considerable decrease in longitudinal stability and elevator control effectiveness as a function of wing flap angle, power setting, and airspeed. In extreme cases, a tail stall upset would occur, which resulted in an uncontrollable nose down pitching motion. Airframe ice contamination also increases drag, reducing climb performance. In another research program, NASA sponsored an activity called the Smart Icing Systems led by the University of Illinois, Urbana-Champaign (UIUC). The Smart Icing Systems took a systems level approach to detecting icing conditions, operating ice protection systems and alerting the flight crew to the status of the aircraft (Ref. 7).

Most recently NASA issued Research Announcement (NRA) NNH06ZEA001N, Appendix B, of the Aviation Safety Program. The research announcement was defined under the Integrated Vehicle Health Management (IVHM) Project, topic IVHM 3.1, Environmental Hazards, which are caused by the "Effects of Icing on Aircraft State". The function of IVHM is to manage the health of the vehicle by detecting, diagnosing, prognosing, and mitigating in-flight environmental hazards. The main objective was to develop tools that measure the state of the aircraft in atmospheric icing conditions and assess the effects of icing on the aircraft for various environmental icing conditions. The original scope for this work included simulation and experimental testing but was later constrained to pilot in the loop simulations. The goals for this work were:

1. Develop a system that performs real time assessment of icing effects on aircraft stability, control, and performance.
2. Provide the flight deck with flight guidance cues, configuration and envelope limits, and related state assessment messaging to avoid upset conditions and loss of control.
3. Enable the pilot to make better tactical decisions regarding flight speed and configuration selections to maintain the aircraft in a safe envelope of flight.

The University of Tennessee Space Institute (UTSI) in partnership with Bihrle Applied Research (BAR) completed a cooperative research effort addressing the IVHM function, objective, scope, and goals. This effort culminated in the development of a real time vehicle state assessment system, which was described by Gingras et al. (Ref. 8) and is referred to as the Icing Contamination Envelope Protection system (ICEPro). The ICEPro system was developed with the philosophy that a knowledge-based system, which compares expected aircraft stability and control characteristics with those existing in real time, could effectively provide envelope protection cues and alerting messages to help the pilot keep the aircraft flying safely. The knowledge base consists of a model for the baseline or clean aircraft, and an ice contamination model with known safe flight envelope limits as demonstrated by either wind tunnel or flight test. Angle of attack (AOA) cues, which are driven by ICEPro, show the pilot safe limits that will protect against either a wing stall or tail stall upset event. Messages alert the pilot to losses in stability and control as a function of flight configuration and condition, and to configuration limits as a function of icing and wing flap setting.

The algorithms in ICEPro were initially developed and tested in a desktop simulation environment, and then integrated and further developed in the NASA Ice Contamination Effects Flight Training Device (ICEFTD). The flight models used in simulation to develop ICEPro for testing and evaluation were based upon the characteristics of the NASA Twin Otter icing research aircraft in a no-ice baseline condition, and a failure of the ice protection system (IPS). The failure case was defined by the ice accretions that would form during a 22.5 min FAR 25 Appendix C icing encounter as calculated by LEWICE version 2.0. The data for the simulator came from a previous NASA project where a 6.5 percent scale Twin Otter

model was tested in the Wichita State University 7×10 Low Speed wind tunnel and BAR's Large Amplitude Multi-Purpose (LAMP) rotary balance wind tunnel using scaled ice shapes (Ref. 9). Flight data from aircraft testing with baseline and failure case ice shapes was also gathered to refine the simulation model data to improve the match full scale flight test results (Ref. 10).

After development and testing in a desktop environment, ICEPro was integrated with the NASA ICEFTD. Researchers from BAR and UTSI completed final development and integration testing to ensure readiness for the planned pilot evaluations. A final check of test readiness was then performed by having two experienced NASA test pilots complete the evaluation profile, and all required pre-test preparation and training. This included a review of: the test plan, NASA web based icing training, standard operating procedures (SOP) for the Twin Otter, the NASA Task Load Index or TLX workload method (Ref. 11), a tutorial on flying with ICEPro displays (only for the pilot using the experimental displays), and post-test survey questionnaire. One NASA pilot was selected to represent the control group and flew with baseline displays. The other was selected to represent the experimental group and flew with the ICEPro modified displays. Before the test began, each pilot was briefed on the entire test process. The test protocol at the time called for minimal training in aircraft handling with hazardous ice formations, somewhat similar to what a typical pilot would receive in an aircraft transition course. However, once testing began, it became apparent that the flight task was so difficult that without practice, there was a high probability of a random "crash" regardless of the displays used. It was apparent that a different approach would have to be taken. After assessing the pilot's comments from the debriefings, it was therefore decided to modify the test protocol and train the pilots in both groups to proficiency for executing the challenging approach task using their respective flight displays. Utility benefits could then be assessed by comparing pilot performance, workload, and opinions between the control and experimental groups who were flying the same task with the same training and preparation, but with different flight displays. This adjustment in the test plan was an essential change, and would not have been discovered without this pre-test. The NASA pilots also completed the NASA TLX forms and answered all the survey questions during their respective evaluations. A few small changes in the survey questions were also required to eliminate ambiguity problems. After these adjustments were made to the test plan, pilot-in-the- loop (PIL) evaluations of ICEPro were scheduled at the Embry Riddle Aeronautical University (ERAU), Daytona Beach, Florida.

However, the simulation could not duplicate all of the real-world conditions that could have first-order effects on system performance, such as those due to real atmospheric turbulence. Therefore, in order to assess system performance under these conditions and minimize the technical risk of an eventual flight-test validation program, the effects of atmospheric turbulence on ICEPro were studied. This led to a one year extension awarded under NASA's Vehicle Systems Safety Technologies (VSST) project.

This contractor report summarizes the results of this research, which focused on the concept, design, development, implementation, and evaluation of the real-time vehicle state assessment system. This evaluation included pilot cueing for flight envelope protection, and evaluation of the effectiveness of the ICEPro system in piloted simulations using the ICEFTD. Sections 2.0 to 9.0 focus on the concept, design, development, and implementation of ICEPro. Section 10.0 explains the methodology used for pilot-in-the-loop testing and overall experiment design. Section 11.0 presents the results and discussions of pilot-in-the-loop testing. Section 12.0 discusses the atmospheric turbulence test methodology and finally Section 13.0 cover conclusions and recommendations. There are five appendices attached to this report. Appendix A is the Symbols List. Appendix B includes the post-test survey questionnaire used in the pilot-in-the-loop simulations. Appendix C includes the results of the post-test survey questionnaire. Appendix D includes the progress report of the effects of atmospheric turbulence on ICEPro through the funded one year extension. Appendix E includes the atmospheric turbulence test plan.

2.0 ICEPro Concept

The ICEPro concept is best summarized by the hypothesis posed by the development team during preliminary stages of the design process.

> *By the real-time processing of measured state and control information, estimates of stability and control can be used in conjunction with a knowledge base, comprised of a-priori data, to provide pilots with envelope-limiting cueing in order to avoid loss-of-control or adverse conditions resulting from in-flight icing.*

The ICEPro system was designed and implemented to identify degradations in airplane performance and flying qualities resulting from ice contamination and to provide safe flight-envelope cues to the pilot. The ICEPro concept relies on the actions of a proficient pilot responding to appropriate cueing and information on the primary and secondary displays in the cockpit. It is believed that, with these cues, the pilot can make informed decisions as to how the airplane should be flown. The ICEPro concept provides envelope protection by issuing advisories, cautions, and warnings in the form of airspeed limits, angle of attack limits, flap position limits, and control effectiveness status. The indications are intended to be consistent with typical advisories and warnings that appear on flight displays, so that they are intuitive and effective. Figure 1 provides a graphic illustrating the cueing that is used in the ICEPro system.

When the system does not detect significant change from the nominal prior airplane characteristics, no cuing or messages appear and the instruments display the nominal flight information. When the system senses icing contamination that exceeds the system thresholds and triggers the latching logic, cues and possibly messages appear in conjunction with the normal display information.

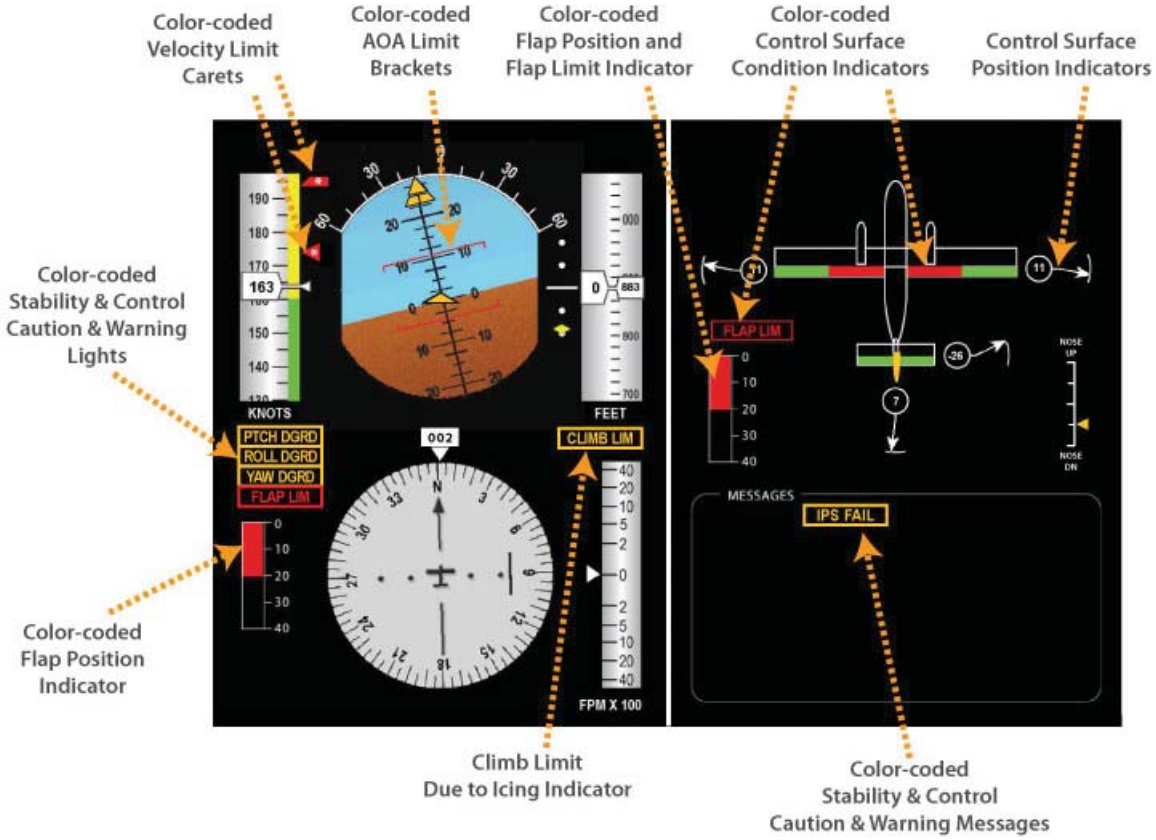

Figure 1.—ICEPro Envelope Protection Cues on the Primary Flight Display (left) and Flight Control Status Page (right)

There are three types of information that are provided when icing contamination is determined. See Figure 1 for illustration.

- Airspeed limit carets and angle of attack limit brackets.

  The airspeed limit carats for icing are to the right of the speed tape and annotated with a * to indicate icing. The angle of attack limit brackets are superimposed on the attitude indicator. The upper bracket indicates the wing stall AOA. The lower bracket indicates the tail stall AOA. The color of the brackets change from white to amber when the AOA is less than 2° lower than stall AOA and then change to red when the AOA reaches the stall AOA. The brackets will also flash for several seconds with each color transition, white to amber, and amber to red.

- Status messages

  These will appear, both on the primary flight display and on the Flight Control Display (FCD) page in the message box. They indicate that there is a control and/or stability degradation in the indicated axis. There is also a message that appears whenever the single-engine climb capability is outside of safe limits. A flap limit message will also appear when the flaps should be retracted to a safer deflection.

- Flight control status indicators

  The FCD page includes a rough diagram of the airplane showing its control surfaces. The surfaces are colored and the color will change whenever degradation is determined in their axis. With no degradation, the surfaces are green and turn amber when there is a caution displayed for that axis and red when there is a warning. The color-coded displays are driven by current estimates of control effectiveness and thresholds defined inside ICEPro.

The basic design architecture of the system is shown in Figure 2. The ICEPro System has three modes of operation: a MONITOR mode that provides initial detection of in-flight icing, IDENTIFICATION or ID mode that provides a diagnosis of the condition, and a REPORTING mode, providing the prognosis of the condition and mitigation through cueing. Details of the system design can be found in Reference 8.

Figure 3 presents a simplified flow chart. Details, such as latching/delatching logic and specific logic for driving each of the caution/warning messages have been omitted to reduce the complexity of the diagram. As indicated in the diagram, the system is heavily dependent on input from two components: 1) The Dynamic Inversion Control Evaluation System (D-ICES), an algorithm that computes what the control surface deflections should be for a clean aircraft compared to what the control deflections actually are, and 2) the Real-Time Parameter IDentification (RT-PID) routine. Results from these components are used to determine an Icing Severity Parameter (ISP) which is used in logic for issuing pilot cues and warnings during the reporting mode.

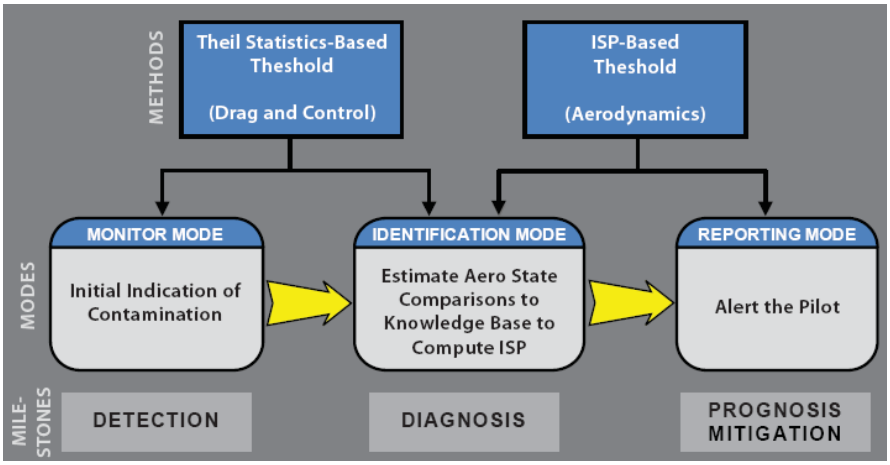

Figure 2.—ICEPro System Architecture

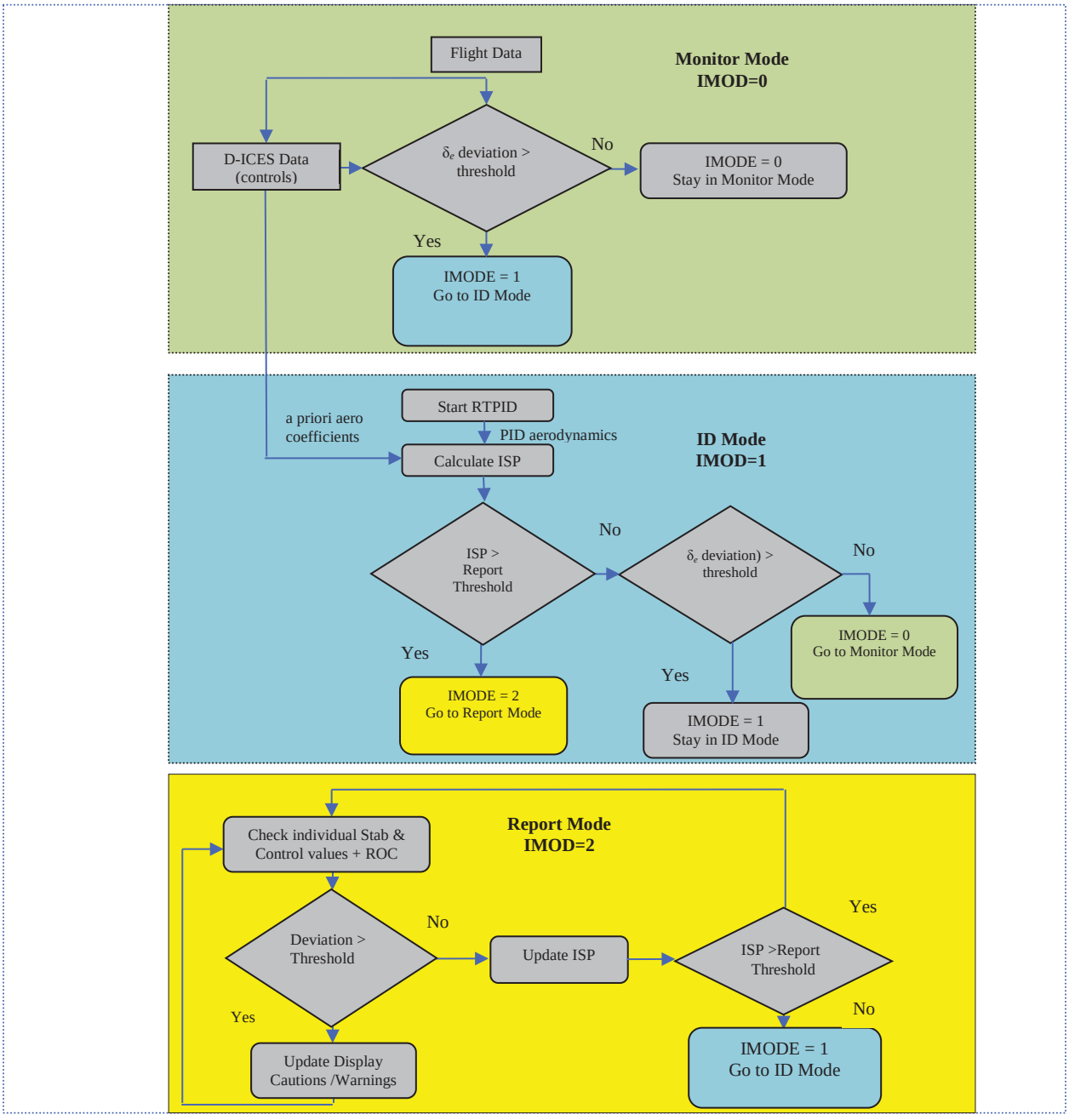

Figure 3.—Simplified ICEPro System Flow Chart

3.0 Flight Characteristic Predictions

Flight predictions are made inside ICEPro using a flight model of a DeHavilland DHC-6 Twin Otter. This flight model was derived from a comprehensive nonlinear 6-degree-of-freedom simulation that was developed by Bihrle Applied Research and engineers at the NASA Glenn Research Center (GRC) (Ref. 9). The model was based on data from extensive wind-tunnel tests using subscale models of the Twin-Otter and supplemented with flight data provided by NASA. This model covers the entire flight envelope including stall and post-stall flight regimes with and without icing effects resulting from ice accretion on the main wing, horizontal tail, and vertical tail. During previous efforts, the model had undergone extensive validation against flight data to achieve high confidence predictions of aerodynamic characteristics in clean configuration, as well as the aerodynamic characteristics from an iced configuration representing an IPS failure situation. Figure 4 contains a flow chart of the process used during this effort to validate the aerodynamic simulation modeling.

Figure 5 contains an example of the resulting comparisons of model output for normal force coefficient, axial force coefficient, and pitching moment coefficient, with flight data from an elevator doublet maneuver on the clean airplane. This process was used to update the aerodynamic simulation model based on flight data. This effort resulted in the knowledge base system or database referred to in this work.

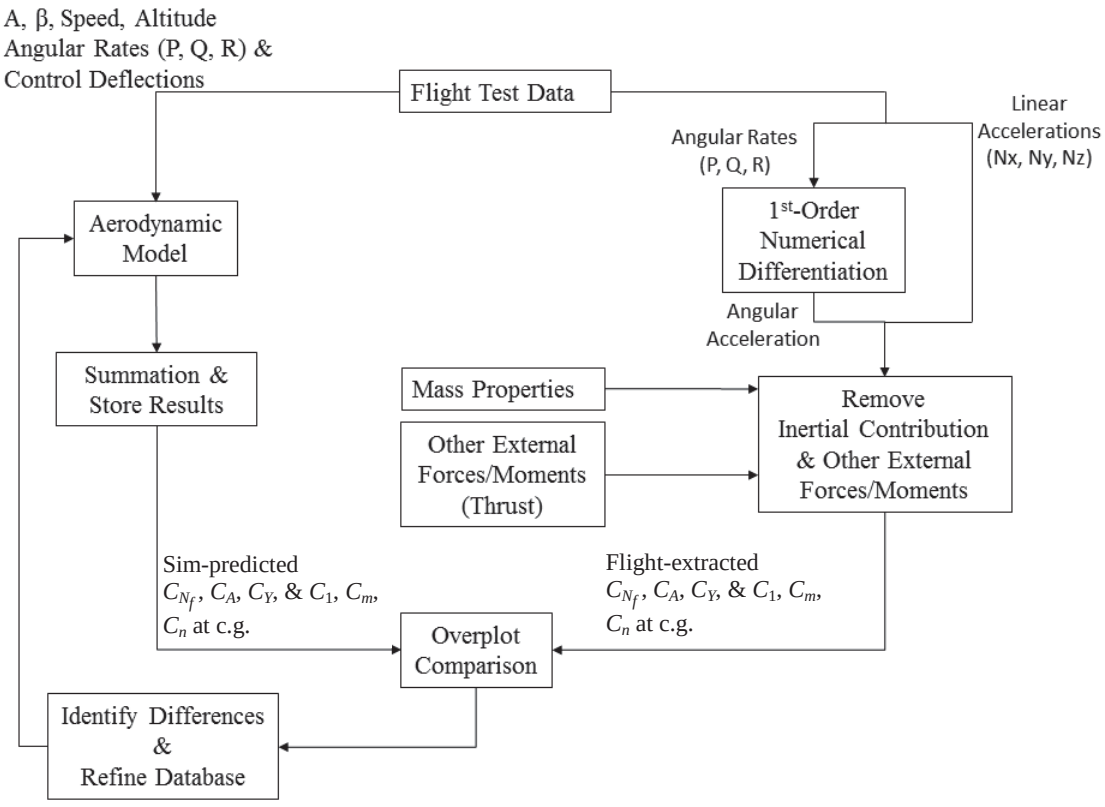

Figure 4.—Process used for Aerodynamic Model Validation

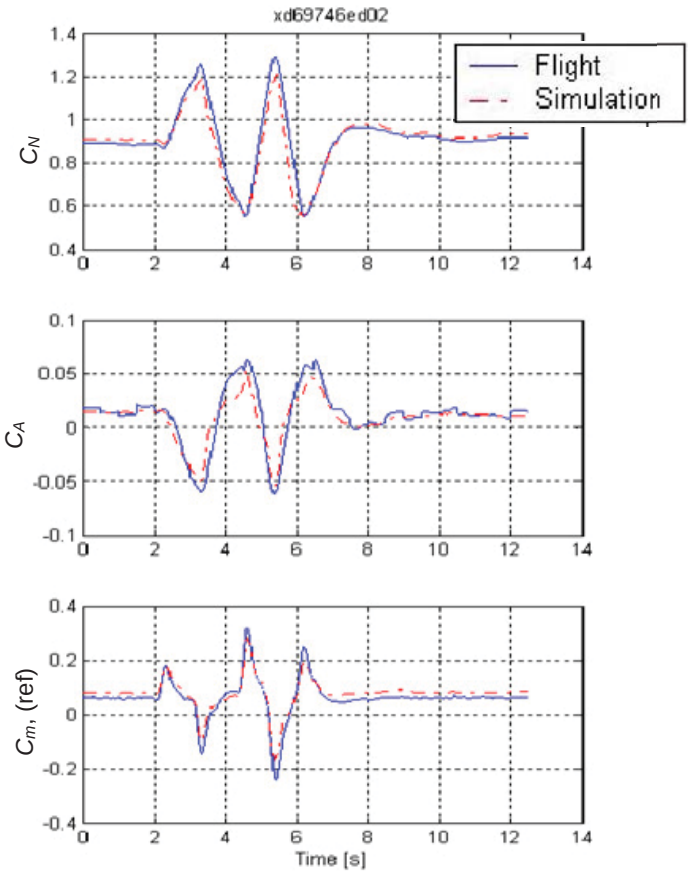

Figure 5.—Example of Comparisons of the Simulation Model and Flight Aerodynamic Coefficients

4.0 Dynamics Inversion Control Evaluation System

This technique, the Dynamics Inversion Control Evaluation System (D-ICES) makes use of the system knowledge base to predict the control deflections necessary to achieve the vehicle motion. D-ICES tracks the current pitch, roll, and yaw rate in each axis using a proportional, integral, and derivative (PID) control with lead compensation, Figure 6. With this tracking, the amount of angular acceleration required to match the aircraft motion is determined. Using information from the knowledge base, predictions of the current "clean" stability of the vehicle are entered into the aircraft equations of motion along with weight and balance information and the tracking accelerations to compute a "residual" acceleration vector.

By assuming this residual acceleration is a direct result of control movement, a prediction of control deflections can be obtained (Eq. (1)). Changes in the vehicle aerodynamic state from the "clean" can be detected by tracking these predictions of the control deflection in flight and comparing them to actual control deflections.

$$\begin{aligned} \dot{x}_{\text{Measured}} &= Ax_{\text{Predicted}} + Bu_{\text{Predicted}} \\ \hat{u}_{\text{Predicted}} &= B_{\text{Control}}{}^{-1}\left[\dot{x}_{\text{Measured}} - A_{\text{Stability}}x_{\text{Predicted}}\right] \end{aligned} \tag{1}$$

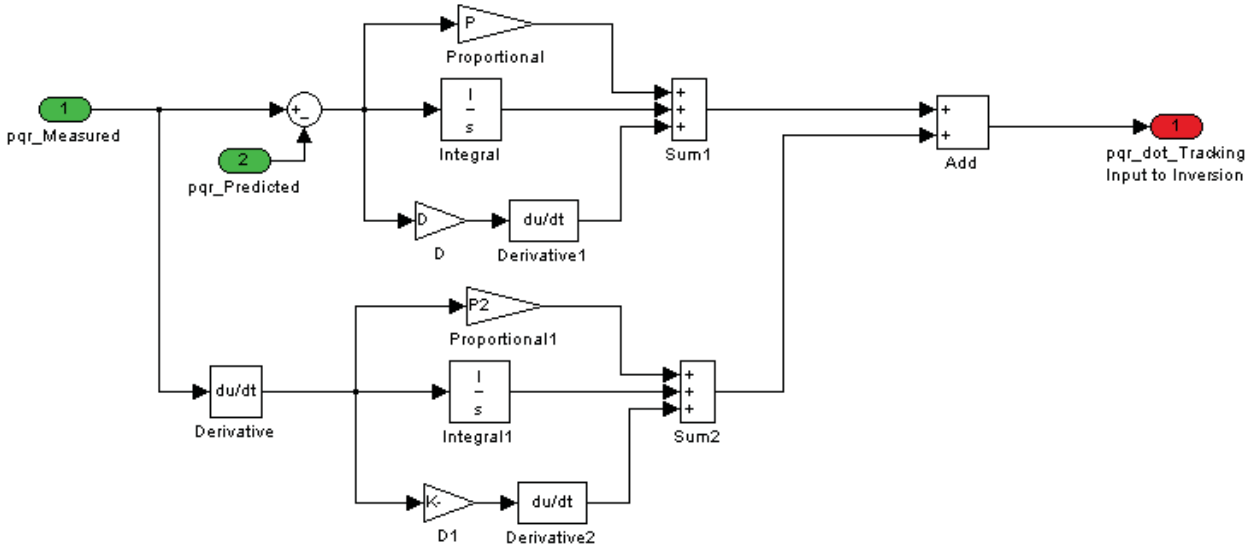

Figure 6.—Tracking algorithm for acceleration signal input to the dynamic inversion scheme

The actual comparisons in the logic are based on the calculated Theil inequality coefficients (Ref. 12) for velocity and elevator deflections. The Theil inequality coefficients are used in a moving time window to evaluate how well the extracted data is matching the expected levels during that time period. These statistics form the basis for the Icing Severity Parameter to be discussed in Section 11.0. The form of the Theil inequality coefficients is shown in Equation (2).

$$U = \frac{\sqrt{\frac{1}{N}\sum_{N}^{1}\left(y-\hat{y}\right)^2}}{\sqrt{\frac{1}{N}\sum_{N}^{1}y^2}+\sqrt{\frac{1}{N}\sum_{N}^{1}\hat{y}^2}} = \frac{LSE}{\sum RMS} \tag{2}$$

Preliminary indications of icing can be assumed when the Theil inequality coefficients for these parameters exceed a threshold level that has been calibrated through simulated exercise of the system.

5.0 Real-Time Model Estimates

Because the system compares model predictions described above with the current state, real-time estimates are used. These estimates are computed by invoking real-time parameter identification (RT-PID). The RT-PID algorithm being employed was developed by Morelli (Ref. 13), and is based on a frequency domain approach implemented in version 2.0 of System Identification Programs for Aircraft (SIDPAC).(Refs. 14 and 15) The approach uses a linearized model of the vehicle dynamics, Equation (3), where *A*, *B*, *C*, and *D* matrices containing stability and control derivatives.

$$\begin{aligned} \dot{x}(t) &= Ax(t)+Bu(t) \qquad x(0)=x_o \\ y(t) &= Cx(t)+Du(t) \end{aligned} \tag{3}$$

Time-varying estimates of the stability and control derivatives are determined using measured airplane control surface deflections and measured states from air data, angular rates, and attitude. Outputs are rotational and translational accelerations. To determine the estimates, a cost function is formulated in the frequency domain from the Fourier transform of the model in Equation (3),

$$
\begin{aligned}
j\omega\,\tilde{x}(\omega) &= A\tilde{x}(\omega) + B\tilde{u}(\omega) \\
\tilde{y}(\omega) &= C\tilde{x}(\omega) + D\tilde{u}(\omega)
\end{aligned}
\tag{4}
$$

The cost function is

$$
J_k = \frac{1}{2}\sum_{n=1}^{m}\left| j\omega_n\,\tilde{x}_k(n) - a_k\,\tilde{x}(n) - b_k\,\tilde{u}(n)\right|^2 \quad \text{for } m \text{ frequencies} \tag{5}
$$

where a_k and b_k are the kth row of matrices A and B, respectively, and $\tilde{x}_k(n) \equiv \tilde{x}_k(\omega_n)$, $\tilde{u}_k(n) \equiv \tilde{u}_k(\omega_n)$. Each line in Equation (4) can be analyzed separately in this way, which implements an equation-error formulation as described in Reference 14. The least squares cost function in each case can be formulated as

$$
J = \frac{1}{2}(Y - X\theta)^{\dagger}(Y - X\theta) \tag{6}
$$

where † indicates complex conjugate transpose,

$$
Y = \begin{bmatrix} j\omega_1\tilde{x}_k(1) \\ \vdots \\ j\omega_m\tilde{x}_k(m) \end{bmatrix} \quad X = \begin{bmatrix} \tilde{x}^T(1) & \tilde{u}^T(1) \\ \vdots & \vdots \\ \tilde{x}^T(m) & \tilde{u}^T(m) \end{bmatrix} \tag{7}
$$

and the unknown parameters from A and B are contained in the parameter vector θ. The least squares parameter vector estimate is obtained as the value of θ that minimizes the cost function in Equation (6) (Ref. 13).

$$
\begin{aligned}
\hat{\theta} &= \left[\mathrm{Re}\left(X^{\dagger}X\right)\right]^{-1}\mathrm{Re}\left(X^{\dagger}Y\right) \\
\mathrm{cov}\left(\hat{\theta}\right) &\equiv E\left[\left(\hat{\theta}-\theta\right)\left(\hat{\theta}-\theta\right)^T\right] = \hat{\sigma}^2\left[\mathrm{Re}\left(X^{\dagger}X\right)\right]^{-1} \\
\hat{\sigma}^2 &= \frac{1}{m}\left(Y - X\hat{\theta}\right)^{\dagger}\left(Y - X\hat{\theta}\right)
\end{aligned}
\tag{8}
$$

Performing the identification in the frequency domain is advantageous for this application because of computational efficiency, robustness to noise and data dropouts, and reliable confidence bounds from the covariance matrix. To ensure reliable estimates, the ICEPro features a self-checking algorithm that examines the confidence bound of the parameter estimates. Table 1 lists the parameters that are being identified in real-time.

TABLE 1.—AERODYNAMIC PARAMETERS IDENTIFIED BY RT-PID

C_{N_α}	$C_{Y_{\delta a}}$	C_{l_p}
$C_{N_{\delta e}}$	$C_{Y_{\delta r}}$	C_l
C_{N_q}	C_{Y_p}	C_{n_β}
C_{m_α}	C_{Y_r}	$C_{n_{\delta a}}$
$C_{m_{\delta e}}$	C_{l_β}	$C_{n_{\delta r}}$
C_{m_q}	$C_{l_{\delta a}}$	C_{n_p}
C_{Y_β}	$C_{l_{\delta r}}$	C_{n_r}

If confidence of the estimated parameters falls below acceptable levels due to lack of data information content (low pilot activity), an automated excitation of the aircraft control surfaces is triggered to improve data information content. This interface with the subject vehicle is performed as though an autopilot is driving control deflections using multi-frequency orthogonal inputs (Ref. 15). Amplitudes of the control deflection inputs are adjusted to provide sufficient excitation in each axis while minimizing vehicle motion.

6.0 System Implementation

The ICEPro system was developed and deployed in Bihrle Applied Research's D-Six PC-Based simulation environment. All of the ICEPro functions, including the software for driving the flight displays are provided in a single computer that runs the software in real time. The system can be interfaced with a desktop simulation, NASA's Ice Contamination Effects Flight Training Device (Ref. 16), ICEFTD (Figure 7), or mounted in the NASA Twin Otter aircraft for flight demonstrations. The system includes all of the Data Acquisition and Executive functions which control the various modules that make up the system.

The data acquisition portion receives data from the data bus on the airplane or from an emulation of the airplane data bus if it is working with the simulator. It then makes the appropriate data available to the various other modules for processing. The Executive portion provides all of the logic and calculation modules required to determine the icing state and what cues should be provided to the pilot.

The ICEPro system was first developed using a desktop simulation running in D-Six. The module development and all of the initial check out and system calibration were executed in this manner. Once the system was sufficiently mature to permit piloted evaluations, it was migrated to the ICEFTD. On the desktop implementation, the ICEPro modules and the Twin Otter simulation were run on the same computer. For the ICEFTD implementation, a separate computer was used for the ICEPro modules. Communication with the ICEFTD was accomplished over an Ethernet connection. This implementation was used to facilitate an eventual implementation in the actual airplane. If this were to occur, the same computer would be similarly connected to the airplane's data acquisition system.

Figure 7.—NASA's Ice Contamination Effects Flight Training Device (ICEFTD)

The ICEFTD piloted simulations provided synthetic environment to assess and tune the final thresholds and latching logic for the cues and messages. They also afforded the opportunity to assess the effect of control surface excitation on the pilot. The piloted simulation was also instrumental in evaluating the appearance and validity of the caution/warning messages, and the development and evaluation of aural and tactile cues. These messages and cues were incorporated for the guest pilot evaluations that were subsequently performed following the development stage.

7.0 Engineering Station

An engineering station was set up that enabled the operator to set key parameters of the ICEPro system, monitor the performance of the system, and interact with the implemented logic during the development and evaluation phases of the program. The engineering station consisted of a set of Graphical User Interfaces (GUIs) that were displayed on two monitors attached to the computer running ICEPro. The first window (Figure 8) shows the status of the system. It shows in which mode the system is currently operating (Monitor, ID, or Report), whether the controls are being excited, the duration and magnitude of the excitations in each axis, as well as the time since reset of both the D-ICES and Real Time Parameter Identification (RT-PID) modules. There is also a window that displays system status messages and buttons to reset the system modules and settings. The duration and magnitude of the surface excitations can be adjusted in this GUI and the excitation can be manually triggered when the system is in the ID or Report modes. It is also possible to manually reset either the D-ICES or RT-PID routines from this window.

There are a series of default thresholds, time delays, etc. that are used by the ICEPro logic modules that are preloaded with the system. All of the default values can be overridden by inputting new values in an included text file. There are two buttons at the bottom of the GUI to either update these system settings from the text file, or to reset them to the default values.

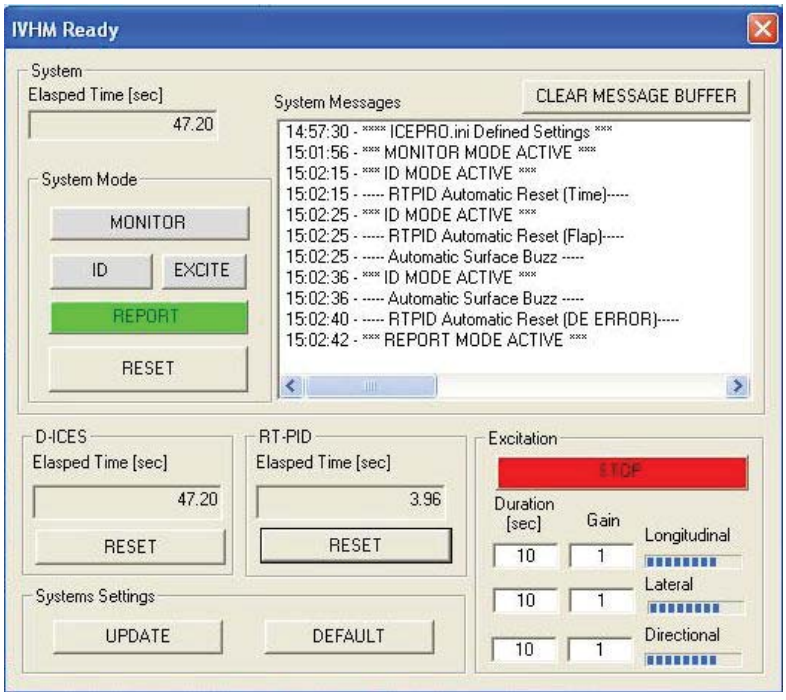

Figure 8.—System Status Window

The D-ICES status window, Figure 9, shows the a priori model values of the longitudinal and lateral-directional derivatives for both the clean and iced (Failure IPS icing shapes) airplanes at the current aircraft states. These linearized derivatives are extracted at the current state from the stored nonlinear database contained in the D-ICES routines. There is also a similar window for the RT-PID routines, Figure 10 that shows comparable real time PID derivatives. The values represented in Figure 9 and Figure 10 are only meant to illustrate the GUI and are not representative.

The RT-PID module only runs in the ID and REPORT modes, therefore, the values are not updated when the system is operating in MONITOR mode. The operator can compare the values from the D-ICES and RT-PID status windows to evaluate the differences between the a priori clean or iced values, and the actual values as determined by RT-PID. A comparison was plotted off-line and is shown in Figure 11.

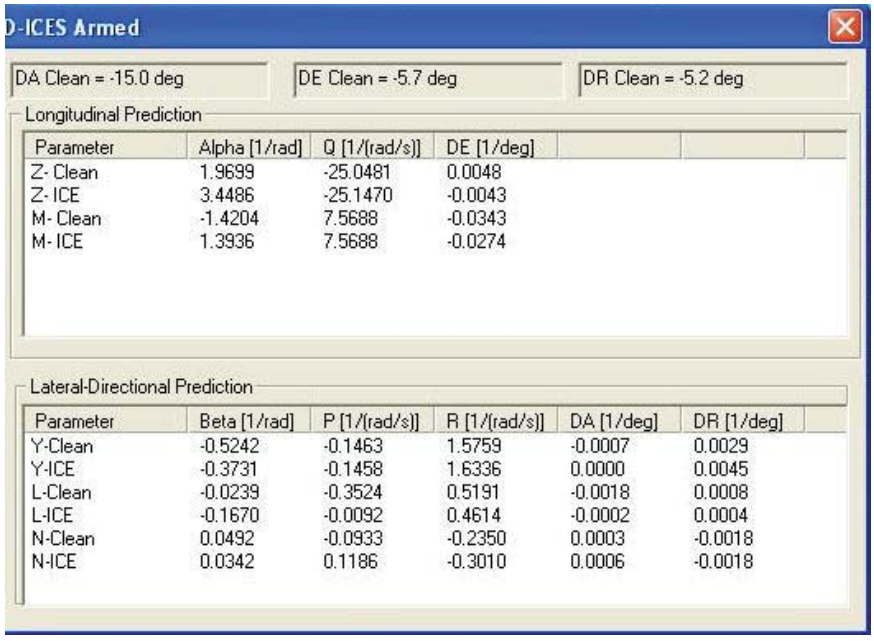

Figure 9.—D-ICES Status Window

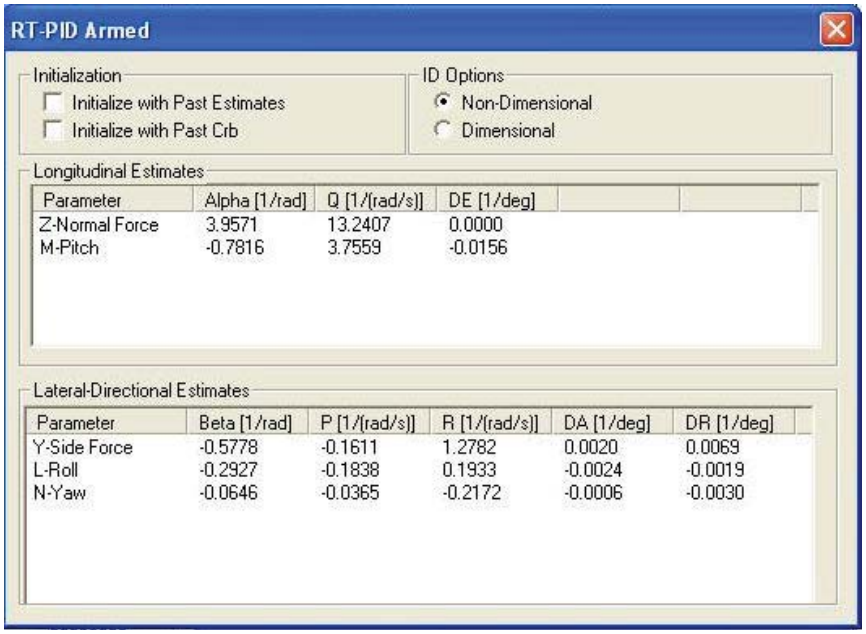

Figure 10.—RT-PID Status Window

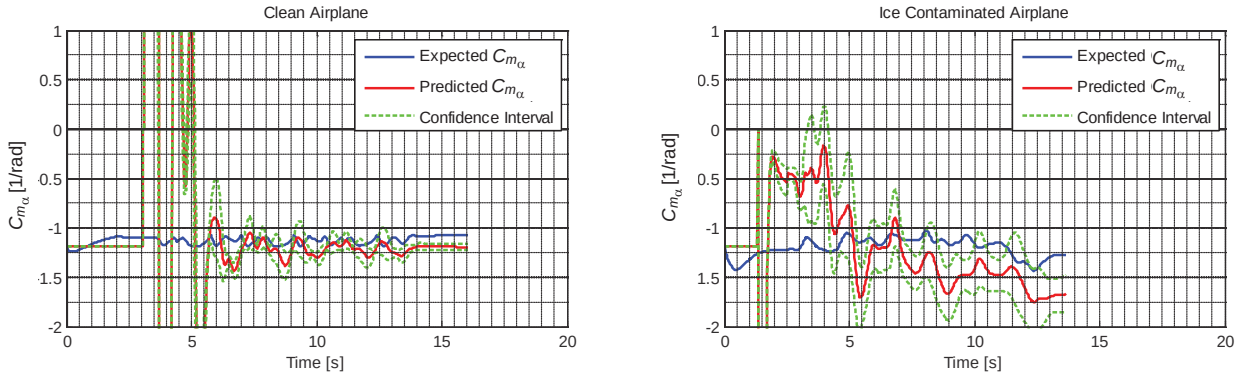

Figure 11.—Comparison of RT-PID Results (red) with D-ICES Predictions (blue), with and without Contamination

Because the ICEPro system modules are running within a D-Six project, all of the normal D-Six interface tools are also available at the engineering station. As a result, any of the aircraft variables that are passed from the ICEFTD are available to monitor in real time listings, strip charts, or as post-run engineering plots. Pertinent ICEPro variables are similarly available for real time monitoring and post-run analysis. At the end of a run, the time histories of these variables can be recorded for subsequent analysis or for play back. The system also provides strip charts of any of the RT-PID derivative values along with their expected values and the calculated error bands.

8.0 System Calibration

A considerable amount of effort was expended fine-tuning the system to provide adequate warning and guidance in an icing encounter without any false indications or nuisance messaging. These efforts included three main areas: determining which terms to include in the ISP calculation, tuning thresholds and latching and delatching logic, and developing reset logic for the RT-PID routines.

8.1 Icing Severity Parameter Determination

As shown in Equation (9), the ISP was formulated as the sum of the difference between the expected (D-ICES clean aircraft) and actual (RT-PID derived values) derivative values divided by the difference between the a priori clean and iced (Failure IPS icing shapes) values for the selected derivatives. The ISP is a single number with a range between 0 and 1. Experimental testing of the system determined that the threshold for ice contamination detection was an ISP of 0.5. During developmental testing, it was found to be impractical to use all of the RT-PID derivative terms. For example, the yawing moment terms for this aircraft did not change appreciably with icing condition, and did not prove useful to include in the ISP calculation. The damping terms, such as C_{m_q} and C_{l_p}, which did show differences with icing, were the most difficult for RT-PID to obtain with great accuracy. These damping terms proved to adversely affect the robustness of the ISP calculation and therefore were not used.

$$ISP = \frac{\sum_{i=1}^{n} \left[\frac{\left(\text{Value}_{\text{expected}} - \text{Value}_{\text{actual}} \right)_i}{\left(\text{Value}_{\text{expected}} - \text{Value}_{\text{iced}} \right)_i} \right]}{n} \tag{9}$$

The control terms, i.e., the δ_e and δ_a moment derivatives, were generally determined with great accuracy, and showed appreciable changes with icing condition. Consequently, these terms were used in

the ISP calculation. The terms for longitudinal and lateral stability, $C_{m\alpha}$ and $C_{l\beta}$ were also used. The final terms included in the ISP calculation were:

$$\begin{array}{ll} C_{m\alpha} & C_{l\beta} \\ C_{m\delta e} & C_{l\delta\alpha} \\ C_{N\alpha} & \end{array}$$

Additional logic was also added to consider the relative predicted error in each term, in the form of

$$\left| \frac{RT - PID\_\text{error}}{RT - PID\_\text{value}} \right| \tag{10}$$

Where, the term (*RT-PID*_error) is the 2 sigma confidence bound of the estimate, and the term (*RT-PID*_value) is the value of the estimate. If the relative predicted error for any term became larger than an experimentally determined threshold, the term was dropped from the ISP calculation. As a result, any term whose error represented a sufficiently large portion of its total value would not adversely influence the ISP calculation. As will be discussed further, the relative error in the pitching moment due to elevator deflection derivative was such a critical value to the ISP calculation (one of the earliest indicators of degraded RT-PID results), that its relative error was used as one of the reset criteria to the RT-PID routines.

8.2 Thresholds and Latching

For each change in mode of operation and messaging, there were thresholds that needed to be met before the change could occur or the message appeared. For example, an experimentally derived ISP threshold of 0.5 is required for the system to transition from monitor mode to ID mode. The value of 0.5 was selected so that the ISP threshold could be satisfied with only one term in the ISP formulation. There was also latching and delatching logic that specified the condition had to be met for a specified period of time before it would appear and, conversely, the condition had to disappear for a period of time before it could be removed. This logic was incorporated so that the messages would not “flash” off and on if the conditions were right on the edge of display thresholds.

8.3 RT-PID Reset

As was mentioned earlier, it was found necessary to force a reset of the RT-PID routines periodically for best operation. The RT-PID calculations make use of past values which works well if there is no change in the aircraft configuration or flight condition. However, when there are changes, the time histories of past values can incorrectly influence the calculations at the new configuration and/or flight condition. Consequently, a reset, which flushes the buffers and essentially restarts the calculations, was required whenever those conditions occurred. In addition, evaluations of the system showed that better results would occur with periodic resets even when no significant changes occurred. For the evaluation phase, the system was set to do an RT-PID reset after 50 sec if one had not occurred for either of the other two specified reasons. While control excitations were not directly commanded upon reset, they generally did occur shortly after the reset unless there was sufficient control activity by the pilot.

8.4 Conditions for Warning/Caution Messages

Messages that warned of deficiencies in a particular axis or of aircraft performance limitations were displayed on the PFD. The conditions under which these messages would appear, and whether they appeared as cautions (amber messages) or warnings (red messages) were based on the amount of

degradation from the baseline clean airplane values. Whenever a caution or warning message is displayed, the corresponding primary control surface on the airplane representation on the FCD page is also colored appropriate to the message (amber for cautions and red for warnings). The caution or warning message is also repeated in the message section of the FCD page.

The initial trials of the ICEPro system considered stability and damping terms in each axis, as well as control effectiveness terms to determine when a caution or warning message should be displayed. In practice, it was found that meaningful stability and damping thresholds were rarely attained. Therefore, these terms were dropped and only the control effectiveness terms were used. Consequently, the conditions that will generate a pitch, roll, or yaw degraded message are as shown below (because the control derivatives are all negative terms, the inequality signs may seem reversed):

$0.50 \cdot C_{m_{\delta e\_no \cdot ice}} \le C_{m_{\delta e}} < 0.25 \cdot C_{m_{\delta e\_no \cdot ice}}$, then amber PTCH DGRD and amber δe on FCD

$C_{m_{\delta e}} \ge 0.25 \cdot C_{m_{\delta e\_no \cdot ice}}$, then red PTCH DGRD and red δ*e* on FCD

$0.50 \cdot C_{n_{\delta r\_no \cdot ice}} \le C_{n_{\delta r}} < 0.25 \cdot C_{n_{\delta r\_no \cdot ice}}$, then amber YAW DGRD and amber δr on FCD

$C_{n_{\delta r}} \ge 0.25 \cdot C_{n_{\delta r\_no \cdot ice}}$, then red YAW DGRD and red δ*r* on FCD

$0.50 \cdot C_{l_{\delta a\_no \cdot ice}} \le C_{l_{\delta a}} < 0.25 \cdot C_{l_{\delta a\_no \cdot ice}}$, then amber ROLL DGRD and amber δa on FCD

$C_{l_{\delta a}} \ge 0.25 \cdot C_{l_{\delta a\_no \cdot ice}}$, then red ROLL DGRD and red δ*a* on FCD

Calculations of single engine rate of climb capability were made using the simulation data and Twin Otter Airplane Flight Manual values. Tables of these values as functions of flap deflection, ice condition, and altitude were stored in the ICEPro routines. Whenever the system was in the Reporting mode and the flight and icing condition resulted in predicted single engine rate of climb levels below specified thresholds, a climb limit caution or warning message would appear on the PFD and in the FCD message box. In addition, a corresponding flap limit message would appear and the flaps representation on the FCD page would be colored either amber or red, corresponding to caution or warning messages. This was meant to alert the pilot that the flap deflection should be reduced for safe operation in the event of an engine failure. The thresholds used during the evaluations were:

0 fpm < SingEngROC ≤ 100 fpm, then amber CLMB LIM and FLAP LIM
SingEngROC ≤ 0 fpm, then red CLMB LIM and FLAP LIM

8.5 Stall Warning and Decluttering

A stall warning was added that consisted of a large red STALL message appearing near the middle of the PFD and an aural two-note tone. The aural warning would come on whenever the calculated stall angle of attack was attained, and the message would appear on the PFD when the angle of attack was 2° above the calculated stall angle. During the system development, it was found that in the low-speed highly dynamic environment present during stall, RT-PID was unable to keep up with the rapid change in aerodynamic characteristics. Extraneous warning/caution messages were observed but would go away after the airplane was stabilized. Rather than spend significant time refining the thresholds and logic, it was decided, based on pilot evaluations during the development, that it was best to eliminate the messaging entirely during a stall and recovery. This allowed the pilot to concentrate on recovering the airplane without the distractions. Consequently, logic was incorporated to “declutter” the PFD by eliminating all ICEPro related messaging during this period. The angle of attack brackets and speed carets did remain on the PFD, since these would aid the pilot during the recovery effort. While these cues do depend on the RT-PID results, the ISP calculation is filtered to yield a more or less steady-state level. Therefore, the ISP calculation is marginally influenced by the rapid changes during a stall and recovery.

8.6 Accommodations for Pilot Evaluations

In preparation for the piloted evaluations that took place during August 2009, several additions were added to the simulation. To represent to the pilot an icing protection system failure, a message stating "IPS failure" was displayed in the FCD message box along with an aural cue. A stick shaker and stick pusher function were added to the longitudinal yoke loader. These were configured to operate in a manner consistent with real-world shakers and pushers and would act as a forceful cue to the pilot that wing stall was about to, or had occurred. The shaker was sufficiently rapid and forceful that it could not be missed during the most intense flight condition. The shaker was configured to come on at the same time as the angle of attack brackets turned from white to amber, which was 2° below the stall angle of attack. The pusher was forceful enough that it would force the airplane back to an unstalled angle of attack. Monitoring when the shaker or pusher was activated proved to be an important tool in interpreting and assessing the performance during post-flight analysis. The stick pusher came on at approximately the same time that the stall message appeared on the PFD.

9.0 Pilot in the Loop Test Methodology

9.1 Experiment Design

The purpose of the pilot in the loop evaluations was to determine if ICEPro had utility for mitigating a potentially hazardous icing encounter (Ref. 17). The independent parameters were the two displays (baseline, and ICEPro with envelope protection), and the dependent parameters were technical performance, workload, and pilot opinion. An ICEPro display is shown in Figure 1. A baseline display is Figure 1 without airspeed limit carets, angle of attack limit brackets, stall messages, and flight control status indicators. A nonparametric, independent measures experiment was therefore selected where differences in the dependent variables were analyzed using the Mann-Whitney "U" (MWU) test (Ref. 18). A critical "U" was determined, based on the statistical one-tailed test where a 95 percent confidence criteria or better was required to correctly reject the null hypothesis (H_0). H_0 assumed that there was no difference between the two groups for the tested variable, therefore the level of significance or alpha level required to reject the null hypothesis was chosen to be $\alpha = 0.05$. The experiment was planned for an evaluation by 30 pilots with relatively similar flight experience. All pilots were Embry-Riddle Aeronautical University (ERAU) instructor pilots with a median flight experience of approximately 1300 flight hours. Each possessed commercial, multi-engine, and instrument ratings, but none had any specific experience in actual icing conditions or any prior training in aircraft handling and upset recovery due to a hazardous icing condition. The 30 pilots were randomly divided into a control group (baseline flight displays and no ICEPro system) and an experimental group (displays modified with ICEPro cues and messages). A scheduling problem resulted in a total of 29 pilot evaluations and unequal sample sizes between the control and experimental groups ($n_c = 14$ and $n_e = 15$). This disparity was accounted for by the MWU methodology as provided for in Reference 18.

9.2 ICEFTD Simulator Description and Capability

The aircraft model and subsystem components for the ICEFTD simulator were assembled in BAR's commercial off the shelf (COTS) proprietary simulator development environment, D-Six. The simulator provided highly representative flight characteristics of the Twin Otter icing research aircraft. Although originally designed as a pilot training device, the ICEFTD's ability to accurately represent aircraft icing characteristics made it a very useful research tool with several advantageous features. One is its capability for accurately representing flight characteristics beyond stall AOA, which permits pilots to experience post-stall gyrations and tail stall hard-over's that can occur during upset conditions. Another is the pitch control system, which can provide control force gradients and deflections that closely match those recorded from flight tests of the NASA Twin Otter during upset events. Lastly, an "aircraft emulator" was designed and integrated in order to represent the same sensor feedback and output response as that of the

NASA Twin Otter research sensors. Figure 12 is an overview of the ICEFTD as modified for this test. The items in red font are those which support ICEPro operation.

The D-Six simulator also provided excellent three-screen graphics of a visual scene, which was an essential element of the final approach and missed approach task. A video recording camera system was also employed for each pilot evaluation run in the event a replay of the pilot's actions needed to be observed. During testing, the evaluation pilot wore a headset and was completely enclosed in the simulator by a system of curtains as shown in Figure 13 and Figure 14. This isolated the pilot from any outside disturbances or distractions, and enhanced the fidelity of the simulation environment.

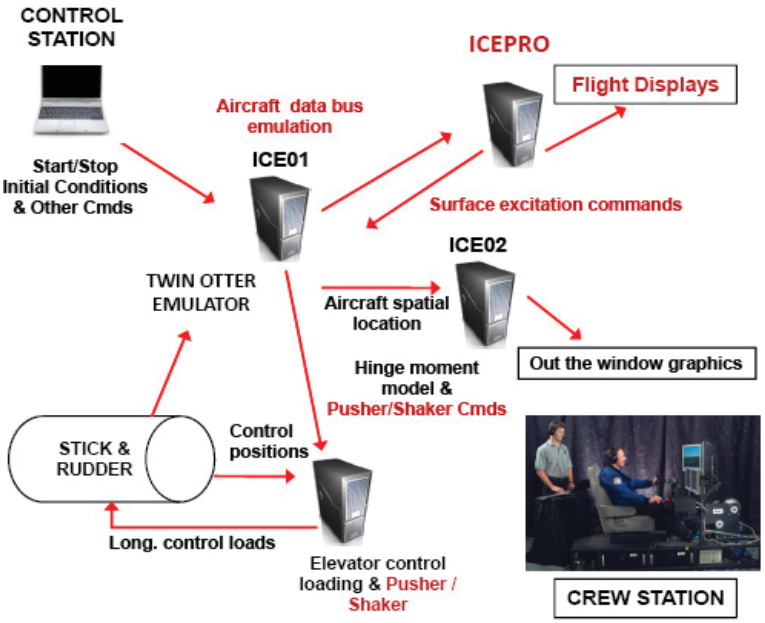

Figure 12.—ICEFTD Configuration for Test and Evaluation of ICEPro

Figure 13.—Evaluation Pilot Station

A member of the test team operated the simulator and performed data acquisition and processing tasks from a remote engineering station. Consequently, this person could not see the ICEFTD instrument panel. Therefore, a copy of the PFD displayed to the pilot was provided as shown in Figure 14.

A second member communicated with the pilot while acting as test conductor and air traffic control (ATC) as shown in Figure 15.

Figure 14.—Engineering Station

Figure 15.—Air Traffic Control Station

9.3 Pre-Test Pilot Proficiency Training

Before performing the evaluation tasks for data collection, each pilot was subjected to approximately 1.5 hr of flight training in the ICEFTD. Pilots were trained for the evaluation task using the respective flight displays depending on whether they were in the control or experimental group. Training began by having each pilot execute the evaluation approach task profile as shown in Figure 16 in a no-ice or baseline configuration under instrument meteorological conditions (IMC). The IMC condition for training and testing was set at 400 ft and 1 nautical mile (n mi) visibility. The white boxes in Figure 16 describe the flight condition and events during the task and the green shaded boxes show the commands given by the test conductor, who acted as ATC at various stages during its execution. The missed approach procedure (MAP) with an engine failure was initiated by the test conductor at the approximate position as shown in red font. Pilots practiced the approach task according to the standard operation procedures (SOP), which specified speeds, configurations, and performance standards throughout the profile. This phase of training was important in order for the test team to determine that each evaluation pilot possessed the requisite instrument flight skills to satisfactorily perform the task.

The next phase of training was conducted up and away under visual meteorological conditions (VMC) to familiarize pilots and develop their skill in dealing with aircraft characteristics due to the ice protection failure case condition. This training emphasized recognition of impending upset conditions and the effects of wing flap configuration and flight speed on aircraft handling and control characteristics. Pilots in the control group were taught how to most effectively use their baseline flight displays to control the aircraft and recognize and recover from upset conditions. Pilots in the experimental group received the same training emphasis, but were taught how to integrate their scan and control strategy with envelope protection cues from ICEPro to facilitate safe flight control and upset recoveries. During this training, evaluation pilots were also instructed to fly with both hands on the yoke. This was a learning experience because nearly all of them were used to one handed operation in aircraft with relatively light control forces.

Once the up and away training was completed, each of the pilots practiced the approach procedure with the hazardous failure case icing condition as would be performed in the actual evaluation. A certain amount of time was also spent having the pilots practice the missed approach procedure under iced conditions. This was the most difficult task to perform because of high pitch control forces and the requirement to null the asymmetric thrust with high rudder forces when an engine was failed. Pilots had to practice this maneuver several times before they could consistently accomplish it in a proficient manner and not lose control. Evaluation pilots were continually reminded to fly according to the SOP, which was intentionally designed to place the aircraft near the edges of the flight envelope at all times. This protocol forced considerable attention to precise aircraft control throughout the approach task, which was essential for making a good utility assessment of ICEPro. The evaluation profile approach task for both groups required considerable mental concentration, physical strength and very aggressive control inputs to prevent or recover from upset conditions. All pilots, regardless of size or gender, were able to effectively perform the approach task where pitch control forces reached 90 to 100 lbf at times. In general, most pilots only required one practice approach before they were ready to begin the evaluation phase.

In addition to the flight training, pilots were briefed on and practiced completing the NASA TLX workload form. Following this training, pilots were critiqued by the test team, and then given a short break before they began their evaluation runs.

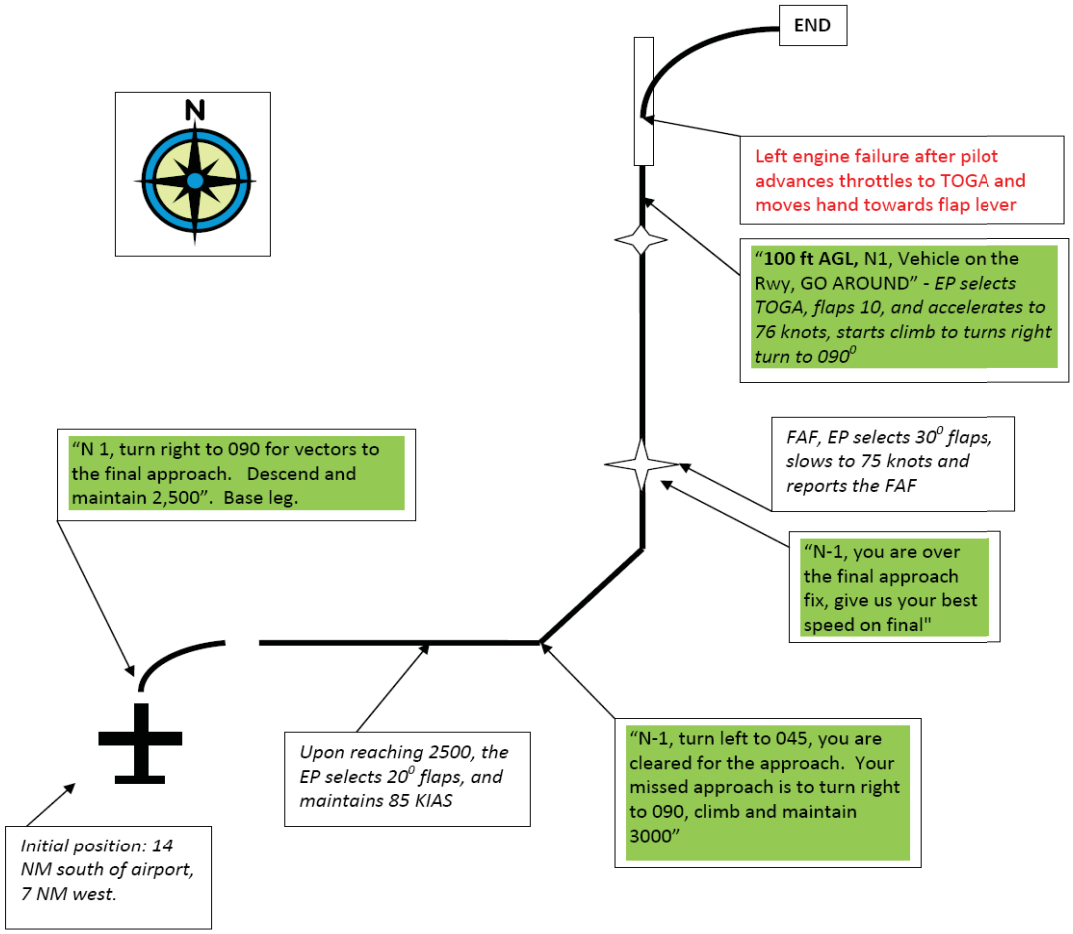

Figure 16.—Evaluation Profile Approach Task Flown by Each Pilot Group During ICEPro Testing and Evaluation

9.4 Simulator Flight Evaluations

The evaluation phase required that a total of three satisfactory approach tasks be performed by each pilot. The test conductor sat behind the ICEFTD and acted as ATC and was able to view the evaluation pilot through a small opening in the rear curtain. During each evaluation run, the pilots were completely enclosed in the simulator cab, and no coaching or extraneous discussions were permitted. As shown in Figure 16, the approach task consisted of "radar vectors" to intercept a precision approach procedure. The pilot would execute the approach according the SOP, and "break out" of the clouds at 400 ft above ground (AGL), and continue the descent to the runway on a visual glide path. At approximately 100 ft AGL, "ATC" would instruct a missed approach procedure, which the pilot would acknowledge and then initiate. As soon as both power levers were fully advanced, the test conductor would fail an engine, and the pilot would continue the procedure while raising the wing flaps from 30° to 10°. The test was terminated when the evaluation pilot was stabilized on the missed approach heading.

Once complete, the evaluation pilot would fill out an electronic TLX form, which automatically computed the numerical workload score, and received a short debriefing from the test team. The pilot would then re-enter the simulator for the next evaluation run.

The entire evaluation process for each pilot including the pre-test training exercises and three evaluation runs took approximately 3 hr, which seemed to be the limit before fatigue became a factor in pilot performance. After testing was completed for each pilot, they were asked to fill out a post-test survey questionnaire, included in Appendix B. This questionnaire consisted of four sections using a

Likert (Ref. 19) style format: Part I provided pilot demographic and experience information; Part II asked about situational awareness; Part III asked for the experimental group's assessment of ICEPro integration; and Part IV asked general questions about workload factors.

9.5 Data Acquisition and Handling

Pilot flight performance data parameters, which were available through a flight data file that was resident in D-Six, were sampled at 10 Hz. MATLAB routines were used to collect and reduce these data for further analysis. For the final approach segment of the task, the Theil inequality coefficient was used to evaluate how closely the pilot's flight path and airspeed agreed with that of a perfectly flown approach. A Theil inequality coefficient was calculated for measured lateral and vertical deviations from the centerline of the approach path, and the airspeed error from the required 75 kt indicated airspeed (KIAS) approach speed. MATLAB routines were also used to record the number of times the stick shaker and pusher fired, and number and depth of tail stall AOA exceedence events over the duration of the entire flight task. In addition to these performance data, other parameters were recorded during each run to provide a more complete picture of the pilot's control strategy which was useful in training and debriefing the evaluation pilots. These included time histories of pressure altitude (H_P), pitch attitude (θ), pitch rate (q), normal acceleration (n_Z), elevator position (δ_e), elevator control force (F_e), and wing flap setting (δ_F). Pilots completed the NASA TLX immediately after each data run, and then completed the survey questionnaire at the termination of the evaluation session.

The pilot performance data quantified how well the pilot flew the approach task, how many stick shaker and pusher events occurred, and the number of times and extent to which the tail stall AOA was exceeded by 5° or more. It should be noted that reaching a tail stall AOA, which was one of the measured parameters, did not always result in an upset as long as the pilot immediately recognized the condition and promptly arrested the negative pitch rate. The added 5° margin took into account pilot reaction time and aircraft dynamic response to the controls. Therefore, tail stall upsets were defined by the number of times the pilot *reached or exceeded the 5° margin*, and the maximum negative AOA achieved in the event. This latter metric was also used to define "upset risk", since the deeper the stall, the lower likelihood of recovery. In addition to pilot performance data, the numerical scores of the TLX workload assessments and the numerical results from the Likert-type post-test questionnaires were analyzed by the MWU process. The TLX analysis was of interest to understand if the added information of the ICEPro displays adversely affected workload. The post-test survey analysis was used to assess if there was a real and positive difference in hazardous aircraft state awareness, and perception of workload between the two groups. Additionally, a section of the survey provided noncomparative information on how well the experimental group felt the ICEPro was integrated with flight displays.

The utility evaluation of ICEPro was based upon assessing real differences between the control and experimental groups. The MWU analysis process began by rank ordering the scores of each group, and computing a "U" value based on the rank sums. In this one directional test, the "U" for the experimental group had to be greater than 144 to ensure a 95 percent probability for correctly rejecting H_0. A cumulative probability p was calculated from the z score and was compared to $\alpha = 0.05$, the requirement for accepting the alternate hypothesis. If this probability was less than 0.05, the null hypothesis was rejected. A negative z score (number of standard deviations) of more than magnitude 1.69 (i.e., less than –1.69) was required to produce the cumulative probability which met this requirement. The parameters which were assessed included all quantified measures of pilot performance, TLX workload, and subjective opinions from the survey questionnaires.

An assessment of recovery from tail stall upsets was also performed. In many cases, when a tail stall event was encountered, a series of pitch oscillations would ensue from which the pilot would have to recover. An analysis of repeated events was performed to determine if the experimental group could recover from these oscillations using ICEPro cueing sooner than the control group, and thereby be less prone to entering an out-of-control condition. A pilot coupling event (PCE) represents a hazardous situation, which if not arrested quickly, could progress to a loss of control. In this context, the risk of an

unrecoverable upset was associated with the number of repeated tail stalls in a PCE scenario, and the depth of each stall beyond the 5° margin previously discussed. A time window analysis was therefore used to analyze the number of tail stalls occurring within a continuous 5, 10, 15, and 20 sec span, while the pilot was attempting a recovery. Search scripts in MATLAB were used to analyze the beginning and ending of each PCE, and total the number and severity of each tail stall within the PCE. The results were then reported in a tabular format for both groups, and analyzed for significance by the MWU method. An important outcome of this analysis was to assess the utility of ICEPro AOA cues for minimizing the recovery time from a PCE, and thereby reduce risk of a loss of control situation.

10.0 Pilot in the Loop Results and Discussion

10.1 Pilot Demographics

All evaluation pilots were instructor pilots in the ERAU professional pilot training program. Thirty pilot volunteers were broken down into two groups—a control group who flew baseline displays, and an experimental group who flew with ICEPro modified displays. All evaluation pilots held FAA commercial licenses with multi-engine and instrument ratings. The demographic data was collected in Part I of the post-test survey questionnaire, and is discussed below. Due to a scheduling problem, the control group consisted of one less pilot that the experimental group. The demographics of the groups were as follows:

Subjects and gender:

14 control group (12 male, 2 female)
15 experimental group (12 male, 3 female)

Median flight hours:

Control group		*Experimental group*	
Total	1350	Total	1250
Multi-engine	122	Multi-engine	100

Icing related experience and training as related from Part I of the post-test survey questionnaire:

- 75 percent had no prior in-flight icing experience
- 89 percent did not feel that their prior icing related knowledge/experience would have prepared them to perform the test scenario (training was required in order for pilots to execute the flight task)
- 72 percent agreed that the NASA videos/web based training gave more information about icing than they had known before (viewing NASA web-based training videos was a pre-test requirement)
- Mixed responses were given for icing related flight training being focused on IPS operation (this depended on the types and classes of aircraft in which pilots had been previously trained)

10.2 Pilot Control Performance

Pilot control performance assessment from the control and experimental groups are summarized in Table 2. Results highlighted in *green* indicate that the significance or real difference criterion for the assessed parameter was met, and the performance of the experimental group was better than that of the control group. Results highlighted in *blue* indicate that the assessed parameter showed better performance by the experimental group, but the result did not meet the real difference criterion. Results highlighted in *orange*, indicate that there was no difference between the performance of the two groups, and results highlighted in *magenta* indicate that the experimental group did not perform as well as the control group.

In general the cumulative pilot performance for the two most critical events, pusher activation and tail stall, met the real difference criterion. These events were considered most important from a safety of

flight standpoint because a wing or tail stall upset had occurred, and potential for loss of control was very high unless the pilot promptly applied the correct sequence of recovery controls. The shaker activation event indicated that the control group had slightly better performance than the experimental group, but this finding can be misleading without considering important aspects of shaker implementation and pilot use of this functionality in a human factors context. This is explained in the following discussion of the results, which were tabulated in Table 2. The first column of Table 2 identifies the event that was evaluated during the approach and missed approach task, the second column indicates the number of standard deviations (z) required in meeting the real difference criterion, the third column indicated the cumulative probability (p), and the last column provides a performance assessment between the experimental and control group based upon the analysis.

10.2.1 Shaker Events—Stall Warning

The results of the pilot performance for avoiding stick shaker events as shown in Table 2 indicate that, cumulatively, the control group had a slightly better performance than the experimental group. Shaker firings typically occurred in banked turns if speed got too low, during positive pitch overshoots incited by a tail stall induced PCE, and when pilots made an overly aggressive recovery after stick pusher firing. The following discussion places these results into perspective and discusses factors that may have affected their outcome. The control group flew with basic aircraft displays and a simple stick shaker functionality, which always provided a 7 percent stall speed margin based upon a clean wing; i.e., no-ice. Therefore, when the shaker fired during the approach task in the icing condition, the actual margin to stall was less than 7 percent.

On the other hand, the experimental group flew with ICEPro generated displays, which provided real time AOA cues and shaker functionality that maintained a 7 percent stall speed margin for the icing

TABLE 2.—SUMMARY OF PILOT CONTROL PERFORMANCE

Pilot control performance by run number and cumulative	z score: $z < -1.69$ for 95% confidence in H_0 rejection	Probability: $p < 0.05$ required to satisfy α (alternate hypothesis)	Group performance: Exp. versus control Positive real difference (PRD), Better (B), Worse (W), Same (S)
Shaker events			
Run 1	1.0474	0.8575	W
Run 2	–0.2837	0.3799	B
Run 3	–0.5892	0.2705	B
Cumulative runs	0.0873	0.5434	S
Pusher events			
Run 1	–0.0655	0.4652	S
Run 2	–1.2875	0.0952	B
Run 3	–2.1822	0.0137	PRD
Cumulative runs	–1.7457	0.0385	PRD
Stall Messages No stall messages appeared for the experimental group			
Tail stall events			
Run 1	–1.2657	0.0989	B
Run 2	–1.8330	0.0318	PRD
Run 3	–1.7894	0.0350	PRD
Cumulative runs	–2.1822	0.0137	PRD
Legend			
	Meets 95% confidence for rejecting H_0		
	Experimental group better over control group but < 95% confidence for rejecting H_0		
	No difference between experimental and control group		
	Experimental group performance worse than control group		

condition. Experimental group pilots could avoid shaker events if they remained below the upper AOA limit bracket as shown in Figure 1. The control group had no AOA information on their basic flight displays. In order to avoid shaker activation, they had to closely maintain the SOP required airspeeds throughout the entire task. Notably, the control group was technically at greater risk when the shaker fired because their stall speed margin was less than 7 percent. A study of the frequency of shaker events is helpful in order to better understand the results of Table 2. Table 3 provides the number of recorded shaker events per run for each group of pilots.

During run one, 14 control group pilots experienced 87 shaker events, whereas 15 experimental group pilots experienced 113 shaker events. On average, the control group experienced 6.21 events per pilot, and the experimental group experienced 7.53 events per pilot. The corresponding MWU analysis for run one in Table 2 clearly shows better (but not significant) performance from the control group. During the subsequent runs, however, the experimental group's performance got better, and this is reflected in the analysis for runs two and three in Table 2. If all three runs are considered cumulatively, the normalized ratio between the two groups is slightly better for the experimental group, but the cumulative results of the statistical analysis shown in Table 2 slightly favors the performance of the control group. Regardless, the differences between control and experimental groups as shown in Table 2 and Table 3 are very small. What is important to observe here is that the experimental group did a much better job of avoiding shaker events during subsequent runs, while the control group's performance remained nearly constant. This was likely due to increased proficiency in using ICEPro AOA cues, which was not fully realized during pre-test training. Unfortunately, practical limits on pre-test training were necessary in order to conduct all required evaluations within time and program cost constraints.

10.2.2 Pusher Events—Wing Stall Upsets

Table 4 summarizes the number of pusher events per run for each group. Pusher events were generally precipitated by the same factors that incited shaker events and occurred when the pilot could not arrest an AOA increase, which resulted in a wing stall upset. This was particularly evident when the missed approach procedure was executed. Here, pilots immediately advanced the throttles to full power, raised the wing flaps to 10° and the nose to the takeoff attitude in one coordinated motion. As soon the power levers reached the full power stop and the evaluation pilot reached for the wing flap lever, the left engine was failed by the test conductor, and the pilot then had to null the yaw and adjust pitch so as to maintain a 76 KIAS climb speed. This was a very dynamic maneuver, and in many cases it precipitated a PCE. As in the case of the shaker events, the experimental group of pilots improved with each evaluation run, whereas the control group actually got worse. The raw data in Table 4 supports the statistical assessment that the ICEPro displays resulted in better pilot control performance and lower risk of an upset due to either wing or tail stall.

TABLE 3.—NORMALIZED SHAKER EVENTS

Control group (14 pilots)			Experimental group (15 pilots)		
Run	Shaker events	Normalized	Run	Shaker events	Normalized
1	87	6.21	1	113	7.53
2	92	6.57	2	86	5.73
3	87	6.21	3	72	4.80
Cum	266	6.33	Cum	271	6.02

TABLE 4.—NORMALIZED PUSHER EVENTS

Control group (14 pilots)			Experimental group (15 pilots)		
Run	Pusher events	Normalized	Run	Pusher events	Normalized
1	12	0.86	1	13	0.87
2	16	1.14	2	10	0.67
3	19	1.16	3	6	0.40
Cum	47	1.05	Cum	29	0.64

10.2.3 Stall Messages

A “STALL” message was incorporated into the PFD in the event the pilot attempted to override the pusher and thereby remain in a stall upset condition. This was a functionality associated with ICEPro displays, and appeared to be unnecessary as all the experimental pilots promptly applied recovery controls to reduce the AOA below the upper bar when the pusher fired. No stall messages appeared during any of the runs flown by the experimental group.

10.2.4 Tail-Stall Upsets and Recoveries

Tail stall upsets resulted when pilots flew too fast, exceeding the speeds specified at various segments of the flight task, or when they allowed the AOA to get too low. This condition was greatly aggravated with increasing wing flap deflections, and was most sensitive during the final approach and missed approach procedure when the flaps were 30° down. As described previously, a tail stall was defined as reaching a negative AOA that was 5° below that where the tail had technically reached a stall condition. This margin was determined experimentally, as it appeared that if a pilot immediately applied recovery controls before reaching this negative AOA, recovery would be prompt and the chance of a PCE minimized. When a tail stall occurs in an aircraft equipped with mechanical controls, such as the one simulated in this test, the pilot feels an immediate increase in pull force and notes a rapid build-up in negative pitch rate. In order to arrest the condition, the pilot must quickly exert very high pull forces (on the order of 90 to100 lbf) to reverse the downward motion of the nose. If successful, the nose starts back up; but, as it does, pitch forces immediately lighten and a positive pitch overshoot can easily occur. This can precipitate a PCE, which can develop into a loss of control situation should a negative AOA be reached that the pilot is not able to physically overcome. Pre-test pilot training acquainted both control and experimental group pilots with these characteristics, and the basic methods for recovery.

During training, pilots practiced tail stall upset recoveries by keeping the pitch divergence to a minimum. Additionally, the experimental group was taught to use the ICEPro displays to facilitate recovery by adjusting pitch during a PCE to remain within the safe envelope defined by the AOA brackets. When pitch rate was negative, the pilot would attempt to pull the nose up, but remain below the high AOA bracket. If the pitch rate was positive, the pilot would push the nose down, but remain above the low AOA bracket. If done properly, this would result is a very expeditious recovery—normally within one or two cycles. Of note, this strategy contributed to fewer pusher events as the experimental group tended to be better at avoiding stall AOA than the control group.

The learning bias evident in the shaker and pusher data seem to indicate that had more time been available for the experimental group to practice with the ICEPro displays, their performance during these events would have been better. Runs 2, 3, and cumulative of the tail stall event clearly show positive real difference in the performance of the experimental group and provide better than 95 percent confidence for correctly rejecting H_0.

10.3 Pilot Precision Approach Performance

The final approach segment required the pilots to intercept and accurately fly a precision approach to the minimum descent altitude of 200 ft. As shown in Figure 1, the flight displays for both groups did not provide computed steering or a flight director format. Therefore, the pilots had to fly what is termed “raw data” and null localizer and glide slope errors by controlling heading and descent rate. As described earlier, this task was also performed in IMC until reaching the ceiling of 400 ft above ground level. When the pilots “broke out” of the cloud at this altitude, they continued their descent to 100 ft and were directed to execute a missed approach. The difficulty in flying the approach task was largely due to control aspects discussed earlier. Some pilots were very smooth and precise throughout the task, and were able to execute it without too much difficulty. This was because they did not allow the attitude of the aircraft to vary much beyond that required to maintain a given flight condition. Generally, these were pilots who had very efficient instrument scans, and who made very small but immediate corrections when required. Pilots whose instrument scans were less efficient and allowed large pitch or roll variations to occur were more prone to get into a pitch axis PCE. A PCE event greatly affected glide slope, course, and airspeed errors, and was reflected in the Theil inequality coefficient values for each of those parameters. Table 5 provides the results

of the MWU analysis of the precision approach errors between the control and experimental groups. It should be noted, that both groups of pilots generally flew the approach procedure within Airline Transport Pilot (ATP) standards (Ref. 20) as required in the SOP. The Theil inequality coefficient values, which were used in the MWU analysis, were basically a means of quantifying the pilot's performance with respect to a perfectly flown approach. A representative localizer Theil inequality value for one such run is shown in Figure 17. Similar plots were obtained for glide slope Theil inequality values. As shown in Table 5, the control group had better cumulative performance in minimizing localizer and airspeed errors. The experimental group had better cumulative performance in minimizing glide slope error, but did not meet the significance criteria required to infer that there was a real difference between the two groups. It would appear, after considering the results from Table 2 and Table 5, that pilots who had the advantage of ICEPro displays tended to prioritize aircraft control over the preciseness at which they flew the localizer and the required airspeed. This is perhaps why the control group, who flew more precise airspeed, had significantly more tail stall upset events than the experimental group and was considered to be at greater risk of entering an out of control situation.

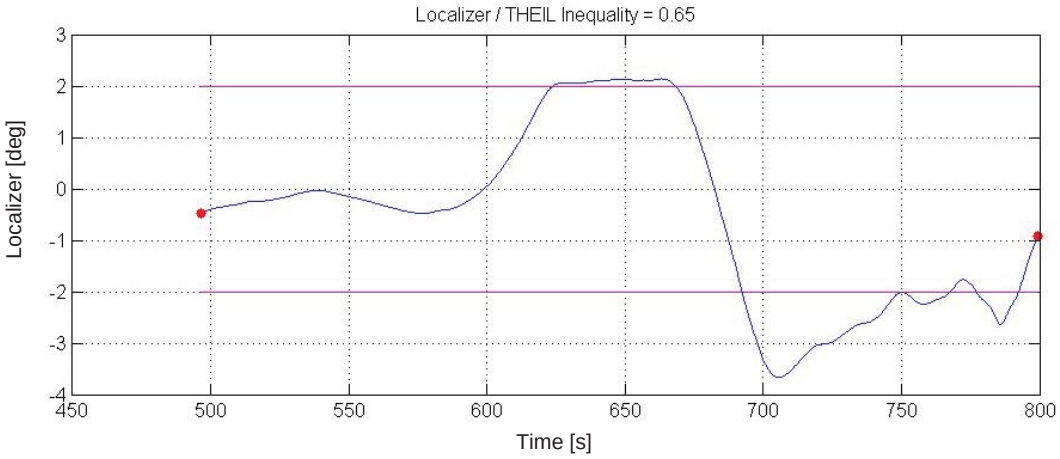

Figure 17.—Localizer performance—THEIL inequality calculation

TABLE 5.—PILOT PRECISION APPROACH PERFORMANCE

Pilot precision approach performance by run number and cumulative	*z* score: $z < -1.69$ for 95% confidence in H_0 rejection	Probability: $p < 0.05$ required to satisfy α (alternate hypothesis)	Group Performance: Exp. versus Control Positive real difference (PRD), Better (B), Worse (W), Same (S)
Localizer			
Run 1	0.6328	0.7436	W
Run 2	0.2619	0.6116	W
Run 3	0.0436	0.5260	W
Cumulative	0.1528	0.5692	W
Glide slope			
Run 1	–1.4402	0.0718	B
Run 2	0.5674	0.7221	W
Run 3	–1.4621	0.0689	B
Cumulative	–0.4364	0.3233	B
Airspeed control			
Run 1	1.8330	0.9681	W
Run 2	1.9640	0.9764	W
Run 3	1.4402	0.9281	W
Cumulative	1.9421	0.9752	W
Legend			
	Meets 95% confidence for rejecting H_0		
	Experimental group better over control group but < 95% confidence for rejecting H_0		
	No difference between experimental and control group		
	Experimental group performance worse than control group		

10.4 Exposure to Risk of an Out of Control Event

A number of tail stalls, which were encountered in the course of the approach procedure, resulted in PCEs before the pilot was able to stop the oscillations and recover to a stable and normal flight condition. This event was described earlier in Section 8.5, and under “Tail-stall upsets and recoveries”, Section 10.2.4. If a quick recovery from a tail stall event (TSE) could not be facilitated by the pilot, there was a risk that repeated oscillations result in a PCE which would deteriorate into a LOC situation. Therefore, the numbers of repeated tail-stalls during PCEs were summed for each group during the final approach segment in four time duration windows of 5, 10, 15 and 20 sec. The methodology began by identifying an initial tail-stall event (TSE), which met the criterion (negative tail-stall AOA plus 5°). If another TSE occurred within 5 sec it would be counted with the first tail stall and considered a PCE. If in this event, TSEs continued to occur within 5 sec of the one previous, they would be added to the PCE until the duration of time between a repeat TSE was greater than 5 sec. This methodology was then repeated for time intervals of 10, 15, and 20 sec. The exposure to risk of reaching a LOC situation was therefore greater during a PCE based upon the number of repeat TSEs in any of the four time frames, the amount of time it took the pilot to recover, and the maximum negative pitch attitude reached during the event. The results of this analysis are provided in Table 6.

The most significant events occurred during the 5 sec interval. By using their ICEPro driven displays, the experimental group had 75 percent fewer PCEs, their events were approximately half as long in duration, and the maximum nose down attitude during the event was about 3.5° less than that of the control group. In effect, the experimental group could arrest a PCE quicker, with fewer oscillations than the control group. Most important however, was the maximum depth of the tail stall, which was measured by the maximum negative pitch attitude achieved during the recovery attempt. The more negative the attitude, the higher the negative column forces, and the more difficult it was for the pilot to arrest the negative pitching moment. Though not shown here in the data, some pilots had to use in excess of 90 to 100 lbf to arrest the negative pitching moment, which was more likely to cause a positive pitch overshoot, and sometimes result in pusher activation.

As previously mentioned, the test profile was intentionally designed to place pilots on the edge of a TSE during the approach, and as a result, most pilots in both groups experienced them, especially when momentarily distracted from their instrument cross-check. However, when a TSE occurred and especially when it deteriorated into a PCE, the experimental group was able to effectively utilize their AOA cues to damp the oscillations more quickly than the control group. They accomplished this recovery while minimizing their time at an unsafe negative AOA, and thereby were at less risk of reaching a LOC situation.

TABLE 6.—EXPOSURE TO RISK BASED UPON PILOT COUPLING EVENTS

Group	Time interval between repeat TSEs (sec)	Total number of PCEs	Mean duration of PCEs in the time interval (sec)	Mean max negative pitch
Control	5	16	15.16	–12.23
Experimental		4	8.66	–8.8
Control	10	69	18.54	–12.06
Experimental		29	17.98	–11.12
Control	15	84	23.08	–12.32
Experimental		36	23.22	–11.37
Control	20	90	27.64	–12.44
Experimental		41	25.85	–11.23

10.5 Workload

After completing each evaluation run, the pilots were asked to complete a TLX workload assessment for the entire task. The flight profile was intentionally designed to place each group of pilots very near the edges of the safe flight envelope especially during the final approach and missed approach segments. Further, the tasks were flown in IMC, and both the cognitive and physical aspects of workload were quite high for both groups, especially when recoveries from TSEs or PCEs were required. Because the experimental group had to integrate more information than the control group, there was a concern that their workload could be adversely affected.

The ICEPro displays provided much more information than the basic displays, and had to be integrated into the pilot's scan along with the instrument flying task. The control group did not have the additional information and thus had less cognitive workload. An analysis was conducted for each of the three runs in both groups. The results shown in Table 7 indicate that overall, the experimental group reported less total workload. Run 2 for example, taken by itself did meet the significance criteria and indicated that ICEPro displays made a real difference in reduced workload. However, on average for all runs, the results did not meet the significance criteria.

Observation of both groups of pilots indicated that as they flew each successive profile, they became more comfortable with the task, and tended to report lower workload. In spite of the lower workload, it was also apparent that, by the second run, fatigue began setting in; this affected pilot concentration and control performance. The entire evaluation was conducted over an approximate 3 hr period with strategically inserted rest breaks, but it was apparent that the performance of the pilots from both groups seemed to peak by the second evaluation and decrease on the third run. The results of the post-test survey questions, which are discussed in the next section, provide further insight into these findings.

10.6 Post-Test Survey Results

The questions in all four parts of the survey solicited pilot opinions to help gain insight of the two pilot groups with respect to their icing experience, perception of situation awareness, how well ICEPro was implemented, and workload issues associated with the flight task. Descriptive analysis was used for responses to Part I—Demographics and Part III—ICEPro Implementation. Parts II—Situation Awareness, and Part IV—Workload, were analyzed via the MWU methodology for real differences. The survey questions solicited either agreement, or frequency of occurrence. A Likert five-answer format was used with numbers 1 to 5 assigned to the answers from left to right. For the MWU analysis of Parts II and IV, the "direction" of the numbered response for each question, i.e., 1 to 5, or 5 to 1, was defined to indicate better performance. The survey questionnaire is provided in Appendix B for the reader's reference, and histograms of the responses to questions in Parts I, II and IV are provided in Appendix C. Descriptive-only assessments of experimental group pilot opinions are provided for Part III.

TABLE 7.—WORKLOAD ASSESSMENT

Pilot workload by run number and cumulative	*z* score: $z < -1.69$ for 95% confidence in H_0 rejection	Probability: $p < 0.05$ to satisfy α (alternate hypothesis)	Group Performance: Exp. versus Control Positive real difference (PRD), Better (B), Worse (W), Same (S)
TLX Workload			
Run 1	–0.5237	0.2926	B
Run 2	–1.8985	0.0274	PRD
Run 3	–1.4621	0.0689	B
Average all runs	–1.0911	0.1328	B

Legend	
	Meets 95% confidence for rejecting H_0
	Experimental group better over control group but < 95% confidence for rejecting H_0
	No difference between experimental and control group
	Control group performance better than experimental group

10.6.1 Part I—Demographics

The two pilot groups were intentionally selected from a relatively homogeneous sample. All pilots were essentially General Aviation (GA) instructor pilots who shared common experience with training, ratings, and types of aircraft flown. All pilots except one were staff instructors at ERAU and subscribed to the same operational and flight standards as defined by the University's professional pilot training program. There was only one outlier in the control group, and that individual's flight hours were not included in the standard deviation calculations as this individual's flight time skewed the data considerably. With the elimination of that pilot's flight hours, the standard deviation of the control group was 1054 hr, and the standard deviation of the experimental group was 698 hr. As shown in Figure C.1 (Appendix C) nearly all pilots had minimal experience with aircraft icing or icing related training before participating in this test.

10.6.2 Part II—Situation Awareness

Table 8 and Appendix B and Appendix C summarize the situational awareness responses to the questions.

TABLE 8.—SITUATIONAL AWARENESS POST-TEST QUESTIONNAIRE RESULTS

Pilot post-test survey questionnaire results	z score: $z < -1.69$ for 95% confidence in H_0 rejection	Probability: $p < 0.05$ required to satisfy α (alternate hypothesis)	Group Performance: Exp. vs. Control Positive real difference (PRD), Better (B), Worse (W), Same (S)
Part II—Situational Awareness			
1. Flight displays were adequate to determine if airframe icing was having an effect on aircraft characteristics.	–3.0987	0.00008	PRD
2. Knew minimum safe speed for a given wing flap setting within 5 kt.	–2.2242	0.0072	PRD
3. Knew how to adjust pitch attitude to avoid a wing stall or a tail stall upset.	–2.5750	0.0047	PRD
4. Knew the wing flap settings for safe rate of climb in event of an engine failure.	–2. 5968	0.0044	PRD
5. Had to rely on aircraft control response to determine icing effects on pitch, yaw, and roll.	–4.4298	0.0000	PRD
6. Confident that the final approach airspeed would prevent stall.	–0.3273	0.3634	B
7. Able to avoid aircraft handling problems or tail stall upsets when selecting wing flaps down.	1.1129	0.8717	W
8. Colored bands on airspeed tape useful to safely fly the aircraft during the entire flight.	–2.7714	0.0026	PRD
9. Relied on stick shaker to prevent inadvertently stalling.	–0.1746	0.4221	B
10. Always knew when approaching a wing or tail stall condition.	–1.8985	0.0274	PRD
Legend			
	Meets 95% confidence for rejecting H_0		
	Experimental group better over control group but < 95% confidence to reject H_0		
	No difference between experimental and control group		
	Experimental group performance worse than control group		

A positive real difference (PRD) indicates that the experimental group had significantly better situational awareness than the control group for the issue in question. As shown in Table 8, MWU analysis of the responses indicated that a PRD existed between the control and experimental groups with respect to questions 1 to 5, 8, and 10. To summarize each of these questions, the experimental group had significantly better ability to:

1. Determine that icing was having an effect on flight characteristics,
2. Know the minimum safe airspeeds to fly for a given wing flap configuration,
3. Adjust pitch to avoid wing or tail stalls,
4. Understand when engine out climb performance was being affected by the wing flap setting, and
5. To know that icing was affecting pitch, roll and yaw characteristics without relying on aircraft control response.

From the responses to question 8 the experimental group of pilots felt the colored bands on the airspeed tape were useful for safely flying the aircraft during the entire flight, while the control group did not. The histogram of the responses, Figure C.3 (Appendix C), clearly reflects this difference, but the result was somewhat confusing since both groups had the same color bands on their airspeed tape (Figure 1), and a real difference was not expected. One explanation however, may have been that the ICEPro speed carets, when overlaid on the baseline PFD display speed tape, provided better low and high speed awareness in relation to the non-iced aircraft condition. Another possibility is that the experimental group misinterpreted the question and thought the “color bands” referred to the ICEPro speed carets. In any case, the wording of the question could have been better to ensure that no misinterpretation of the nomenclature was made.

Question 10 indicated that the experimental group felt they had significantly better awareness when approaching a flight condition that could lead to a wing or tail stall than the control group. Many of the experimental pilots verbally commented during their test runs that the real time computed AOA brackets were most useful in that respect.

The responses to questions 6 and 9 respectively, indicated that the experimental group was more confident that their final approach airspeed would avoid wing stall, and that they did not have to rely as much on the shaker to avoid stalling. These results, although better for the experimental group, did not meet the significance criteria. This better, but not significantly better result may have been due to the fact that the experimental group knew that they could safely fly to just below the AOA upper bracket and avoid the shaker firing. If the brackets started flashing coincident with the aircraft attitude indication and the shaker did fire, they could immediately reduce AOA and avoid stall. The combination of AOA brackets and shaker gave the experimental group good low speed and incipient stall awareness. The control group on the other hand, had to rely on basic (clean aircraft) shaker settings and the likewise basic (clean aircraft) airspeed bands on their PFD to avoid stalling.

Fortunately for the control group, the failure case icing configuration in the simulation model resulted in a very small stall speed increase and concurrent stall AOA decrease. As a result, if the shaker fired for the control group, or if they flew into the amber stall warning band on the airspeed indicator, they were generally able to react with a decreased pitch input in time to avoid stall. Had a more severe ice shape been modeled and the stall margin been less, or even negative, the control group responses may have been different as they could have stalled before the shaker fired. The responses to question 7 indicated that the experimental group felt less able to avoid handling problems or tail stall upsets while extending the wing flaps than the control group. Referring to Figure C.3 (Appendix C), it is apparent that the greatest number of responses from the control group agreed that they could manage their control inputs to avoid handling problems, while there were an equivalent number of disagreement responses from the experimental group. This result was somewhat puzzling because it was apparent from the data in Table 6 that quantitatively, the experimental group was significantly better than the control group in avoiding tail stalls. One possible explanation is that the experimental group was provided with displays that clearly showed the effects of wing flap extension on the safe AOA envelope, but were required by the test

protocol to ignore those indications and extend the wing flaps regardless. This could have led to their response choice because they *expected* handling problems as wing flaps were extended, and knew that they were unavoidable. The question may have been poorly worded in that respect.

10.6.3 Part III—ICEPro integration

The experimental group was asked 15 questions regarding the integration of ICEPro displays. Since these questions only affected that group, a descriptive statistical approach was taken in the analysis of the data. The primary goal of these survey questions was to understand if the implementation of real time state assessment into flyable pilot cues did provide utility to the pilot. The key findings that follow list the percentage of responses on either side of a "neutral" opinion.

Figure 18 and Figure 19 represent the agreed / disagreed and always / frequently and infrequently / never responses recorded for the experimental group, respectively.

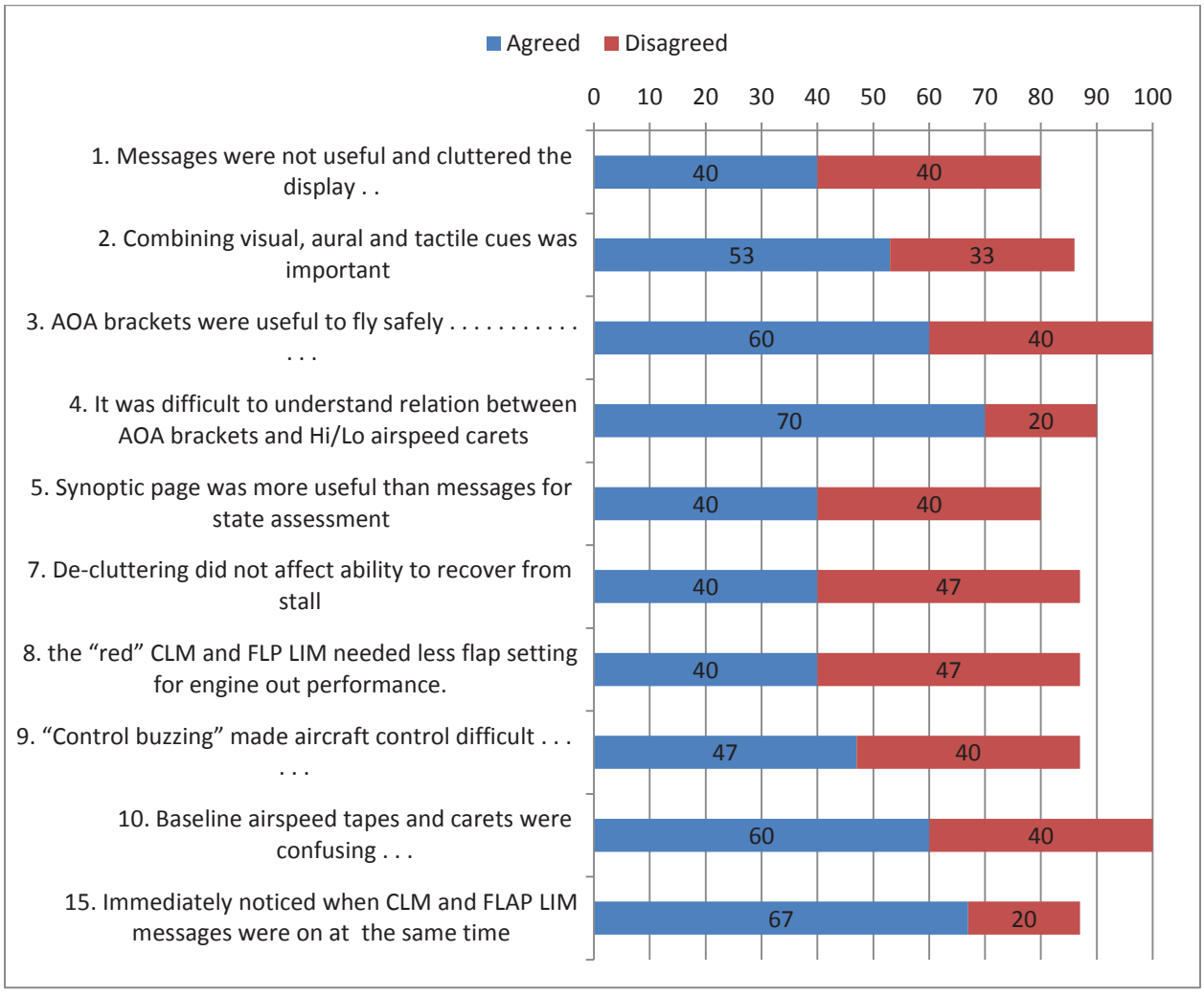

Figure 18.—Agreed versus Disagreed survey responses

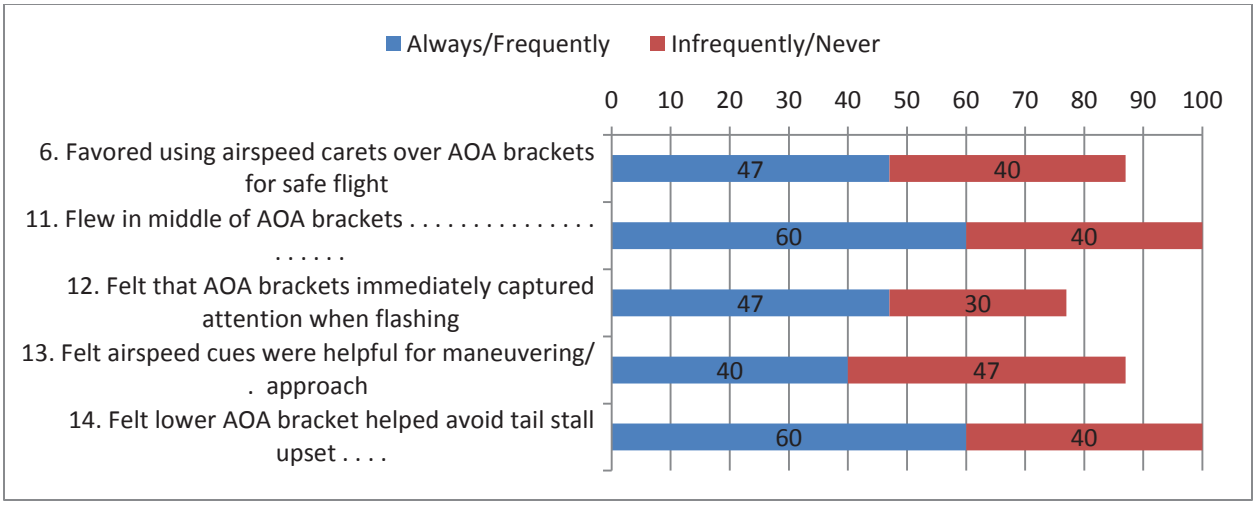

Figure 19.—Additional survey responses

Summarizing these key findings, the experimental group felt that the AOA brackets were very useful in all phases of flight, and were effectively able to use the brackets to keep the aircraft in a safe flight envelope. However, many had difficulty understanding the relationship between AOA and airspeed. None of the participating pilots had experience with flying AOA prior to this test, and it is felt that this response was largely the result of this lack of experience.

More pilots felt that presenting both the baseline airspeed along with the ICEPro generated airspeed carets was confusing. The original design intent of the ICEPro displays was to present the computed real time speeds as “advisory” information. This way, the pilot would always have a reference to the baseline aircraft, which would prove useful if a system anomaly was encountered. There was a concern for the manner in which this would be done to avoid confusion and the survey seemed to bear this concern out. Along those same lines, pilots were essentially ambivalent as to the usefulness of the ICEPro speed carets when maneuvering and flying the approach task as shown in Figure 16. A majority of pilots felt that the integration of visual, aural, and tactile cues was important, but providing redundant messages on two displays was not necessary.

Lastly, one major concern was the assessment of the multi-axis control excitation or “buzzing”, which was commanded by the ICEPro logic for aircraft state assessment. Some pilots were bothered by the buzzing, and some were not. It appeared that because it was expected, pilots accommodated to this as they would if having to fly through turbulence. In any case, there did not seem to be a strong opinion one way or the other regarding control buzzing.

10.6.4 Part IV—Workload

Workload assessments via the NASA TLX format were gathered after each run for each pilot. Post-test questionnaires were solicited in an attempt to understand some of the important factors that influenced the scores that pilots gave to workload assessment. The survey answers from the control and experimental was assessed via the MWU methodology. Table 9 provides the results from the survey questionnaire. Pilot workload was not measurably affected by ICEPro cueing. The data indicated the following:

1. Controlling vertical speed on glide slope was more difficult for experimental group (60 versus 43 percent). It appears that the control group prioritized safe flight over strict airspeed control.
2. Flight control inputs were more physically demanding for the control group (73 versus 60 percent), possibly due to the fact that the control group was not aware of the magnitude of AOA divergence.

3. The control group reported that it took more concentration and effort for flying MAP safely (87 versus 80 percent). The results however did not meet the significance criterion, but did show that the experimental group did better.
4. Staying on glide slope without pitch upset was more difficult for control group (79 versus 67 percent). This was likely because the control group made corrections without knowledge of AOA limits. On the other hand, the experimental group had a real time display of AOA limits and could remain within those limits while correcting to the glide path. By "respecting" these limits, the experimental group tended to give greater priority to remaining in a safe flight conditions and were less aggressive in maintaining a precise vertical flight path. It should be noted however, that both groups flew the approaches within ATP standards as previously discussed.
5. Maintaining glide slope detracted from localizer control. This affected the experimental group more than the control group (64 versus 47 percent). This is thought to be a result of AOA cueing, which captured the pilot's attention.

In summary, the workload was not measurably affected by the addition of ICEPro system. Pilots seemed to accommodate to those displays rather quickly during their training, and appeared to use them quite effectively to perform the flight task. TLX data showed clearly that the flight task was very demanding for both groups of pilots, and the physical difficulty of it far outweighed other workload dimensions.

TABLE 9.—PILOT WORKLOAD SURVEY RESULTS

Pilot post-test survey questionnaire results	*z* score: $z < -1.69$ for 95% confidence in H_0 rejection	Probability: $p < 0.05$ required to satisfy α (alternate hypothesis)	Exp. versus Control Positive real difference (PRD), Better (B), Worse (W), Same (S)
Part IV—Workload			
1. It was difficult to control vertical speed when on glide slope.	0.7856	0.7902	W
2. Operating the flight controls to avoid an upset condition when on final approach was a physically demanding effort.	–0.5455	0.2852	B
3. I felt it took a considerable amount of concentration and effort to safely execute the missed approach procedure.	–1.2002	0.1108	B
4. Keeping the aircraft on the glide slope without experiencing a pitch upset was a very demanding task.	–0.8074	0.2034	B
5. On final approach I spent so much time trying to fly the glide slope that I was unable to maintain good localizer course control.	0.5674	0.7221	W

Legend	
	Meets 95% confidence for rejecting H_0
	Experimental group better over control group but < 95% confidence for rejecting H_0
	No difference between experimental and control group
	Control group performance better than experimental group

11.0 Atmospheric Turbulence Test Methodology

The pilot-in-the-loop simulations could not duplicate all of the real-world conditions that could have first-order effects on system performance, such as those due to real atmospheric turbulence. Therefore, in order to assess system performance under these conditions and minimize the technical risk of an eventual flight-test validation program, the effects of atmospheric turbulence on ICEPro were studied. This led to a one year extension awarded under NASA's Vehicle Systems Safety Technologies (VSST) project. This section summarizes the study which is fully reported in the Year 5 progress report that can be found in Appendix D.

11.1 Experiment Design

Four tasks and their measures of success (MOS) were defined in the ICEPro atmospheric turbulence test plan (Appendix E). These tasks involved studying the source of the scatter in RT-PID estimates in turbulence, understanding the effect of sensor noise and turbulence on RT-PID and D-ICES, determining the performance characteristics of a turbulence probe, and studying the effect of turbulence in different phases of flight. In order to test each task as described below, a test matrix was developed. The test matrix included representative flight phases in terms of airspeeds, attitude, and configuration. Utilizing D-Six scripting capabilities, a series of scripts were developed to explore the test matrix through batch testing.

11.2 Task Descriptions

This summary will describe the questions asked in each of the four tasks. For more detail, please see Appendix D.

11.2.1 Task 1: Simulating Real World RT-PID Performance in Turbulence

Determine whether the scatter in the turbulence estimates arise from, 1) colored noise in the regressor(s), and if so what is the source of the colored noise and in which regressor(s), 2) insufficient model structure, and if so how should the model structure be adjusted or, 3) some other means. In the system identification process, regressor(s) are defined as the independent variables.

11.2.2 Task 2: Effect of Sensor Noise and Turbulence

Modify, test, and validate the use of RT-PID and D-ICES algorithms with atmospheric turbulence as an input for various levels of atmospheric turbulence, and to identify an acceptable error in the wind measurement during turbulence for RT-PID and D-ICES algorithms. Additionally, verify MOS during straight and level flight for varying atmospheric turbulence levels and icing conditions.

11.2.3 Task 3: Effect of Turbulence for Different Flight Phases at Selected Noise Level

Modify, test, and validate the use of RT-PID and D-ICES algorithms with atmospheric turbulence as an input. Select an acceptable atmospheric turbulence measurement error based on findings from Task 2 and commercially available atmospheric turbulence sensors. Verify MOS during each phase of flight for varying atmospheric turbulence levels and icing conditions.

11.2.4 Task 4: Evaluate the Effectiveness of Manual Pilot Inputs Alone for Making High Confidence Vehicle State Estimates When Performing Typical Maneuvering Flight Tasks Under Varying Levels of Atmospheric Turbulence

Determine the portion or portions of the maneuvers, which provide frequency content at the natural frequency of the short period, dutch-roll, and roll modes and thereby support the achievement of high confidence parameter estimates from RT-PID. This effort was not performed due to time and funding constraints.

11.3 Measures of Success

To ensure that test objectives are attained, measures of success (MOS) have been formulated. A MOS is defined as a comparative requirement which must be satisfied by the results of testing. The overall measure of success for the primary and secondary objectives will be that the error bounds and accuracy in RT-PID and Theil inequality coefficients in D-ICES algorithms meets or exceeds its non-atmospheric turbulence performance in atmospheric turbulence. This success criterion focuses on the performance of these two algorithms and not on ICEPro's utility to mitigate a potentially hazardous icing encounter or on the pilot's performance during such encounter. It assumes that if the RT-PID and D-ICES algorithms perform equally in and out of atmospheric turbulence, the ICEPro system will perform equally. The following MOS are defined for the primary objective.

RT-PID Algorithm

1. Message accuracy

   Message error will be determined by the error bounds and accuracy of its associated stability and control coefficient. For example, the red (warning level) pitch degrade logic is a function of elevator control power

   $$C_{m_{\delta e}} \geq 0.25 \cdot C_{m_{\delta e\_no \cdot ice}}$$

   The elevator control power must meet or exceed its non-atmospheric turbulence error bound and accuracy in atmospheric turbulence. This is repeated for all ICEPro messages.

2. ISP accuracy

   ISP error will be determined by comparing the true ISP value with the estimated ISP value. ISP is a function of five stability and control coefficients: Longitudinal static stability, elevator control power, dihedral effect, aileron control power, and normal lift coefficient. The true ISP value is known since the five true stability and control parameters are known to the simulation. The ISP error must meet or exceed its non-atmospheric turbulence error bound and accuracy in atmospheric turbulence.

D-ICES Algorithm

1. Control deflection accuracy

   Control deflection error is determined by comparing the estimated deflection Theil inequality coefficient with the baseline no turbulence case. The control deflection error must meet or exceed its non-atmospheric turbulence error in atmospheric turbulence.

11.4 Changes to ICEPro Logic

Several specific features were added to the ICEPro module for the current effort. The new features included adding several input parameters within the D-Six variable list. These parameters permitted overriding ICEPro's logic in the Monitor mode forcing the system into Identification mode. In addition, user specified surface buzzing times were created to override normal ICEPro buzzing logic. Buzzing refers to exercising the controls through a set of orthogonal multi-sine inputs to provide additional control content for RT-PID operation. Finally, the use of these new features was optional allowing ICEPro to operate in an unmodified logic set.

Utilizing D-Six scripting capabilities, a series of scripts were developed to facilitate batch testing. These scripts interfaced an Excel file containing the test matrix, set up the simulation initial conditions, stepped through the simulation using control inputs provided by virtual pilot logic contained in the

scripts, recorded selected time history variables, stopped the simulation, and exported the recorded data to MATLAB. The script virtual pilot logic used the differences between the desired flight path angle, heading, and airspeed and the current actual values as inputs to the elevator, aileron, and throttles as control inputs. Sideslip feedback to the rudder was also used to coordinate turns. Equations (11) show the basic control laws used by the virtual pilot. The gains were set to low values that worked satisfactorily for the no turbulence cases, but were less than optimal with turbulence. These values were used for all cases to minimize excessive control movements during turbulent conditions. For some cases, the throttle commands were set to zero to eliminate excessive throttle movements encountered with turbulent conditions.

$$\delta e_{\text{command}} = K_{\gamma}\left(\gamma_{\text{desired}} - \gamma\right) + K_{\dot{\gamma}}\dot{\gamma} + \int\left(\gamma_{\text{desired}} - \gamma\right)dt \tag{11a}$$

$$\delta a_{\text{command}} = K_{\psi}\left(\psi_{\text{desired}} - \psi\right) + K_{\phi}\varphi \tag{11b}$$

$$\delta r_{\text{command}} = K_{\beta}\beta \tag{11c}$$

$$\delta_{\text{Throttle}} = K_{V}\left(V_{\text{desired}} - V\right) + K_{\dot{V}}\dot{V} \tag{11d}$$

11.5 Atmospheric Turbulence Probe

In support of Task 3, a search was conducted to identify candidate COTS turbulence probes. Several probes were identified using state of the art LIDAR technology. Unfortunately, the accuracy of such technology requires an order of magnitude improvement for the present work. The Atmospheric Integrated Meteorological Measurement System AIMMS-20 probe by Aventech Research was chosen because 1) It provides the most accurate wind determination out of the candidate probes and 2) it is already part of GRC's inventory. Table D.1 in Appendix D summarizes the AIMMS-20 performance based on an error analysis.

12.0 Atmospheric Turbulence Results and Discussion

A detailed discussion of Tasks 1 to 3 results can be found in the Year 5 progress report (Appendix D). The following results and discussion provide a short summary.

12.1 Task 1 Simulating Real World RT-PID Performance in Turbulence

Several practical issues related to real-time parameter estimation for a linear longitudinal dynamics model in atmospheric turbulence using indirect turbulence measurements were examined and discussed. The frequency response of the airflow vanes, wing response to atmospheric turbulence, and the structural response of the air data boom were identified as sources of colored noise. The frequency response of the airflow vanes for a wide variety of combinations of natural frequency and damping ratio did not adversely impact parameter estimation results in turbulence, except for C_{Z_q} and $C_{Z\delta e}$. This was attributed to noisy explanatory variables in the atmospheric turbulence implementation and relatively low aerodynamic contributions as compared to C_{Z_α}. Airflow vane dynamics do not substantially contribute to the scatter in the estimates, because all of the added dynamics are outside the range of frequencies analyzed. The structural modes of the boom lead to similar conclusions, because the natural frequencies of the boom structural modes are outside the range of frequencies used for dynamic modeling.

A major source of colored noise was identified as the frequency-dependent upwash and time delay induced by the wing-bound vortex system and the longitudinal separation between the AOA measurement and the wing. It was also surmised that the frequency-dependent sidewash was a major source of colored

noise. The frequency-dependent upwash and time delay appear to be significant contributors to biasing and increased scatter and uncertainty for parameter estimates in atmospheric turbulence.

Practical issues were examined using data from a Twin Otter DHC-6 longitudinal linear simulation, with realistic noise sequences added to the computed aircraft responses. This allowed a clear view of the effect of each source of colored noise to the modeling problem, because the true values of the model parameters were known. This approach was used initially to show that real-time parameter estimation can be done accurately in all atmospheric turbulence conditions if the AOA and angle of sideslip measurements are accurate. Flight test data from the GRC DHC-6 Twin Otter aircraft was used to validate the effect of the identified colored noise sources.

Based on these findings, several practical recommendations for flight testing in atmospheric turbulence are suggested, as well as areas for future study. First, mount the air data boom at the nose of the aircraft to minimize the effect of the wing-bound and wing-tip vortices. Second, if the air data boom is mounted on the nose of the aircraft, an upwash and time delay calibration as a function of frequency is required. Third, airflow angle measurements must be corrected for frequency dependent upwash, sidewash, and time delay corrections.

The following Task 2 and Task 3 results were carried out assuming that these precautions had been taken care of. This assumed that the frequency response was adequate (Good assumption based on the results of this section for a well calibrated, stiff, nose mounted sensor). This left the sensor's static performance to be evaluated in Task 2 and Task 3. In other words, if these precautions are taken, the RT-PID estimates will behave similarly inside and outside of atmospheric turbulence.

12.2 Task 2: Effect of Sensor Noise and Turbulence

RT-PID

- In general, the original MOS for message accuracy were not achieved since the errors in the estimates and in the error bounds increase as a function of turbulence intensity. A new MOS criterion was formulated where the error in the estimates and in the error bounds with atmospheric turbulence is tolerated as long as the ICEPro messages and AOA brackets are equivalently displayed inside and outside of turbulence.
- In practice, for flight in zero, light, and moderate atmospheric turbulence the average airflow angles are similar. In severe turbulence, the average airflow angles are significantly different due to wing stall. The differences do not affect message accuracy, but do affect the AOA bracket accuracy. The data from stalled runs was not considered useful because stalled flight does not produce reliable data. As a result, all severe turbulence test conditions have been omitted from Task 2 analysis.
- With the exception of the roll degrade message in calm atmosphere, there were no false positives or false negatives. The roll degrade message was caused by low pilot activity resulting in poor RT-PID estimates. In each of the turbulence cases, the additional aileron inputs provided by the virtual pilot improved the RT-PID estimates so that no false positives (roll degrade message) were annunciated.
- In general the new MOS message criterion was considered to be successful.

D-ICES

- It was found that the application of turbulence and sensor noise on D-ICES had minimal impact on performance without filtering.
    - Only one condition was found that yielded a false positive that would have caused the system to enter ID Mode when no icing was present.
    - There was one condition where the elevator deflection Theil inequality Coefficient for an iced airplane failed to exceed the threshold and two where the value originally exceeded the threshold, but with time decreased until it was below the threshold.

- However, when the state vectors were low pass filtered to remove higher frequency disturbances due to turbulence and noise, D-ICES accurately detected all icing conditions in the presence of turbulence and sensor noise. Filtering did not have any adverse ramifications on logic, thresholds, or other system parameters or functions.
- Three potential false positive cases were found that showed the elevator Theil Coefficient built up over time to exceed the threshold when no ice was present. An examination of the data in this region led to supposition that the D-ICES inversion process had trouble determining the correct elevator deflection with pitch due to elevator characteristics at those flight conditions. This condition is specific to the Twin Otter flight model.

Using the results of Task 2, it was determined that the objective to identify an acceptable error in the wind measurement was not required and that the performance of an air data probe such as the AIMMS-20 probe was satisfactory.

12.3 Task 3 Effect of Turbulence for Different Flight Phases at Selected Noise Level

For the purpose of this task the four phases of flight are defined as:

Phase 1. Flaps up straight and level flight at 110 KIAS and 2500 ft – 30 sec duration
Phase 2. Flaps up straight and level flight at 110 KIAS and 2500 ft followed by a constant altitude flap transition (0° to 20°) and deceleration to 80 KIAS – 1 min duration
Phase 3. Heading capture at 80 KIAS, 2500 ft, and flaps 20° from 090° to 360° – 30 sec duration
Phase 4. Descent from 3000 ft at 75 KIAS and flaps 20° followed by a flap transition (30°) and deceleration to 70 KIAS with localizer and glide slope tracking – 2 min duration

RT-PID

- Phase 1 runs had no pitch degrade, climb limit, or flap limit messages for zero, light and moderate turbulence levels. The MOS criterion for AOA bracket was applied to Phase 1 and considered to be successful.
- Phase 2 runs had no pitch degrade, yaw degrade, climb limit, or flap limit messages for zero, light, and moderate turbulence levels. The MOS criterion for AOA bracket was applied to Phase 2 and considered to be successful.
- Phase 3 runs had no pitch degrade, climb limit, or flap limit messages for zero, light and moderate turbulence levels. The MOS criterion for AOA bracket was applied to Phase 3 and considered to be successful.
- Phase 4 runs had no pitch degrade or yaw degrade messages for zero, light or moderate turbulence levels.
- The MOS criterion for AOA bracket was applied to Phase 4: Applying the MOS criterion would be unsuccessful in this phase since a pilot is able to discern the unconservative variation in the AOA brackets. It is recommended that additional piloted runs be conducted to verify this conclusion by the virtual pilot.

D-ICES

- Phase 1 runs were a repeat of the Task 2 conditions and the results were similar.
- Phase 2 runs experienced no false positives during this scenario.
- In Phase 3 runs, a false negative was seen for the iced airplane with no turbulence, but correctly predicted positives for the low and moderate turbulence levels. The false positive was believed to be due to a singular condition where there was little difference between the iced and clean

airplane's control effectiveness at the chosen flight condition. This condition is specific to the Twin Otter flight model.

- In Phase 4 runs, there were no false indications, even though the results remained close to a singular condition seen in the level turning flight case. However, the Theil inequality coefficient values are still sufficient to exceed the threshold for transitioning to ID mode for all of the iced conditions.
- In most cases, D-ICES performed as designed in the presence of turbulence and noise. However, the exceptions noted above, especially the false negatives, do indicate that some further development of the system is warranted. One possible area to examine would be utilizing other terms related to the Theil inequality coefficient, namely the bias, variance and covariance terms in some way to develop a more robust detection scheme.
- In general, it was found that the performance of the AIMMS-20 probe and the new MOS criterion were satisfactory for Task 3.

13.0 Conclusions and Recommendations

13.1 ICEPro System Design and Implementation

In keeping with the NASA goal to improve the safety of commercial and general aviation aircraft, an envelope protection system was developed using no direct ice detection devices. Through the use of measured data, a priori information, and real-time stability and control estimates, this system computes an icing severity parameter. This parameter is used to trigger appropriate pilot cueing to warn the pilot of hazardous conditions and provide guidance for action to mitigate the situation. The main advantage of the system is that it uses data that are readily available in modern avionics systems and once adjusted to specific aircraft makes and models, and mated to modern display systems, should provide sufficient pilot cueing for envelope protection against icing related incidents.

13.2 Pilot in the Loop Test and Evaluation of ICEPro

The utility of the Icing Contamination Envelope Protection (ICEPro) system for mitigating a potentially hazardous icing condition was evaluated by 29 pilots using the ICEFTD. The pilots participating in this test were divided into two groups; a control group using baseline displays without ICEPro, and an experimental group using ICEPro driven display cueing. Each group flew identical precision approach and missed approach procedures with a simulated ice protection failure icing configuration. Pilot performance, workload, and survey questionnaires were collected for both groups of pilots. Results showed that real time assessment cues were effective in reducing the number of potentially hazardous upset events and in lessening exposure to loss of control following an incipient upset condition. Pilot workload with the added ICEPro displays was not measurably affected, but pilot opinion surveys showed that real time cueing greatly improved their situation awareness of a hazardous aircraft state. The conclusions from this test indicate that the experimental group of pilots, who flew with ICEPro displays, demonstrated significantly better control performance in dealing with aircraft handling problems under icing conditions and had better awareness of a hazardous aircraft state. Pilot workload was not affected by the additional display information provided by ICEPro, but pilot opinions of the implementation of that system indicate that improvements could be made.

13.3 Atmospheric Turbulence and Sensor Noise

The conclusions from this task confirm the hypothesis that the scatter in the estimates observed during flight in turbulence is due to airflow angle colored noise. Several important sources of colored noise were identified and tested. A major source of colored noise was identified as the frequency-dependent upwash and time delay induced by the wing-bound vortex system and the longitudinal

separation between the AOA measurement and the wing. It was also surmised that the frequency-dependent sidewash was a major source of colored noise. The frequency-dependent upwash and time delay appear to be significant contributors to biasing and increased scatter and uncertainty for parameter estimates in atmospheric turbulence.

These findings also disproved the hypothesis that additional model structure was needed. Additionally, several precautions should be taken for improved estimates in atmospheric turbulence. 1) Mount the flow angle sensors as far forward of the wing as practical, preferably on the nose of the aircraft. This will minimize airframe flex and the amplitude of the upwash correction. 2) Calibrate the change in upwash and sidewash correction versus frequency. 3) Eliminate the use of booms for flow angle sensors. This will minimize boom flex. In general, it was found that the performance of the AIMMS-20 probe was satisfactory for Task 2 and Task 3. Acceptable noise error was therefore defined by current specification of AIMMS-20 probe. As long as booms are not used and the calibration for wing response to turbulence has been taken care of, ICEPro performed similarly inside and outside of atmospheric turbulence.

Subsequent analysis of the RT-PID and D-ICES algorithms in Task 2 and Task 3 demonstrated good performance with few exceptions. Additional recommendations have been made to look at the exceptions.

14.0 Recommendations

1. Flight displays in this test were not optimized from a human factors standpoint, nor were the envelope protection cues coupled with a flight director. Based upon the opinions extracted from the pilot survey, pilot control performance and state awareness may be improved by addressing those issues in future pilot in the loop testing.
2. Execute Task 4 in the one year VSST extension. This task evaluates the effectiveness of manual pilot inputs alone for making high confidence vehicle state estimates when performing typical maneuvering flight tasks under varying levels of atmospheric turbulence.
3. Flight test to validate RT-PID findings based on colored AOA regressor findings.
4. Flight test to validate ICEPro.

References

1. Green, Stephen D., “A Study of U.S. Inflight Icing Accidents and Incidents, 1978 to 2002,” 44th AIAA Aerospace Sciences Meeting and Exhibit, 9-12 January 2006, Reno, NV, AIAA 2006-82.
2. Nagel, David C., “Human Error in Aviation Operations,” Human Factors in Aviation, Chapter 9, eds. Weiner, E.L, Nagel, D.C., Academic Press, 1988.
3. National Transportation Safety Board, Safety Recommendation to Mitigate the Existing Risk to the Cessna 208 Fleet during the Current Icing Season. A-06-01 through -03, January 17, 2006.
4. National Transportation Safety Board, Safety Recommendation to Mitigate the Existing Risk to the Saab 340 Fleet When Operating in Icing Conditions. A-06-48/51, July 10, 2006.
5. Russell, P., Pardee, J., “Joint Safety Analysis Team- CAST Approved Final Report Loss of Control JSAT Results and Analysis,” December 2000.
6. Ratvasky, T.P., Van Zante, J.F., Sim, A., “NASA/FAA Tailplane Icing Program: Flight Test Report,” NASA/TP—2000-209908, DOT/FAA/AR-99/85, March 2000.
7. Bragg, M.B., Basar, T., Perkins, W.R., Selig, M.S., Voulgaris, P.G., Melody, J.W., Sarter, N.B., “Smart Icing Systems for Aircraft Icing Safety,” AIAA 2002-0813, January 2002.
8. Gingras, D.R., Barnhart, B., Ranaudo, R., Ratvasky, T., and Morelli, E., “Envelope Protection for In-Flight Ice Contamination,” AIAA-2009-1458, NASA/TM—2010-216072, January 2009.
9. Barnhart, B.P., Dickes, E., Gingras, D.R., and Ratvasky, T.P., “Simulation model Development for Icing Effects Flight Training,” SAE 2002-01-1527, NASA/TM—2003-212115.
10. Ratvasky, T., Blankenship, K., Rieke, W., Brinker, D., “Iced Aircraft Flight Data for Flight Simulator Validation,” SAE-2002-01-1528, April 2002.

11. Hart, S., and Lowell, S., “Development of NASA-TLX: Results of Empirical and Theoretical Research,” Human Mental Workload, eds. Hancock, P., and Meshkati, N., North Holland Press, Amsterdam, 1988, pp. 239-250.
12. Theil, H. (1967). Economics and Information Theory. Amsterdam: North Holland.
13. Morelli, E.A., “Real-Time Parameter Estimation in the Frequency Domain,” Journal of Guidance, Control, and Dynamics, Vol. 23, No. 5, September-October 2000, pp. 812-818.
14. Morelli, E.A., “System IDentification Programs for AirCraft (SIDPAC),” AIAA-2002-4704.
15. Klein, V and Morelli, E.A., Aircraft System Identification Theory and Practice, American Institute for Aeronautics and Astronautics Inc., Reston, VA, 2006.
16. Barnhart, B.P., Dickes, E., Gingras, D.R., and Ratvasky, T.P., “Simulation model Development for Icing Effects Flight Training,” SAE 2002-01-1527.
17. Ranaudo, R., Martos, B., Norton, B., Gingras, D., Barnhart, B., Ratvasky, T., and Morelli, E., “Piloted Simulation to Evaluate the Utility of a Real Time Envelope System for Mitigating In-Flight Icing Hazards,” presented at AIAA Atmospheric and Space Environments Conference, August 2–5, 2010, Toronto, Ontario, Canada, AIAA 2010-7987.
18. Sheskin, D. J., The Handbook of Parametric and Nonparametric Statistical Procedures, CRC Press, Boca Raton, FL, 1997, pp., 181-190.
19. Trochim, William M., “Likert Scaling”. Research Methods Knowledge Base, 2nd Edition. October 20, 2006
20. Federal Aviation Administration, Airline Transport and Aircraft Type Rating Practical Test Standards for Airplane, FAA-S-8081-5F, July 2008, pp 2-20 – 2-27.

Appendix A.—Abbreviations and Symbols List

Abbreviations

AOA	angle of attack
D-ICES	Dynamic Inversion Control Evaluation System
ERAU	Embry-Riddle Aeronautical University
FCD	Flight Control Display
H_0	null hypothesis
ICEFTD	Ice Contamination Effects Flight Training Device
ICEPro	Icing Contamination Envelope Protection system
IPS	Ice Protection System
ISP	Icing Severity Parameter
J	cost function
LSE	least-squared error
PCE	Pilot Coupling Event
RT-PID	Real Time Parameter Identification
PFD	Primary Flight Display
RMS	root-mean square
SLD	Super-cooled Large Droplet

Symbols

A	stability matrix
B	control matrix
C	stability matrix
C_{l_β}	rolling moment due to sideslip angle derivative, $\partial C_l / \partial \beta$
$C_{l_{\delta a}}$	rolling moment due to aileron deflection derivative, $\partial C_l / \partial \delta_a$
$C_{l\delta r}$	rolling moment due to rudder deflection derivative, $\partial C_l / \partial \delta_r$
C_{lp}	rolling moment due to nondimensional roll rate derivative, $\partial C_l / \partial (pb/2V)$
C_{l_r}	rolling moment due to nondimensional yaw rate derivative, $\partial C_l / \partial (rb/2V)$
$C_{m\alpha}$	pitching moment due to AOA derivative, $\partial C_m / \partial \alpha$
$C_{m\delta e}$	pitching moment due to elevator deflection derivative, $\partial C_m / \partial \delta_e$
C_{mq}	pitching moment due to nondimensional pitch rate derivative, $\partial C_m / \partial (q\bar{c}/2V)$
$C_{N\alpha}$	normal force due to AOA derivative, $\partial C_N / \partial \alpha$
$C_{N\delta e}$	normal force due to elevator deflection derivative, $\partial C_N / \partial \delta_e$
C_{Nq}	normal force due to nondimensional pitch rate derivative, $\partial C_N / \partial (q\bar{c}/2V)$
$C_{n\beta}$	yawing moment due to sideslip angle derivative, $\partial C_n / \partial \beta$
$C_{n\delta a}$	yawing moment due to aileron deflection derivative, $\partial C_n / \partial \delta_a$
$C_{n\delta r}$	yawing moment due to rudder deflection derivative, $\partial C_n / \partial \delta_r$

C_{np}	yawing moment due to nondimensional roll rate derivative, $\partial C_n / \partial (pb/2V)$
C_{nr}	yawing moment due to nondimensional yaw rate derivative, $\partial C_n / \partial (rb/2V)$
$C_{Y\beta}$	side force due to sideslip angle derivative, $\partial C_Y / \partial \beta$
$C_{Y\delta a}$	side force due to aileron deflection derivative, $\partial C_Y / \partial \delta_a$
$C_{Y\delta r}$	side force due to rudder deflection derivative, $\partial C_Y / \partial \delta r$
C_{Yp}	side force due to nondimensional roll rate derivative, $\partial C_Y / \partial (pb/2V)$
C_{Yr}	side force due to nondimensional yaw rate derivative, $\partial C_Y / \partial (rb/2V)$
U	Theil inequality coefficient
a_k	k^{th} row of matrix A
b_k	k^{th} row of matrix B
b	reference span
$\bar{c}$	mean aerodynamic chord
t	time
u	control vector
$\hat{u}$	control vector predicted from inversion routine
$\tilde{u}_k$	control
V	true velocity, ft/s
x	state vector
$x0$	state vector initial condition
$\tilde{x}_k$	state
$y,\ \hat{y}$	measured and predicted output
α	alternate hypothesis
ω	frequency, rad/s
θ	parameter vector
$\hat{\theta}$	estimated Parameter
$\hat{\sigma}$	confidence bound

Appendix B.—Post-Test Survey Questionnaire

Part I. Demographics

Name: _____ Male☐ Female ☐

Pilot Number: _____

Total Flight Hours: _____

Multi – Engine Hours: _____

FAA Ratings: Commercial ☐ Multi☐ CFI ☐ CFII ☐

Aircraft Flown and Hours in Type:

_____

_____

Icing related training and experience:

1. In my all my prior flying experience, I encountered in-flight icing

Never Rarely Sometimes Very often Always

2. I felt that my prior icing related knowledge and experience would have adequately prepared me to perform this test scenario without the familiarization training I received on aircraft handling characteristics.

Strongly Disagree Strongly Agree Disagree Undecided Agree

3. The NASA videos and web based training materials provided me with information about icing that I had never known about before.

Strongly Disagree Disagree Undecided Agree Strongly Agree

4. Before this test, my icing related flight training was mostly focused on how to operate the ice protection system.

Strongly Disagree Disagree Undecided Agree Strongly Agree

Part II. Situation Awareness

1. My flight displays were adequate for me to determine when airframe icing was having an effect on aircraft characteristics.

Never Rarely Sometimes Very often Always

2. I felt as though I knew the minimum safe speed I could fly for a given wing flap setting within 5 kt.

Never Rarely Sometimes Very often Always

3. I knew how to adjust my pitch attitude to avoid a wing stall or a tail stall upset.

Never Rarely Sometimes Very Often Always

4. I wasn't always sure which wing flap settings would allow a safe rate of climb in the event of an engine failure.

Strongly Disagree Disagree Undecided Agree Strongly Agree

5. I relied solely on aircraft control response to determine how icing affected pitch, yaw, or roll characteristics.

Strongly Disagree Disagree Undecided Agree Strongly Agree

6. I was confident that the final approach airspeed I chose to fly after I departed the final approach fix would prevent me from stalling.

Strongly Disagree Disagree Undecided Agree Strongly Agree

7. While I was putting the flaps down during the approach and landing, I felt I could effectively manage my control inputs and airspeed to avoid aircraft handling problems or tail stall upsets.

Strongly Disagree Disagree Undecided Agree Strongly Agree

8. The various colored bands on the airspeed tape were useful for me to safely fly the aircraft during the entire flight.

Never Infrequently Sometimes Frequently Always

9. I relied upon the stick shaker to prevent me from inadvertently stalling.

Never Rarely Sometimes Very Often Always

10. I could always tell when I was approaching a wing or tail stall condition.

Strongly Disagree Disagree Undecided Agree Strongly Agree

Part III. Implementation of Envelope Protection Cueing (Experimental ICEPro Group Only)

1. I felt that it was important to combine the visual cues from ICEPro with aural alerts, and tactile feedback from the stick shaker.

Strongly Disagree Disagree Undecided Agree Strongly Agree

2. The ROL DGRD, PTCH DGRD, or YAW DGRD messages on the PFD did not provide useful information, and only cluttered the display.

Strongly Disagree Disagree Undecided Agree Strongly Agree

3. When flying at slow speeds, I could easily use the AOA bars as a good pitch control reference for safely flying the airplane.

Strongly Disagree Disagree Undecided Agree Strongly Agree

4. I had difficulty understanding the relationship between the AOA bars and the high and low speed carets on the airspeed tape.

Strongly Disagree Disagree Undecided Agree Strongly Agree

5. The color coded flight control surfaces on the flight control synoptic were more useful than the messages for assessing degraded control state.

Strongly Disagree Disagree Undecided Agree Strongly Agree

6. I favored using the airspeed carets rather than the AOA bars to remain within a safe operating condition.

Never Infrequently Sometimes Frequently Always

7. When I unintentionally got into an upset condition, the disappearance of all ICEPro messages except the AOA bars on the PFD did not affect my ability to recover the airplane. (Answer only if a wing stall or tail stall upset occurred).

Strongly Disagree Disagree Undecided Agree Strongly Agree

8. When I extended the wing flaps and the red CLIMB LIM and FLAP LIM messages came on together, I immediately knew if an engine failed I would have to reduce my flap setting in order to climb.

Strongly Disagree Disagree Undecided Agree Strongly Agree

9. The occasional “buzzing” of the flight controls by ICEPro made flying the aircraft very difficult.

Strongly Disagree Disagree Undecided Agree Strongly Agree

10. I tended to confuse baseline airspeed limits with the airspeed limits (carets) that were posted by ICEPro.

Strongly Disagree Disagree Undecided Agree Strongly Agree

11. I tended to fly so as to keep my pitch attitude in the middle of the AOA bars when they were presented by ICEPro

Never Infrequently Sometimes Frequently Always

12. When the AOA bars started flashing, they immediately captured my attention.

Never Infrequently Sometimes Frequently Always

13. I felt that the airspeed carets from ICEPro were useful for helping me determine safe flight speeds when maneuvering during approach and landing.

Never Infrequently Sometimes Frequently Always

14. The low AOA cue on the PFD enabled me to avoid a tail stall upset.

Never Infrequently Sometimes Frequently Always

15. I immediately noticed when the CLIMB LIM and FLAP LIM messages were on at the same time.

Strongly Disagree Disagree Undecided Agree Strongly Agree

Part IV. Workload

1. I found it difficult to control vertical speed when on glide slope.

Never Infrequently Sometimes Frequently Always

2. Operating the flight controls to avoid an upset condition when on final approach was a physically demanding effort.

Never Infrequently Sometimes Frequently Always

3. I felt it took a considerable amount of concentration and effort to safely execute the missed approach procedure.

Strongly Disagree Disagree Undecided Agree Strongly Agree

4. Keeping the aircraft on the glide slope without experiencing a pitch upset was a very demanding task.

Strongly Disagree Disagree Undecided Agree Strongly Agree

5. On final approach I spent so much time trying to fly the glide slope that I was unable to maintain good localizer course control.

Never Infrequently Sometimes Frequently Always

Appendix C.—Results of Survey Questions from Parts I, II, and IV

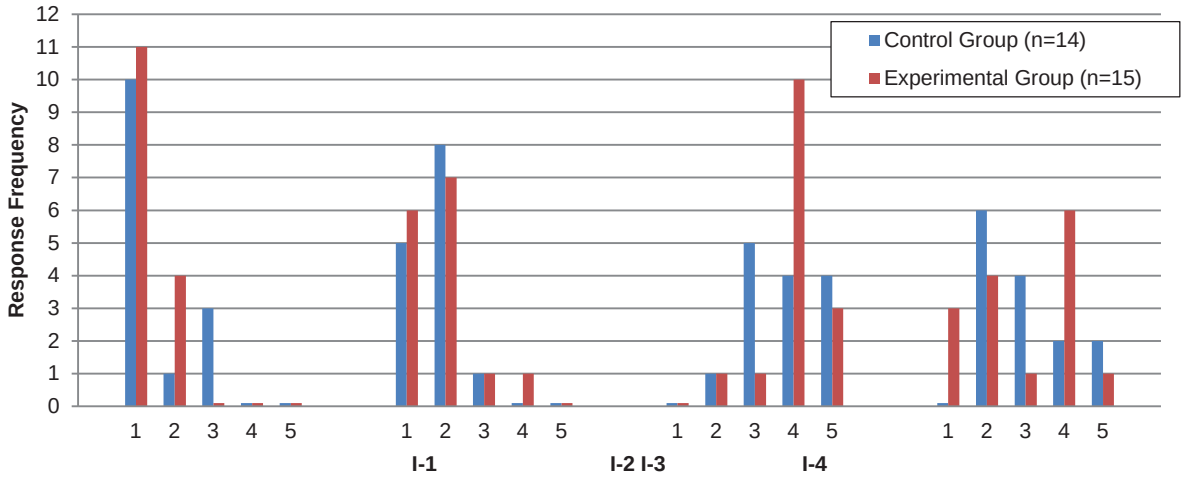

Figure C.1.—Pilot demographics—Part I Survey questions 1 to 4

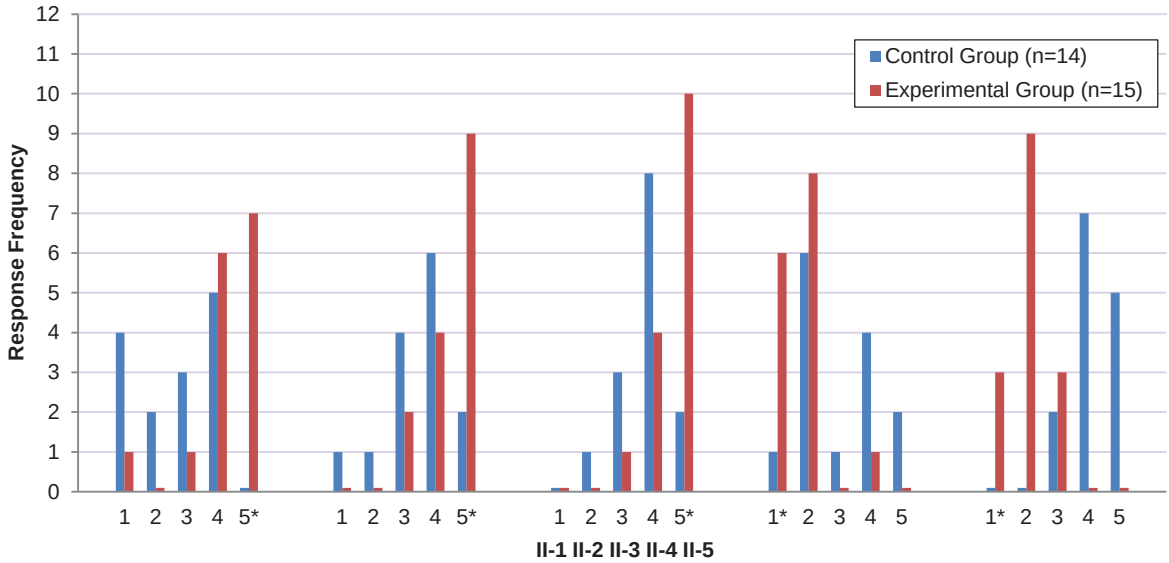

Figure C.2.—Situational Awareness—Part II Survey questions 1 to 5

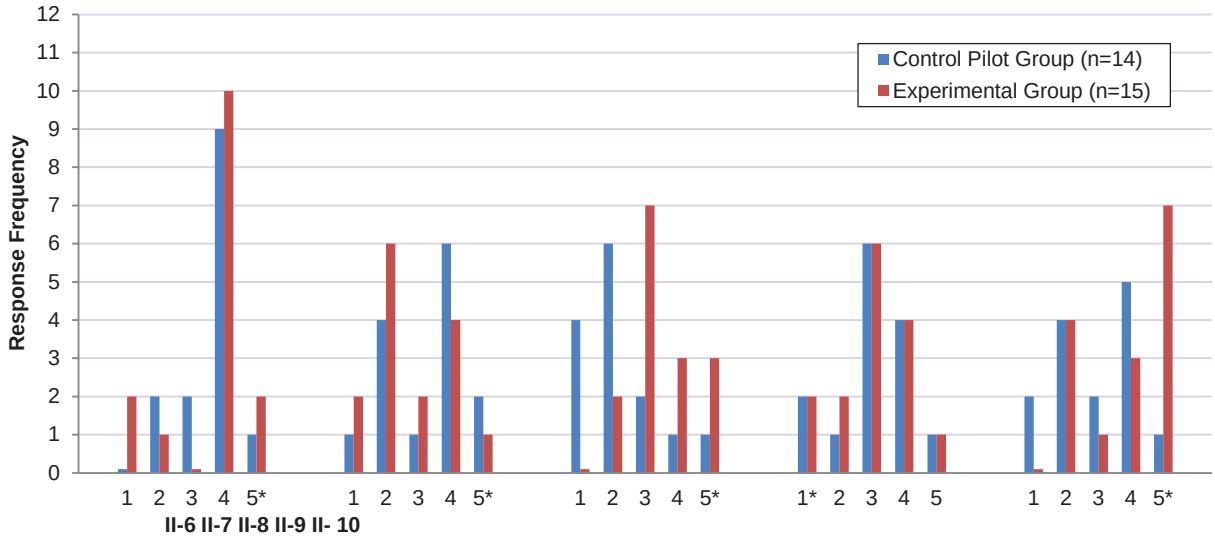

* Direction of responses that indicated better situational awareness

Figure C.3.—Situational Awareness—Part II Survey questions 6 to 10

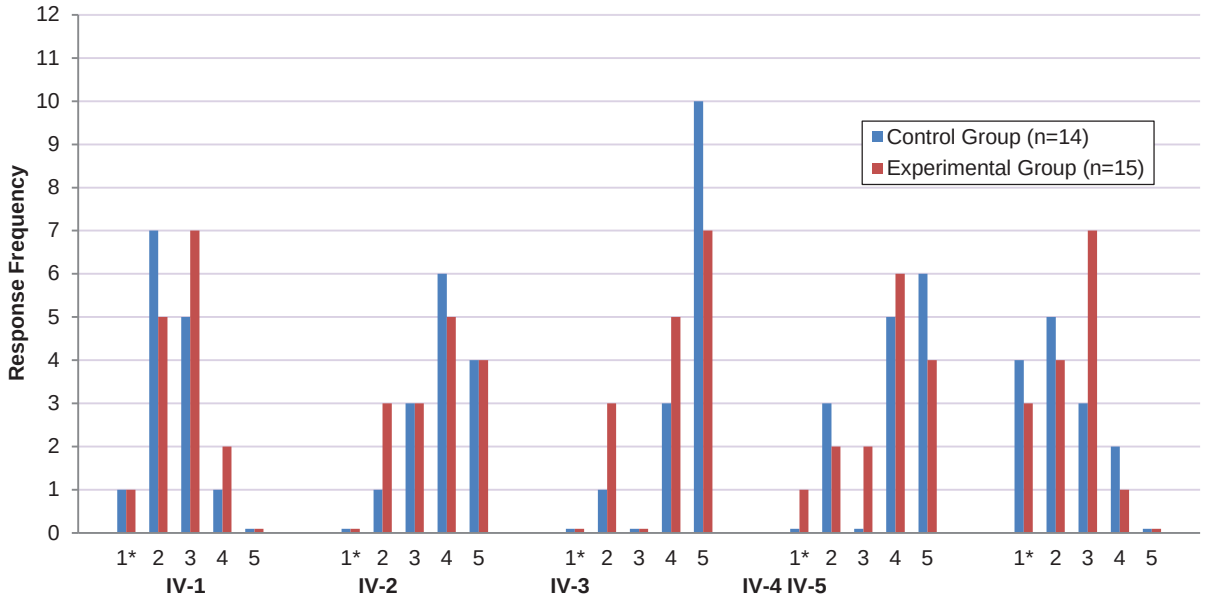

* Direction of responses that indicated lower workload

Figure C.4.—Workload—Part IV Survey questions 1 to 5

Appendix D.—One Year Atmospheric Turbulence Extension Final Report—Effect of Turbulence and Sensor Noise On ICEPro

Progress Report: Year 5

Borja Martos, Principal Investigator
University of Tennessee Space Institute (UTSI)
411 B. H. Goethert Pkwy
Tullahoma, TN 37388-9700

and

Ryan Oltman, David Gingras, and Billy Barnhart
Bihrle Applied Research (BAR)
81 Research Drive,
Hampton VA 23666

Cooperative Agreement: NNX07AD58A

List of Symbols and Abbreviations

Abbreviations

AIAA	American Institute of Aeronautics and Astronautics
AIMMS-20	Atmospheric Integrated Meteorological Measurement System-20
AOA	angle of attack
ATP	Airline Transport Pilot
BAR	Bihrle Applied Research
COTS	commercial off the shelf
D-ICES	Dynamic Inversion Control Evaluation System
D-Six	Bihrle Applied Research's Simulation Environment Software
I0	no ice condition
I2	20 min ice accumulation condition
ICEFTD	Ice Contamination Effects Flight Training Device
ICEPro	Icing Contamination Envelope Protection System
ID	identification
ISP	icing severity parameter
IVHM	Integrated Vehicle Health Monitoring
KIAS	knots indicated airspeed
LIDAR	light detection and ranging
MIL	military handbook
MOS	measure of success
NASA	National Aeronautics and Space Administration
GRC	NASA Glenn Research Center
LaRC	NASA Langley Research Center
NASA TLX	NASA Task Load Index
OBES	Onboard Excitation System
PFD	Primary Flight Display
PFLF	power for level flight
RMS	root mean square
ROC	rate of climb
RT-PID	Real Time Parameter Identification
SFTE	Society of Flight Test Engineers
T0	no turbulence condition
T1	light turbulence condition
T2	moderate turbulence condition
T3	severe turbulence condition
TMS	Turbulence Model Structure
TOGA	Take Off - Go Around
UTSI	University of Tennessee Space Institute
VIAS	velocity indicated airspeed
VMC	visual meteorological conditions
VSST	Vehicle Systems Safety Technology

Symbols

A_X	longitudinal acceleration
A_Y	lateral acceleration
A_Z	vertical acceleration

$\bar{c}$	mean aerodynamic chord
$C_{l\beta}$	dihedral effect stability coefficient
$C_{l\delta a}$	aileron effectiveness stability coefficient
$C_{m\alpha G}$	gust longitudinal static stability coefficient
$C_{m\alpha S}$	rigid body longitudinal static stability coefficient
$C_{m\alpha}$	longitudinal static stability coefficient
C_{mO}	pitch stability coefficient
C_{mq}	pitch damping stability coefficient
$C_{m\delta e}$	elevator effectiveness stability coefficient
$C_{N\alpha}$	normal lift coefficient
$C_{N\delta r}$	rudder effectiveness stability coefficient
deU	Theil inequality coefficient
g	gravitational acceleration constant
H_P	pressure altitude
$\vec{V}_g$	aircraft velocity relative to the earth
$\vec{V}_t$	true airspeed
$\vec{V}_w$	true wind velocity vector
V_D	velocity down
V_E	velocity east
W_D	wind velocity, down
W_E	wind velocity, east
W_N	wind velocity, north
V_N	velocity north
V_S	stalling airspeed
V_T	true airspeed
p	roll rate
q	dynamic pressure
q	pitch rate
r	yaw rate
u	longitudinal velocity
v	lateral velocity
w	vertical velocity
Δ	change
α	angle of attack
α_m	measured angle of attack
β	angle of sideslip
β_m	flow sideslip angle
δ_F	flap deflection
δ_e	elevator deflection
θ	pitch angle
ϕ	roll angle
ψ	yaw angle

D.1 Abstract

A team comprised of personnel from The University of Tennessee Space Institute, Bihrle Applied Research, Inc., NASA Glenn Research Center (GRC), and NASA Langley Research Center (LaRC), has successfully developed a prototype Icing Contamination Envelope Protection System (ICEPro). The ICEPro system facilitates flight envelope protection by making continuous real time vehicle state assessments, which are synthesized into flyable pilot cueing along with visual and aural alerts during in-flight icing conditions. The simulation could not duplicate all of the real-world conditions that could have first-order effects on system performance, such as those due to real atmospheric turbulence. Therefore, in order to assess system performance under these conditions and minimize the technical risk of an eventual flight-test validation program, the effects of atmospheric turbulence on ICEPro are studied in this extension.

This extension focused on the impact turbulence has on the ICEPro system. Turbulence will degrade the quality of air data sensing. This study explored the accuracy of ICEPro's ice detection and parameter estimation with perfect sensing and degraded sensing to determine an acceptable amount of degradation that would allow the ICEPro system to function correctly. Finally, after an acceptable error in air data collection was defined, it would be possible to determine whether the tolerance was obtainable in a commercially available air data sensor.

D.2 Introduction

D.2.1 Research Background

D.2.1.1 Previous Studies and Results

A team comprised of personnel from The University of Tennessee Space Institute (UTSI), Tullahoma, Tennessee, Bihrle Applied Research Inc (BAR), Hampton, Virginia, NASA Glenn Research Center (GRC), Cleveland, Ohio, and NASA Langley Research Center (LaRC), Hampton, Virginia, has successfully developed a prototype Ice Contamination Envelope Protection System (ICEPro). ICEPro was developed using a DH-6 Twin Otter simulation for development and evaluation. The aerodynamic math models of the Twin Otter were derived from a series of wind tunnel tests for both the clean and iced airplanes. The math models were then validated against NASA flight data for both the clean aircraft and the test aircraft flown with artificial ice shapes. The Twin Otter was chosen because of the availability of the flight test data.

The ICEPro system facilitates flight envelope protection by making continuous real time vehicle state assessments, which are synthesized into flyable pilot cueing along with visual and aural alerts during in-flight icing conditions. Detection of degraded aircraft stability and control and performance due to icing is carried out by a dynamic inversion control evaluation system (D-ICES) that compares expected aircraft response from *a-priori* knowledge base with the current response. When differences reach defined thresholds, real time parameter identification (RT-PID) methods are invoked to estimate current state parameters, which continuously support pilot cueing and alerts. The development effort included simulation-based design, testing, and verification. A pilot in-the-loop study was conducted to gather pilot performance data and opinions of the utility of ICEPro during simulated icing encounters. Results of the study indicated that the system performed as expected and pilot performance benefited from the envelope protection cues.

Figure D.1 presents a flow chart of the ICEPro system. (Some aspects of the system such as mode latching/delatching and logic for displaying messages, logic to force flushing the D-ICES and RT-PID buffers, etc. are not shown for clarity). The system starts in Monitor mode where D-ICES calculates, via an inversion technique using an a priori clean aircraft aerodynamic model, what the elevator deflection should be for the flight condition. This is compared with the actual elevator deflection using a statistical parameter called the Theil inequality coefficient. If this coefficient exceeds its threshold the system transitions to the ID mode. In the ID mode, the Real Time Parameter Identification (RT-PID) module is started and it predicts, based on flight state parameters, the linearized aerodynamic coefficients. These coefficients in conjunction with comparable clean and iced coefficients provided by D-ICES are used to calculate an Icing Severity Parameter (ISP). If the ISP becomes larger than its threshold, the system transitions to the Report mode where pilot cues and messages are displayed indicating the degraded aircraft's condition and providing limits for safe operation of the aircraft.

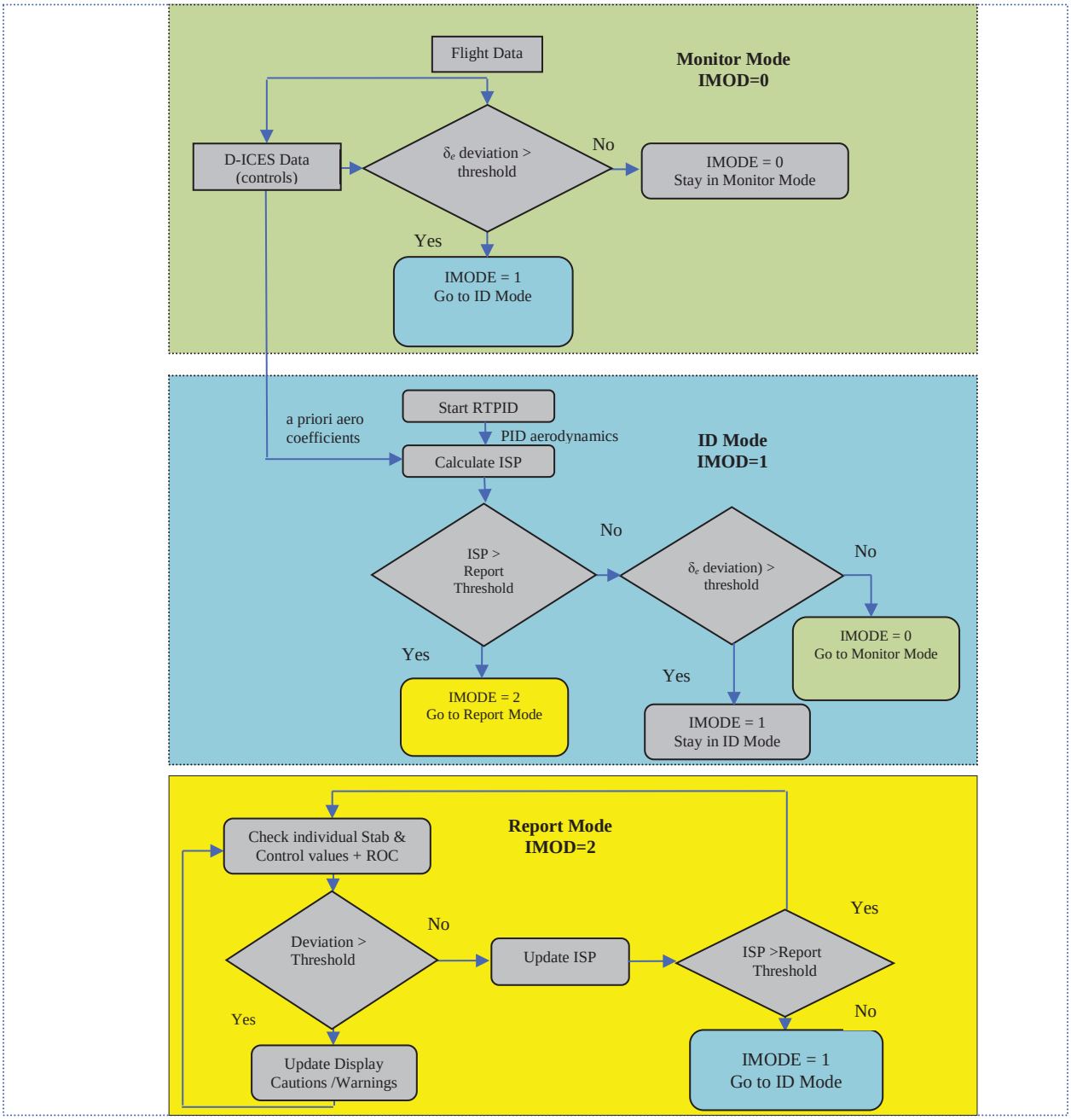

Figure D.1.—ICEPro System Flow Chart

D.2.1.2 Current Year Five Study

The simulation used for the development and evaluation did not duplicate all of the real-world conditions that could have first-order effects on system performance, such as those due to real atmospheric turbulence. Therefore, in order to assess system performance under these conditions and minimize the technical risk of an eventual flight-test validation program, the effects of atmospheric turbulence on ICEPro are studied in this extension.

This extension focused on the impact turbulence has on the ICEPro system. Turbulence will degrade the quality of air data sensing. This study explored the accuracy of ICEPro's ice detection and parameter

estimation with perfect sensing and degraded sensing to determine an acceptable amount of degradation that would allow the ICEPro system to function correctly. Finally, after an acceptable error in air data collection was defined, it would be possible to determine whether the tolerance was obtainable in a commercially available air data sensor.

D.2.2 Research Objectives

Four tasks and their measures of success (MOS) have been defined in the ICEPro atmospheric turbulence test plan (see Appendix E). This summary will describe the questions asked in each of the first three tasks and a brief introduction into the software tools developed to accomplish this work. The effort on Tasks 1 to 3 exhausted the allowed time and remaining funds, therefore no Task 4 results were included.

D.2.2.1 Task 1: Simulating Real World RT-PID Performance in Turbulence

Determine whether the scatter in the turbulence estimates arise from, 1) colored noise in the regressor(s), and if so what is the source of the colored noise and in which regressor(s), 2) insufficient model structure, and if so how should the model structure be adjusted or, 3) some other means. In the system identification process, regressor(s) are defined as the independent variables.

D.2.2.2 Task 2: Effect of Sensor Noise and Turbulence

Modify, test, and validate the use of RT-PID and D-ICES algorithms with atmospheric turbulence as an input for various levels of atmospheric turbulence, and to identify an acceptable error in the wind measurement during turbulence for RT-PID and D-ICES algorithms. Additionally, verify MOS during straight and level flight for varying atmospheric turbulence levels and icing conditions.

D.2.2.3 Task 3: Effect of Turbulence for Different Flight Phases at Selected Noise Level

Modify, test, and validate the use of RT-PID and D-ICES algorithms with atmospheric turbulence as an input. Select an acceptable atmospheric turbulence measurement error based on findings from Task 2 and commercially available atmospheric turbulence sensors. Verify MOS during each phase of flight for varying atmospheric turbulence levels and icing conditions.

D.2.2.4 Changes to ICEPro Logic

Several specific features were added to the ICEPro module for the current effort. The new features included adding several input parameters within the DSix variable list. These parameters permitted overriding ICEPro's logic in the Monitor mode forcing the system into identification mode. In addition, user specified surface buzzing times were created to override normal ICEPro buzzing logic. Buzzing refers to exercising the controls through a set of orthogonal multi-sine inputs to provide additional control content for RT-PID operation. Finally, the use of these new features was optional allowing ICEPro to operate in an unmodified logic set.

Utilizing DSix scripting capabilities, a series of scripts were developed to facilitate batch testing. These scripts interfaced an Excel file containing the test matrix, set up the simulation initial conditions, stepped through the simulation using control inputs provided by virtual pilot logic contained in the scripts, recorded selected time history variables stopped the simulation, and, exported the recorded data to MATLAB. The script virtual pilot logic used the differences between the desired flight path angle, heading, and airspeed and the current actual values as inputs to the elevator, aileron, and throttles as control inputs. Sideslip feedback to the rudder was also used to coordinate turns. Equations (D.1) show the basic control laws used by the virtual pilot. The gains were set to low values that worked satisfactorily for the no turbulence cases, but were less than optimal with turbulence. These values were used for all cases to minimize excessive control movements during turbulent conditions. For some cases, the throttle commands were set to zero to eliminate excessive throttle movements encountered with turbulent conditions.

$$\delta e_{\text{command}} = K_p\left(\gamma_{\text{desired}} - \gamma\right) + K_{\dot{p}}\dot{\gamma} + \int\left(\gamma_{\text{desired}} - \gamma\right)dt \tag{D.1a}$$

$$\delta a_{\text{command}} = K_{\psi}\left(\psi_{\text{desired}} - \psi\right) + K_{\phi}\varphi \tag{D.1b}$$

$$\delta r_{\text{command}} = K_{\beta}\beta \tag{D.1c}$$

$$\delta_{\text{Throttle}} = K_{V}\left(V_{\text{desired}} - V\right) + K_{\dot{V}}\dot{V} \tag{D.1d}$$

D.3 Discussion of Study and Results

There are at least two ways to account for turbulence in system identification algorithms, 1) model the turbulence mathematically and estimate the corresponding parameters and 2) measure the turbulence. In the first approach, the identification of dynamic models containing turbulence is classified as a system with state and measurement noise. In the second approach, favored in this work, turbulence is measured indirectly since air turbulence is imbedded in the true wind velocity vector. This approach is favored because it makes it possible to use commercial off the shelf sensors to measure the atmospheric turbulence and treat it as a measured explanatory variable in the system identification problem. The true wind velocity vector, $\vec{V}_w$, of atmospheric air relative to the surface of the Earth is found from the vector subtraction:

$$\vec{V}_w = \vec{V}_t - \vec{V}_e \tag{D.2}$$

Where $\vec{V}_t$ the true aircraft velocity relative to the air mass and $\vec{V}_e$ is the velocity of the aircraft with respect to the Earth. Since $\vec{V}_w$ is the difference between two large quantities it is essential that $\vec{V}_t$ and $\vec{V}_e$ are measured as accurately as possible in order to minimize errors in $\vec{V}_w$. The details of these calculations can be found in flight test engineering handbooks (Refs. 1 to 3) The most obvious difficulty in measuring air turbulence from an aircraft is the removal of the aircraft's velocity with respect to the Earth. Additional difficulties arise since the aircraft distorts the airflow around itself. This requires precise measurement of $\vec{V}_t$ and $\vec{V}_e$. Any inaccuracies in the measurements or calibrations will affect the derived wind, and consequently the aerodynamic estimates. It is only recently that COTS technology has been developed with sufficient measurement accuracy.

A search was conducted to identify candidate COTS atmospheric turbulence sensors. Several sensors were identified using state of the art LIDAR technology with an airflow angle accuracy of 1.0°. In comparison, flight test air data booms with traditional air data technology are calibrated to an accuracy of 0.1°. The cutoff accuracy for this work was set at 0.1°. Unfortunately, the accuracy of LIDAR based sensors requires an order of magnitude improvement to be useful for the present work. Several additional sensors were identified using traditional air data technology. The AIMMS-20 probe by Aventech Research was chosen because 1) It provides the most accurate wind determination out of the candidate probes and 2) it is already part of GRC's inventory. Table D.1 summarizes the AIMMS-20 performance based on an error analysis.

Turbulence was tested as calm, light, moderate, and severe. Turbulence implementation and levels were defined per MIL-F-8785C and were based on the Dryden Turbulence Spectrum. According to MIL-F-8785C, the probability of exceeding light turbulence levels is between 10^{-1} and 10^{-2}, for moderate turbulence, the probability is approximately 10^{-3}, and for severe turbulence it is approximately 10^{-5}, as shown in Figure D.2 (Ref. 4) derived from MIL-F-8785C. Therefore, severe turbulence levels are not very likely to be encountered. The RMS turbulence wind speed values are also shown in Figure D.2 as a function of altitude. The turbulence velocity components were generated randomly within the guidelines of the Dryden spectrum and added to the aircraft velocity components to generate the total velocity components. A random number was used to generate the velocity components from the turbulence spectrum. By specifying a constant initial random number seed, the sequence of random numbers become reproducible allowing an "apples to apples" comparison of results. This method is referred to as a "fixed"

seed. Likewise, using a varying random number seed results in unique sequences of random numbers from test to test. The three velocity components from the turbulence calculations were added to their appropriate wind frame velocity components (u, v, w) that were generated from the aircraft dynamics so that the velocity components used for the vehicle motion calculations included the components from the turbulence model.

TABLE D.1.—AIMMS-20 PROBE PERFORMANCE

Parameter	1 Sigma Error
Longitudinal acceleration, A_X, (g)	0.003
Lateral acceleration, A_Y, (g)	0.003
Normal acceleration, A_Z, (g)	0.05
Angle of attack, α, (deg)	0.10
Angle of sideslip, β, (deg)	0.10
Pitch rate, q, (dps)	0.01
Roll rate, p, (dps)	0.07
Yaw rate, r, (dps)	0.01
Pitch attitude, θ, (deg)	0.20
Roll attitude, ϕ, (deg)	0.20
Yaw attitude, ψ, (deg)	0.20
GPS velocity down, V_D, (mps)	0.10
GPS velocity north, V_N, (mps)	0.10
GPS velocity east, V_E, (mps)	0.10
True airspeed, V_T, (mps)	0.20
Wind velocity down, W_D, (mps)	0.30
Wind velocity north, W_N, (mps)	0.30
Wind velocity east, W_E, (mps)	0.30

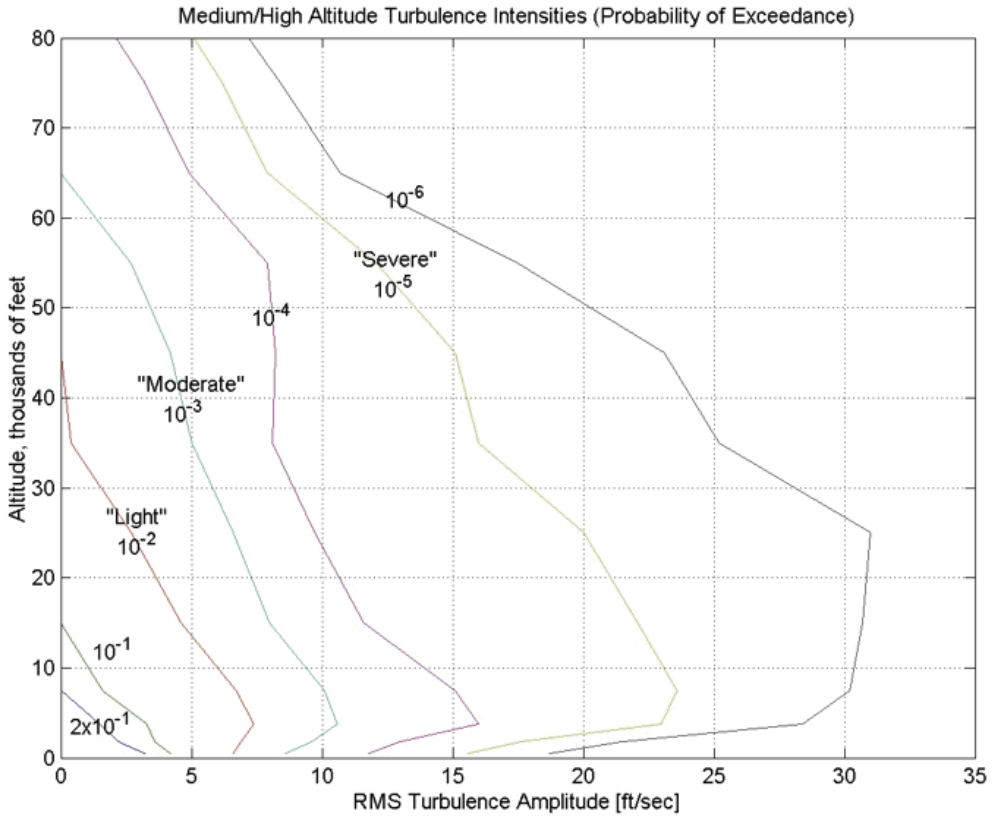

Figure D.2.—Turbulence Definition (derived from MIL-F-8785C).

D.3.1 Task 1

The following results are representative of the effect of turbulence on aircraft system identification. Data were collected using NASA's AIRSTAR T2 model during atmospheric turbulence conditions. NASA's T2 model is a 5.5 percent dynamically-scaled generic transport model. It is outfitted with typical flight test instrumentation and air data booms with flow vanes on each wingtip. In Figure D.3, each color represents a different run, and only the last estimate of each real-time parameter estimation run is shown. A total of nine runs are represented; six in high turbulence and three in low turbulence.

Simulating the correct cause and effect due to atmospheric turbulence on aircraft parameter identification is an ongoing research topic. It is known that colored measurement noise causes scatter and bias (Refs. 5 and 6) in the parameter estimates, which is observed in Figure D.3 during repeated flight test maneuvers in atmospheric turbulence. However, it is unknown whether the scatter in the turbulence estimates arise from 1) colored noise in the regressor, and if so what is the source of the colored noise and in which regressor 2) inadequate model structure, and if so how should the model structure be adjusted or 3) some other means.

D.3.1.1 Hypothesis

Colored AOA regressor noise and/or inadequate model structure is the cause of scatter in aircraft system identifcaiton estimates in atmospheric turbulence.

D.3.1.2 Sources of Scatter in Estimates

Based on the hypothesis a literature search was carried out to examine previous related work. The results are summarized in the following sections.

D.3.1.2.1 Colored Regressor Noise

Based on the literature search, the most likely causes of colored regressor noise are the wing aerodynamic response, the frequency response of long air data booms, and the frequency response of airflow angle vanes in atmospheric turbulence.

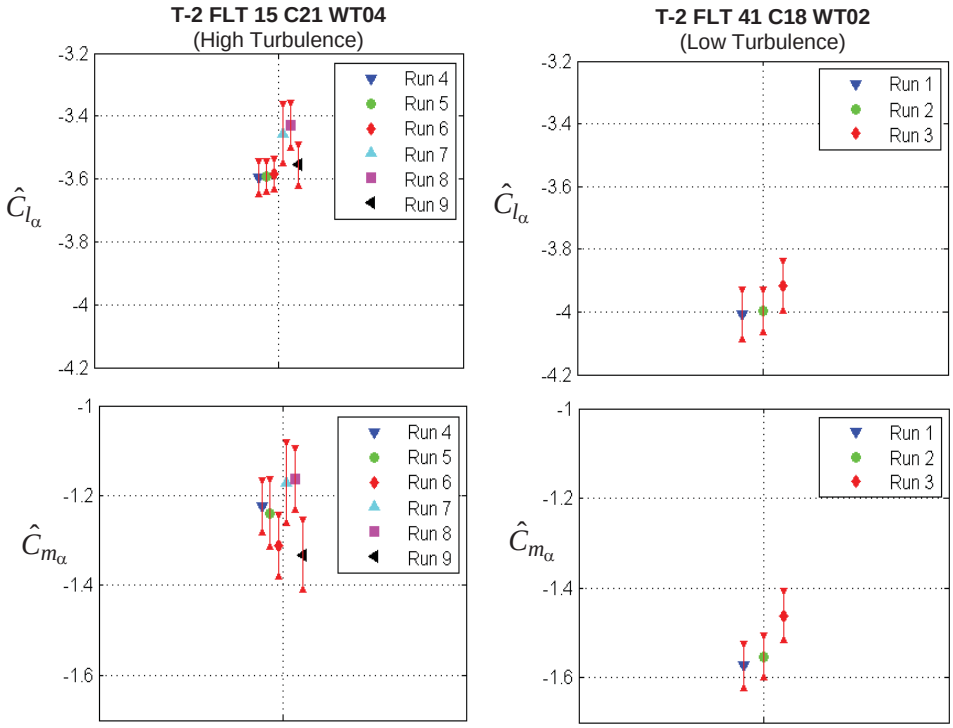

Figure D.3.—Effect of Turbulence on Modeling Results
(Dr. Eugene A. Morelli, personal communication, April 24, 2011)

D.3.1.2.1.1 Flexure of AirData Boom

During low-level flight tests over the terrestial and marine boundary layer, a Long EZ research aircraft was used to measure atmospheric turbulence (Ref. 7). Details of the aircraft and its instrumentation system are found in the cited reference. The boom motion with respect to the center of gravity (accelerometers were mounted at each location) is summarized in the following figure (Ref. 7) during light atmospheric turbulence. The phase trace compares fuselage and probe accelerometer sensors, whereas the magnitude traces represent each individual accelerometer sensor.

Figure D.4 illustrates the complexity of motion for this particular boom-airframe combination. Significant difference is apparent in Figure D.4 between the vertical motion of the probe and the CG. Below 0.6 Hz the coherence between the two accelerations is 1.0 with zero phase shift. Between 0.6 Hz and 2.0 Hz the coherence decreases and the phase changers from zero to –45°. Beyond 6 Hz there is no significant relationship between the two accelerations. In other words, in the frequency range of interest for rigid body aircraft dynamics (0.1 to 2.0 Hz), the drop in coherence and phase indicates that the AOA is different between locations. This in turn results in colored noise in the α regressor. No doubt there would be similarities for other boom-airframe combinations but with different frequency responses.

In order to investigate the in-flight structural response of the air data boom, airflow angle flight data collected in a DHC-6 Twin Otter during multiple parameter etstimation maneuvers was analyzed in the frequecy domain using Fourier coefficients. Figure D.5 shows the frequency response data for the entire frequency range, up to the Nyquist frequency at 25 Hz. The longitudinal and lateral natural frequencies for the dominant structural mode of the air data boom are approximately 8 and 9 Hz. These natural frequencies are associated with the AOA and angle of sideslip measurements respectively. In Figure D.5, the Fourier coeffcients for the AOA near 8 Hz are at the noise floor. Therefore, the structural response of the nose boom on which the AOA sensor is mounted, and from fuselage bending, is not a source of colored noise in the AOA. Similar results were calculated for angle of sideslip but the results are not shown.

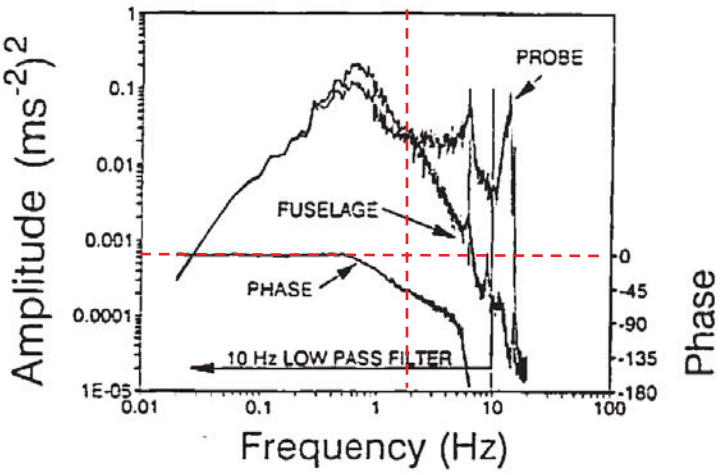

Figure D.4.—Comparison between vertical accelerations of the boom and airplane center of gravity

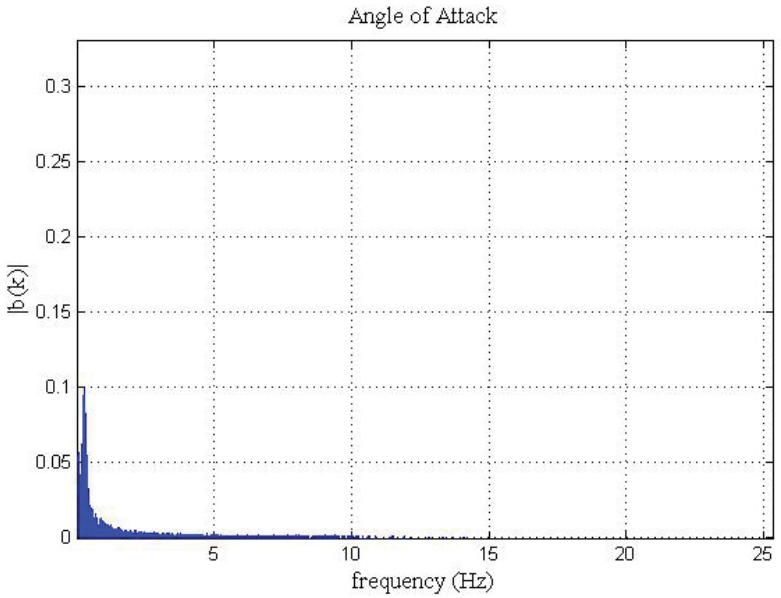

Figure D.5.—Fourier coefficients for measured AOA

D.3.1.2.1.2 Wing Response to Turbulence

During flight tests in the marine boundary layer, a Twin Otter research aircraft was used to study the aerodynamic effects on wind turbulence measurements(Ref. 8). Details of the aircraft and its instrumentation system are found in the cited reference. Although mounted on the wing the airdata boom was not used as the primary source of air data measurements. Instead a flush air data system was mounted on the nose of the Twin Otter. The flush air data system avoids the vibration and frequency response problems of a long boom mounted on the nose of the aircraft (Ref. 9). The wing response to atmospheric turbulence can be summarized in Figure D.6 during a 30 km flight in light atmospheric turbulence. Figure D.6 represents the estimated AOA scale upwash correction versus frequency.

The frequency dependant upwash correction is caused by chordwise and spanwise upwash varations as a result of the wing vortex system response to atmospheric turbulence (Refs. 8 and 9). The frequency scale is the reduced frequency k_b based on the half wing span where ω is the angular frequency, b is the wingspan, and U is the airspeed. The AOA upwash correction $(1 + k_u)^{-1}$ is explained by examining a sensor model:

$$\alpha_M = (1 + k_u)\alpha_T + \alpha_B \tag{D.3}$$

where

α_B = AOA bias

α_M = measured AOA

α_T = true AOA

In Figure D.6, the vertical axis $(1 + k_u)^{-1}$ represents the correction required to calculate the true AOA from measured data.

$$\alpha_T = (1 + k_u)^{-1}(\alpha_M - \alpha_B) \tag{D.4}$$

At low frequencies (representing flight in a calm atmosphere) the scale factor is approximately 0.75 and increases to 0.90 as k_b approaches 2.0. A k_b value of 2.0 (using the DHC-6 Twin Otter wing span and 110 kt cruise airspeed) corresponds to approximately 2.0 Hz. Therefore, over the frequency range of

interest for rigid body aircraft dynamics (0.1 to 2.0 Hz), the scale factor changes from 0.75 to 0.90 due to atmospheric turbulence. It was also surmised that the frequency-dependent sidewash was a major source of colored noise but this was not tested.

Figure D.7 depicts the time delay as a function of frequency. The time delay is caused by the separation between the nose boom mounted airflow vanes (measurement position) and the wing tip (lift and upwash generation), along which turbulence eddies travel.

The magnitude of the time delay represents the correction required to calculate the true AOA from measured data. In the frequency range of interest for rigid body aircraft dynamics (0.1 to 2.0 Hz), the time delay is approximately 0.1 sec.

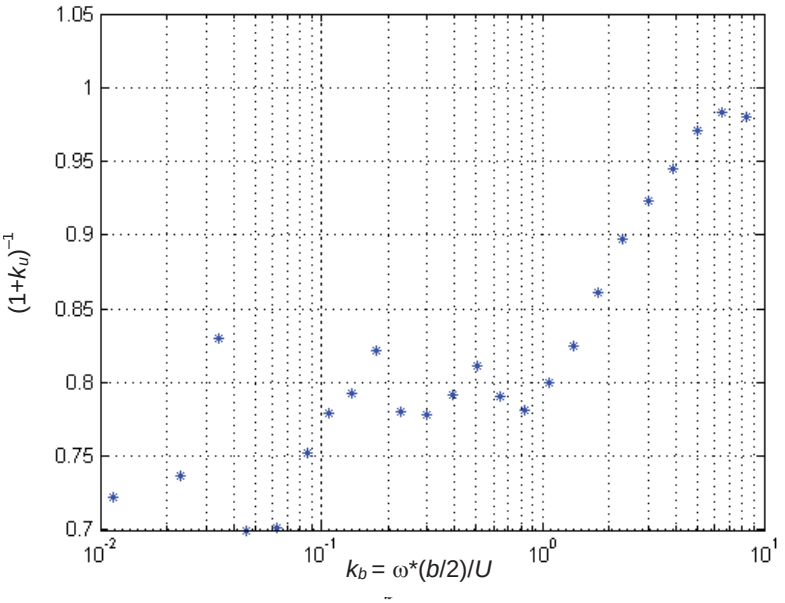

Figure D.6.—Angle of attack upwash versus frequency

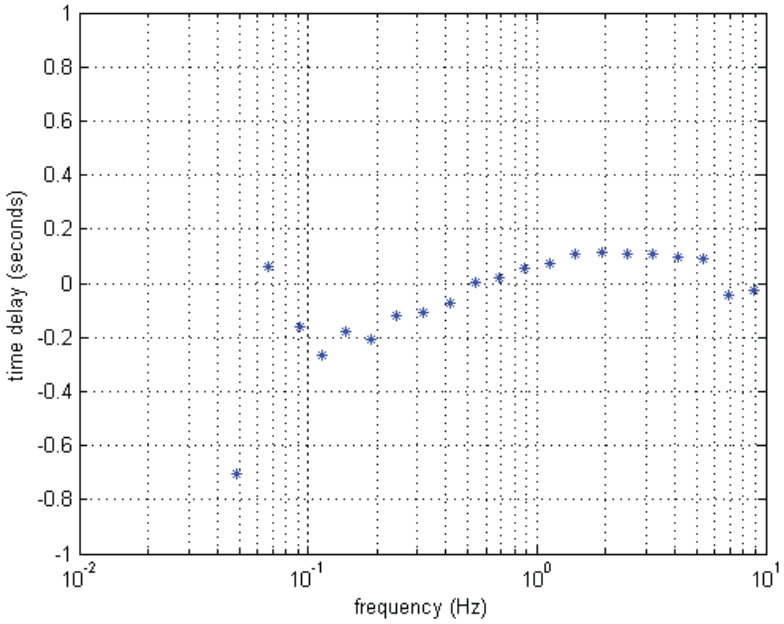

Figure D.7.—Time delay versus frequency

D.3.1.2.1.3 Frequency Response of Airdata Vanes

Although References 10 to 12 were found to determine the frequency response of airdata vanes via natural frequency and damping ratio, no analysis was found confirming that the frequency response of airdata vanes was adequate in atmospheric turbulence.

D.3.1.2.2 Model Structure

It is conceivable that the aerodynamic coefficients are different in atmospheric turbulence that in smooth air although such differences have not been documented in flight (Ref. 13). The new model structure—referred to as the Turbulence Model Structure (TMS)—includes new coefficients $C_{m\alpha_S}$ and $C_{m\alpha_G}$.These parameters represent the nondimensional pitching moment due to α_S (rigid body dynamics) and the nondimensional pitching moment due to α_G (atmospheric turbulence) respectively. Similar coefficients were implemented for the normal force. These coefficients represent different contributions due to the effect of atmospheric turbulence on the aircraft. Stated differently, knowing the effect of atmospheric turbulence on α sensor does not imply that the effect of atmospheric turbulence on the aircraft response can be calculated by simply multiplying α by the usual α coefficients. It is assumed that the effect of turbulence on aircraft response is proportional to the effect of turbulence on the α sensor; therefore, turbulence coefficients are estimated using turbulent α as a regressor to capture its effect. So it's not really a turbulent α coefficient as much as it is an effect of turbulence using the best measure of turbulence. Both aerodynamic model structures are presented in Section D.3.1.3.1.

D.3.1.3 Modeling

For this study, a simplified Twin Otter aircraft simulation was generated outside the DSIX software environment using the MATHWORKS SIMULINK software. The simulation simplified the nonlinear equations of motion (Ref. 14) to 3 degrees of freedom (3-DOF) longitudinal dynamics and a linear aerodynamics model. The simulation rate was 50 Hz and the pertinent output variables were corrupted with gaussian noise with magnitudes that resulted in a signal to noise ratio of 50 for the measured outputs. The use of this simplified simulation was warranted to avoid changes to the high fidelity DSIX database as model structure changes were investigated.

D.3.1.3.1 Model Equations

For reference purposes, a detailed listing of the 3-DOF longitudinal equations of motion (Ref. 14) for a symmetric rigid aircraft is included.

Force Equations:

$$\dot{u} = qw - g\sin\theta + (X + T_X)/m \tag{D.5a}$$

$$\dot{w} = qu + g\cos\theta + (Z + T_Z)/m \tag{D.5b}$$

Moment Equation:

$$I_Y\dot{q} = M + M_T \tag{D.6}$$

Kinematic Equation:

$$\dot{\theta} = q \tag{D.7}$$

Navigation Equations:

$$\dot{p}_N = u\cos\theta + w\sin\theta \tag{D.8a}$$

$$\dot{h} = u\sin\theta - w\cos\theta \tag{D.8b}$$

Atmospheric Turbulence Contributions:

$$u = u_{\text{aerodynamics}} + u_{\text{turbulence}} \tag{D.9a}$$

$$w = w_{\text{aerodynamics}} + w_{\text{turbulence}} \tag{D.9b}$$

Where the atmospheric turbulence velocity components, $u_{\text{turbulence}}$ and $w_{\text{turbulence}}$, were calculated using MIL-F-8785C specification and the Dryden Turbulence SIMULINK block for calm, light, moderate, and severe turbulence. Nondimensional aerodynamic force and moment coefficients for an aircraft can be computed from flight measurements as follows:

$$C_X = \left(ma_X - T_X\right)/\bar{q}S \tag{D.10a}$$

$$C_Z = \left(ma_Z - T_Z\right)/\bar{q}S \tag{D.10b}$$

$$C_m = \left[I_Y\dot{q} - M_T\right]/\bar{q}S\bar{c} \tag{D.10c}$$

The nondimensional aerodynamic force coefficients are transformed from the body axis to the wind axis as follows:

$$C_L = -C_Z\cos\alpha + C_X\sin\alpha \tag{D.11}$$

For local modeling over a short time period, the force and moment coefficients computed from Equations (D.10) can be modeled using linear expansions in the aircraft states and controls:

$$C_L = C_{L_\alpha}\Delta\alpha_S + C_{L_{\delta e}}\Delta\delta e + C_{L_O} \tag{D.12a}$$

$$C_m = C_{m_\alpha}\Delta\alpha_S + C_{m_q}\frac{\Delta q\bar{c}}{2V} + C_{m_{\delta e}}\Delta\delta e + C_{m_O} \tag{D.12b}$$

Atmospheric Turbulence Model Structure

$$C_L = C_{L_\alpha}\Delta\alpha_S + C_{L_{\alpha_G}}\Delta\alpha_G + C_{L_{\delta e}}\Delta\delta e + C_{L_O} \tag{D.12c}$$

$$C_m = C_{m_\alpha}\Delta\alpha_S + C_{m_{\alpha_G}}\Delta\alpha_G + C_{m_q}\frac{\Delta q\bar{c}}{2V} + C_{m_{\delta e}}\Delta\delta e + C_{m_O} \tag{D.12d}$$

The Δ notation indicates perturbation from a reference condition. In Equations (D.12b) and (D.12d), C_{m_O} represents the nondimensional pitching moment at a reference condition, and similarly for the other expansions.

D.3.1.3.2 Wing Response to Turbulence

In order to investigate the effects of upwash correction as a function of frequency and time delay as a function of frequency the recursive Fourier transform in the RT-PID algorithm was modified. The recursive Fourier transform is defined as:

$$\tilde{X}_{n+1} = \tilde{X}_n + x_{n+1}e^{-j2\pi f_k(n+1)\Delta t} \tag{D.13}$$

Where the frequency vector is defined as f = [0.1:0.04:2.0], the time delay is modeled as:

$$\phi(f) = e^{-j2\pi * \text{time delay}}$$
$$\tilde{X}_{n+1} = \tilde{X}_n + \phi x_{n+1} e^{-j2\pi f_k (n+1)\Delta t} \tag{D.14}$$

Where *time delay*, is a vector of time delays for each frequency f = [0.1:0.04:2.0]. The upwash correction $1 + k_u(f)$is a vector of upwash corrections for each frequency f = [0.1:0.04:2.0]. The updated recursive Fourier transform is defined as:

$$\tilde{X}_{n+1} = \tilde{X}_n + x_{n+1}\left[1 + k_u(f)\right]\left[\phi(f)\right] e^{-j2\pi f_k (n+1)\Delta t} \tag{D.15}$$

D.3.1.3.3 Vane Sensor Model

In order to investigate the frequency response of airflow angle vanes, a second-order airflow vane sensor dynamic model was studied. A natural frequency of ω_n = 9 Hz and a damping ratio ζ = 0.35 were chosen as representative values for a dynamic model of the airflow vanes (Ref. 10 to 12). Typical natural frequency and damping ratio values range from 5 to 20 Hz and 0.2 to 0.6, respectively. Equation (D.6) represents a second order continous-time transfer function:

$$G(s) = \frac{\omega_n^2}{s^2 + 2\zeta\omega_n s + \omega_n^2} \tag{D.16}$$

The transfer function representation does not support non-zero initial conditions; therefore, the vane sensor model was converted to a state space representation which supported a trim α initial condition.

D.3.1.4 Testing

The hypothesis was tested using the SIMULINK model described and the following test conditions:

1. Baseline run with a perfect AOA measurement and the aerodynamic model structure defined in Equation (D.12).
2. Based on findings in Section D.3.1.3.3, repeat test condition 1 with a representative frequency response model for the airflow angle vanes.
3. Repeat test condition 2 with varying AOA magnitude and time delay as a function of frequency.
4. Based on findings in Section D.3.1.2.2, add turbulence coefficients to the aerodynamic model structure and a perfect α measurement.

D.3.1.5 Results and Analysis

The following parameters are common to all four test conditions.

1. Aircraft trimmed at 10,000 ft and 140 kt
2. 20 sec runs
3. Orthogonal multi-sine inputs (Ref. 14) invoked from 1 to 11 sec
4. Model parameter estimates taken at the end of each 20 sec run
5. 200 runs per atmospheric turbulence intensity (calm, light, moderate, and severe)
6. Fourier transform frequency spacing 0.04 Hz
7. Fourier transform frequency range [0.1 2.0] Hz
8. Signal-to-noise ratio of 50
9. 50 Hz data rate

The following comments are common to all of the figures associated with test conditions one to four:

1. Green line—truth value of the parameter
2. Red dashed line—confidence interval using ±10 percent of truth value of the parameter
3. Red diamond—parameter estimate
4. Blue bars—estimated two sigma error bounds

In the dynamic modeling process, no attempt was made at estimating the drag coefficients, because the aircraft excitations did not appreciably changed airspeed, resulting in a low signal-to-noise ratio for the axial force coefficient parameter estimation. Additionally, contributions from the lift damping coefficient C_{Lq} were small and omitted from the model and the estimation process. In total, five coefficients were estimated, $C_{L\alpha}$, $C_{L_{\delta e}}$, $C_{m\alpha}$, C_{mq}, and $C_{m_{\delta e}}$.

D.3.1.5.1 Test Condition 1

As shown in Figure D.8, the baseline model estimates for $C_{Z\alpha}$ resulted in improved estimates with increasing atmospheric turbulence. This is not representative of actual flight data and is attributed to perfect α measurement given the additional excitation caused by atmospheric turbulence.

As shown in Figure D.9, the baseline model estimates for $C_{m_{\delta e}}$ resulted in greater scatter as turbulence intensity increased. This is caused by noisy explanatory variables (Ref. 15) from the atmospheric turbulence implementation in Equation (D.9). Similar patterns were observed with the remaining coefficients C_{Zq}, $C_{Z_{\delta e}}$, $C_{m\alpha}$, and C_{mq}, although the results are not shown. These simulations demonstrate that all if the AOA measurements are perfect, all model parameters can be estimated accurately for any level of turbulence.

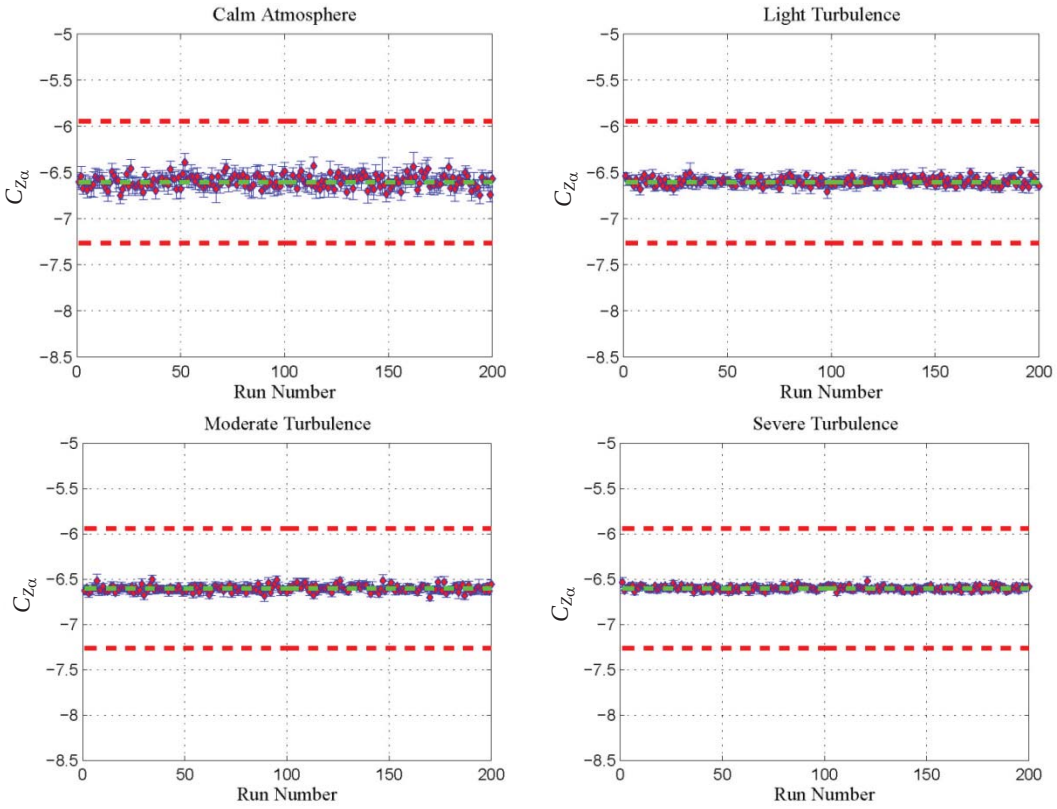

Figure D.8.—Test Condition 1—Effect on C_{Z_α}

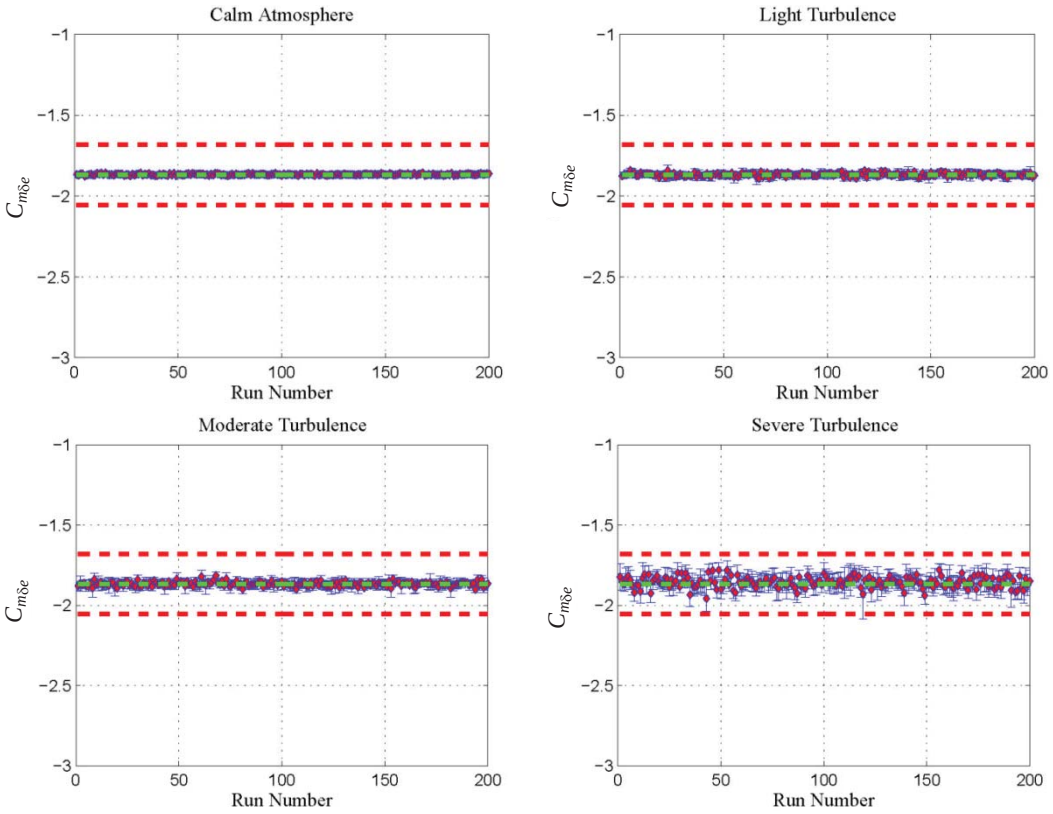

Figure D.9.—Test Condition 1—Effect on $C_{m_{\delta e}}$

D.3.1.5.2 Test Condition 2

Estimates for C_{Z_α} using the second-order vane sensor model of Equation (D.6) (ω_n = 9 Hz and ζ = 0.35) caused degradations and biasing in the estimates with increasing turbulence intensities, as shown in Figure D.10. This is representative of actual flight data.

As shown in Figure D.11, the baseline model estimates for $C_{m_{\delta e}}$ resulted in greater scatter as atmospheric turbulence intensity increased. This is caused by noisy explanatory variables (Ref. 15) from the atmospheric turbulence implementation in Equation (D.9), and the vane sensor model. Similar patterns were observed with the remaining coefficients C_{Z_q}, $C_{Z_{\delta e}}$, C_{m_α}, and C_{m_q}, although the results are not shown.

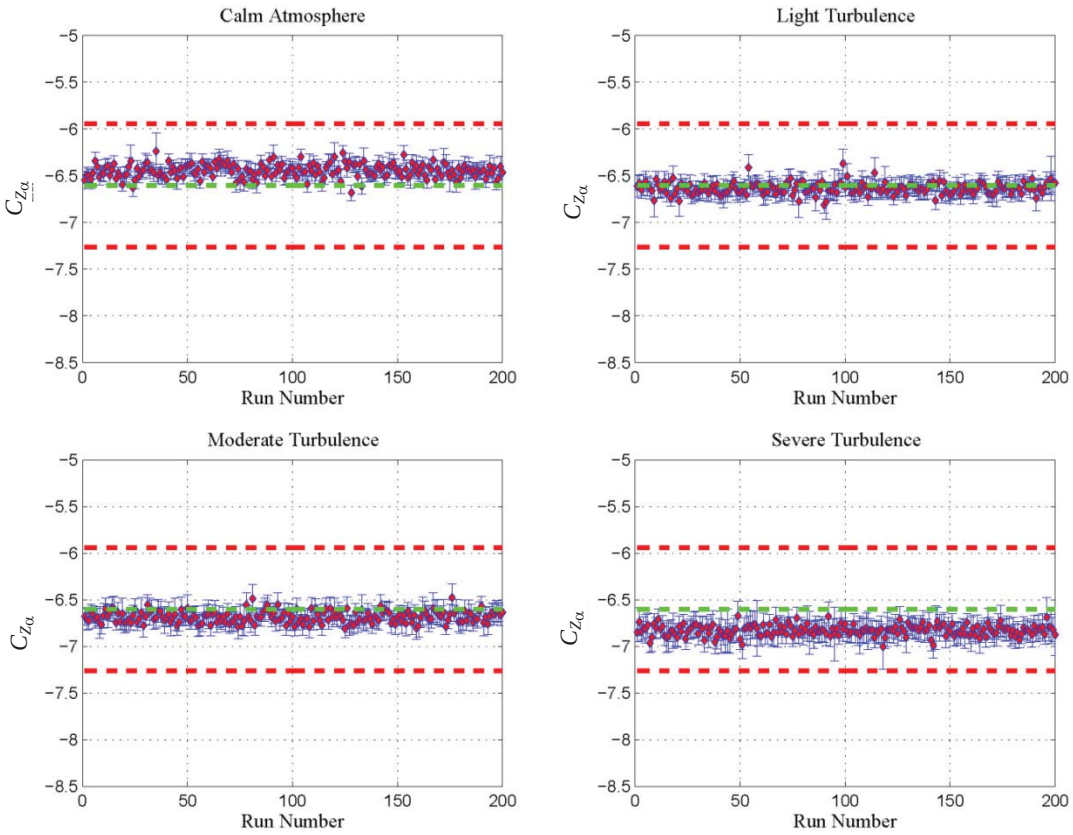

Figure D.10.—Test Condition 2—Effect on C_{Z_α}

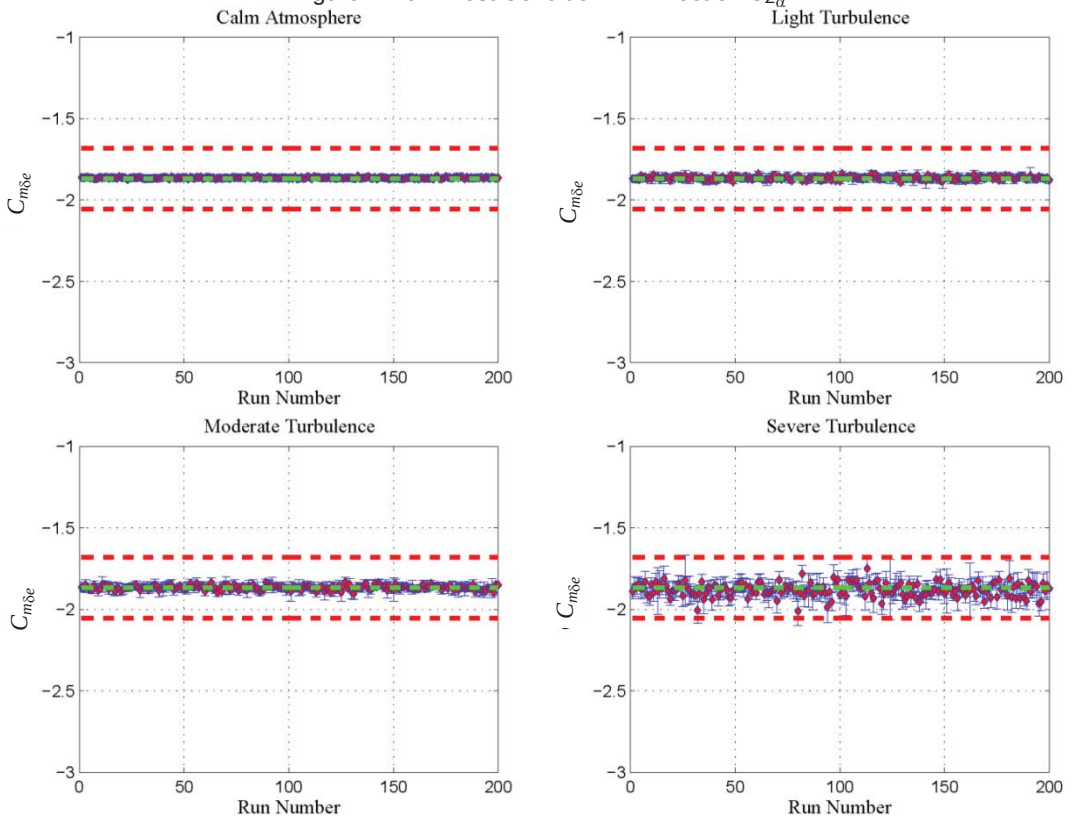

Figure D.11.—Test Condition 2—Effect on $C_{m_{\delta e}}$

D.3.1.5.3 Test Condition 2—Expanded Testing

Although no quantitative analysis was done, qualitatively, small differences were observed between a perfect and typical vane frequency response in test conditions 1 and 2. This is expected because the vane dynamics do not substantially contribute to the scatter in the estimates, since all of the added dynamics are outside the range of frequencies analyzed.

To further validate this claim, additional testing was carried out using the same simulation. A total of 121 different combinations of flow angle vane natural frequency and damping ratios were tested. The natural frequency values tested were 5 through 15 in 1 Hz increments. The damping ratio values tested were 0.01, 0.05, 0.1, 0.15, 0.2, 0.25, 0.3, 0.35, 0.4, 0.45, and 0.6. Since the AIMMS-20 probe approaches a gain of one and zero phase shift, it is characterized by the results of test condition 1. The AIMMS-20 probe offers superior frequency response performance to mechanical vanes by using 1) a 5 hole pressure probe , 2) short tube lengths (air data tubes are typically less than 5 in. long), and 3) the resonance frequency of the silicon pressure diaphragm is in the kilohertz region. The following figures depict the results of 121 combinations, times 4 turbulence levels, times 200 runs per case. This totaled 96,800 runs. Figure D.12 depicts the results of 96,800 runs for C_{Z_α}. As an example, the bottom left corner block in severe turbulence is light blue. The color represents the number of exceedances of C_{Z_α} from ±10 percent of truth. The remaining 120 blocks are dark blue representing less than 10 exceedances. Figure D.12 suggests that any combination of natural frequency and damping ratio tested provides adequate performance. Similar results were obtained for C_{m_α} and C_{m_q} results are not shown.

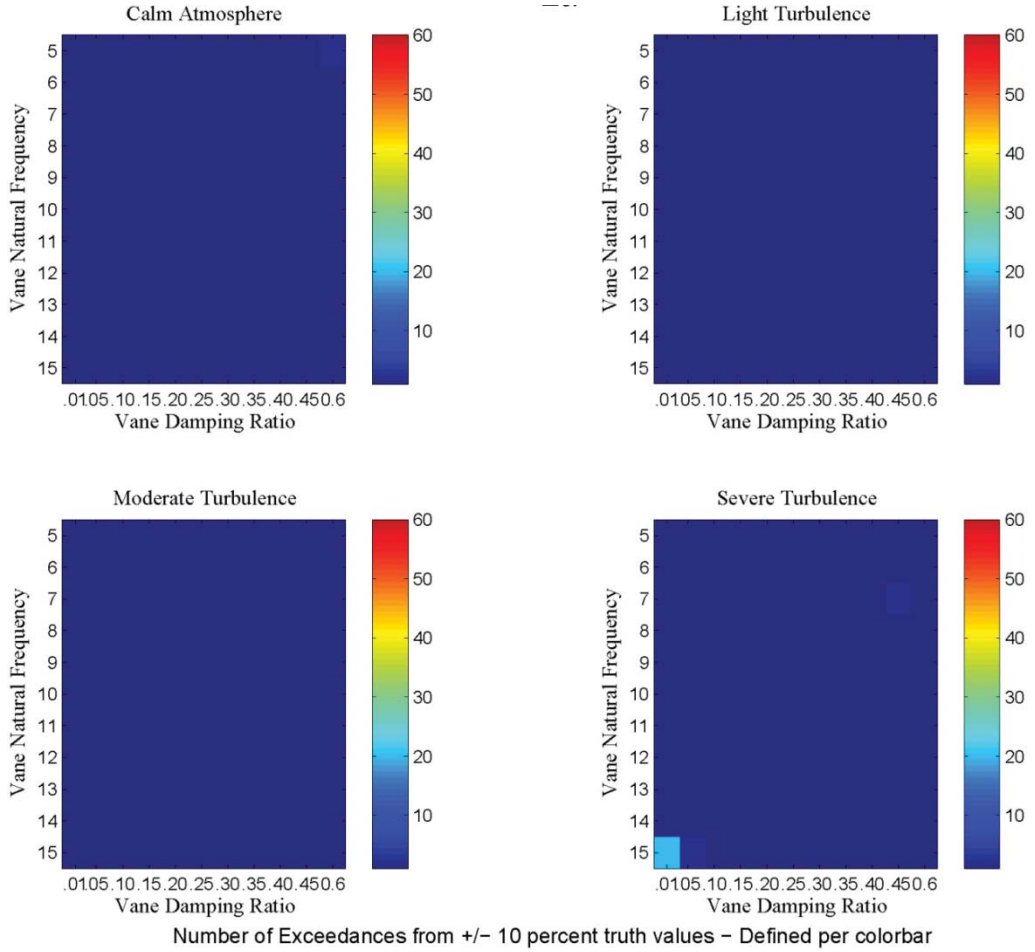

Figure D.12.—Number of exceedances for C_{Z_α}

Figure D.13 shows that independent of the natural frequency and damping ratio tested, accurate estimates of $C_{m_{\delta e}}$ are feasible in atmospheric turbulence. This is expected due to strong elevator control authority.

Results for C_{Z_q}, not shown, demonstrate that independent of the natural frequency and damping ratio tested, exceedances less than 20 out of 200 or ±10 percent of truth are not feasible in any level of atmospheric turbulence except calm. For the remaining stability and control estimates, the results show that most combinations of natural frequency and damping ratio tested provide adequate performance in calm, light, moderate, and severe atmospheric turbulence.

D.3.1.5.4 Test Condition 3

As shown in Figure D.14, estimates for C_{Z_α} resulted in degraded estimates with increasing atmospheric turbulence for varying AOA magnitude and time delay as a function of frequency implemented using the data in Figure D.6 and Figure D.7. The degradation is seen as biasing in the estimates and increased scatter and uncertainty estimate error bounds. This is representative of actual flight data.

As shown in Figure D.15, the estimates for $C_{Z_{\delta e}}$ also resulted in degraded estimates with increasing atmospheric turbulence. The degradation is seen as biasing in the estimates and increased scatter and uncertainty estimates. The increase in biasing and uncertainty compared to C_{Z_α} estimates is caused by the relatively small contribution of the elevator term to the normal force coefficient.

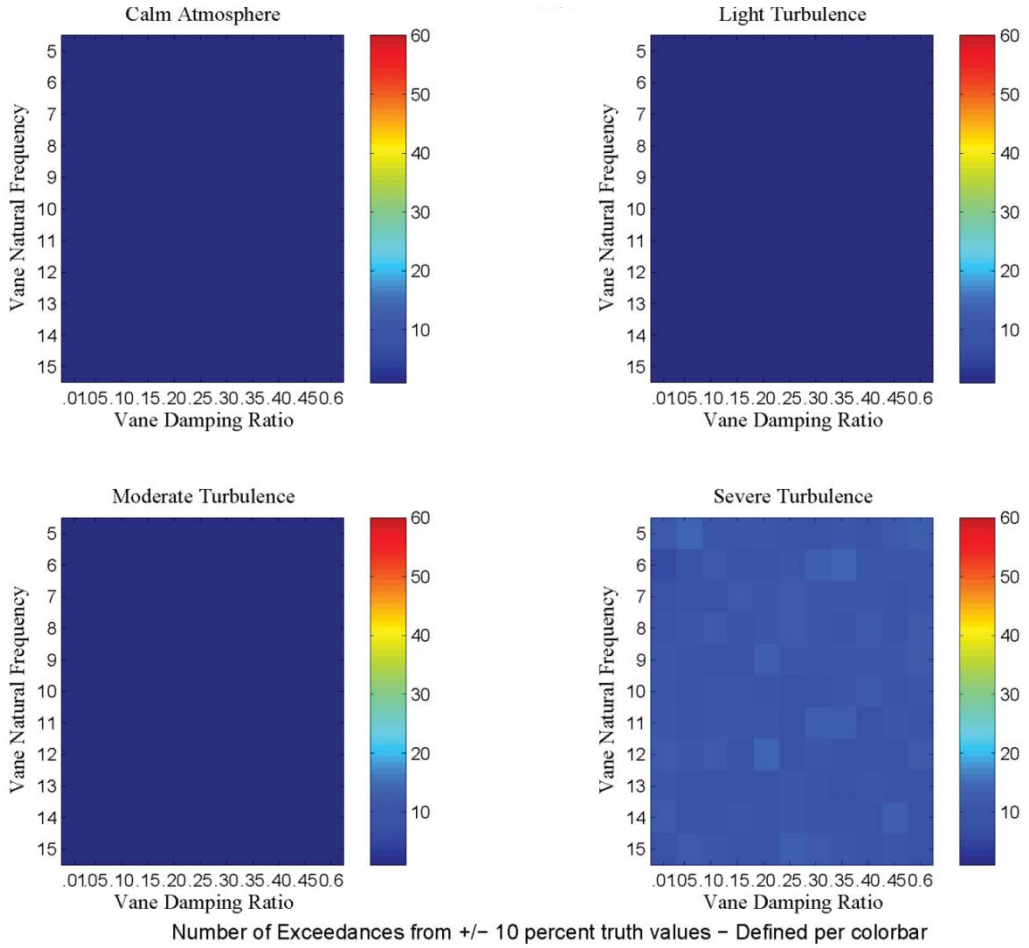

Figure D.13.—Number of exceedances for $C_{m_{\delta e}}$

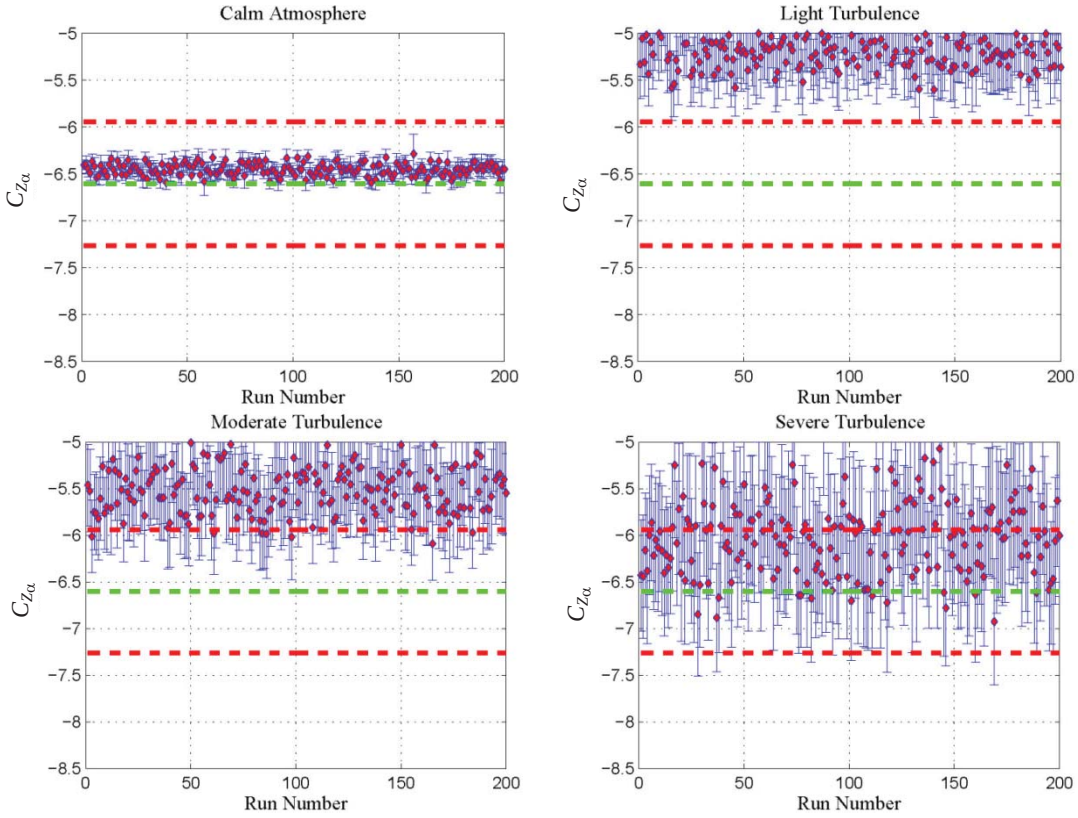

Figure D.14.—Test condition 3—Effect on C_{Z_α}

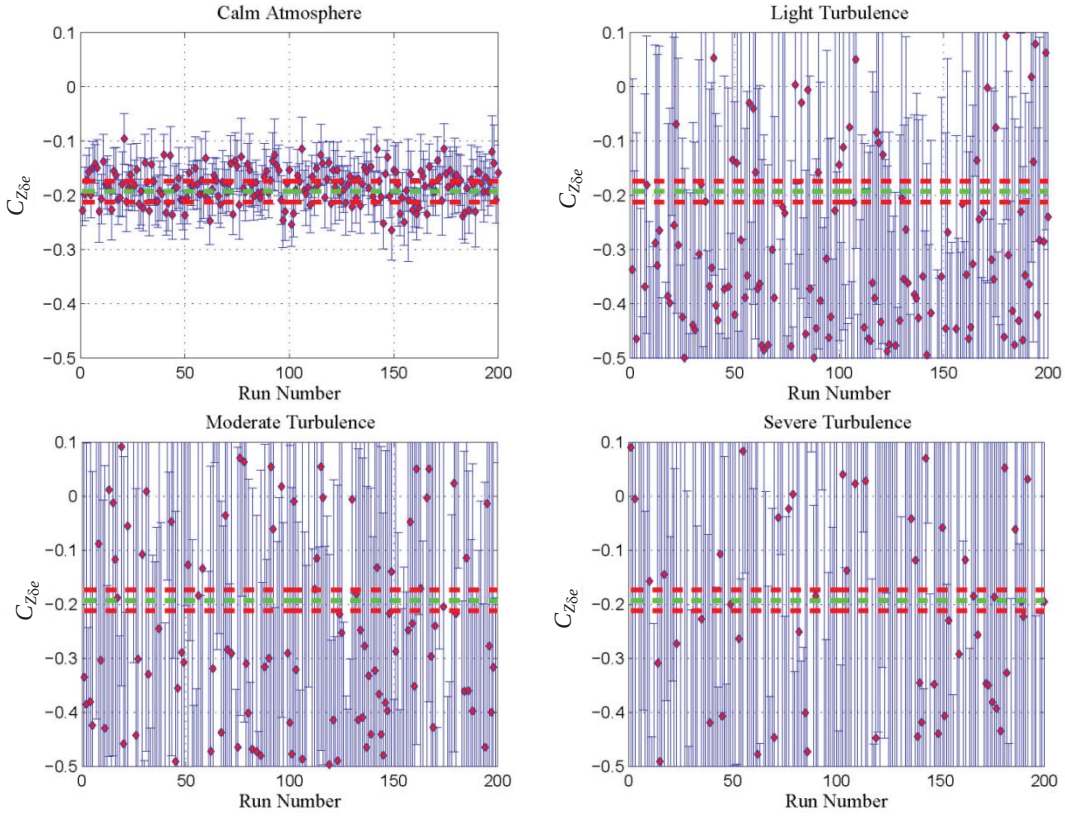

Figure D.15.—Test condition 3—Effect on $C_{Z_{\delta e}}$

Figure D.16 shows that the estimates for $C_{m\alpha}$ degraded with increasing atmospheric turbulence. The degradation is seen as biasing in the estimates and increased scatter and uncertainty estimates. This is representative of actual flight data.

As shown in Figure D.17, the estimates for C_{mq} degraded with increasing atmospheric turbulence. The degradation is seen as biasing in the estimates and increased scatter and uncertainty estimates. The estimates for C_{mq} resulted in the largest biasing of all the aerodynamic estimates considered because angular velocity model parameters are most susceptible to time delays (Ref. 16).

Figure D.18 shows that the estimates for $C_{m\delta e}$ degraded with increasing atmospheric turbulence. The degradation is seen as a scatter in the estimates and increased scatter and uncertainty estimates. This is representative of actual flight data and correlates with the flight results presented in Figure D.3.

Corrupting the AOA measurement by a frequency-dependent magnitude and time delay affected all of the estimated stability and control coefficients. The estimates of $C_{m\alpha}$ and $C_{m\delta e}$ exhibited moderate biasing and increased scatter and uncertainty, $C_{Z\alpha}$ and C_{mq} estimates had large biases and increased scatter and uncertainty, and $C_{Z\delta e}$ estimates showed the largest biases and increases in scatter and uncertainty. Previous work on the effects of time-shifted data on flight determined stability and control estimates (Ref. 16) using the output-error method in the time domain demonstrated similar trends in the biasing and increased uncertainty, compared to the results shown here due to atmospheric turbulence.

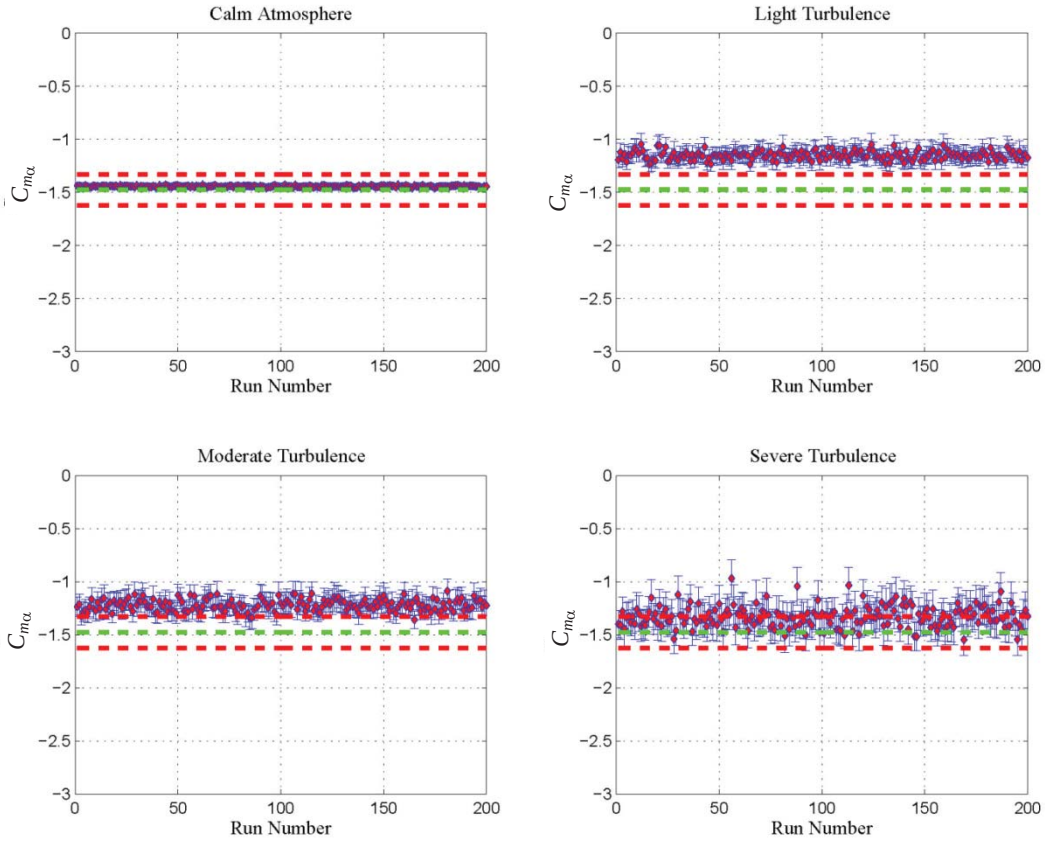

Figure D.16.—Test condition 3—Effect on C_{m_α}

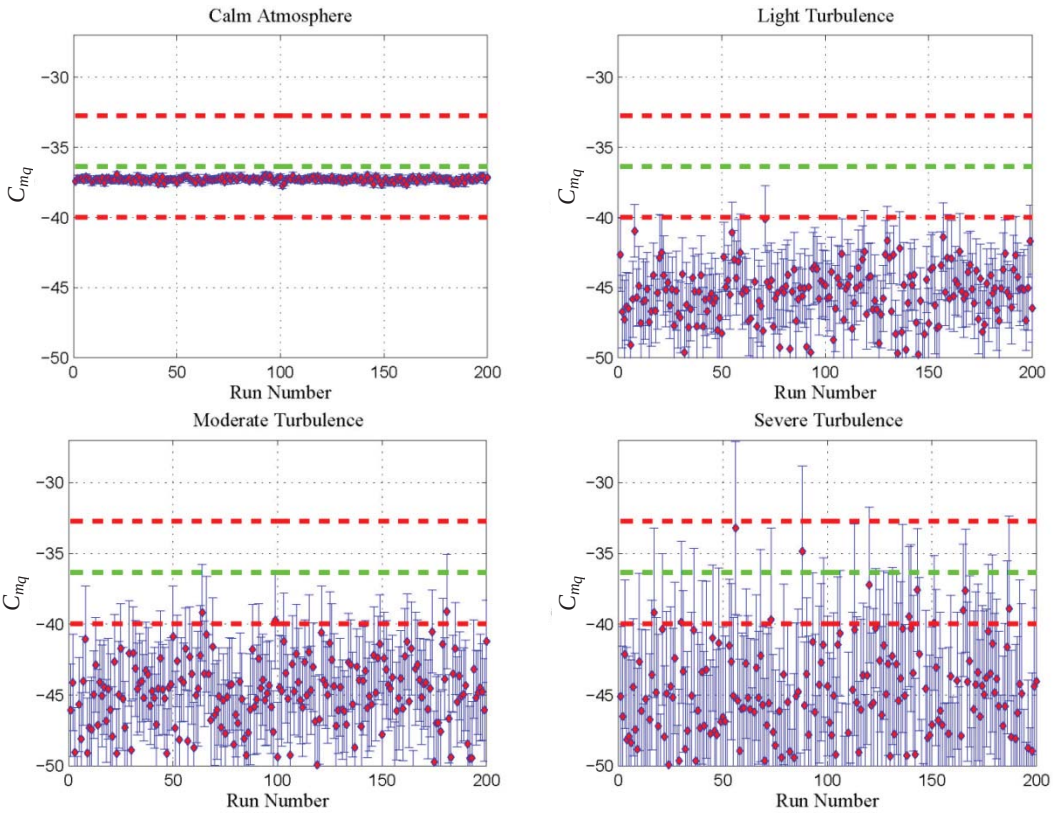

Figure D.17.—Test condition 3—Effect on C_{m_q}

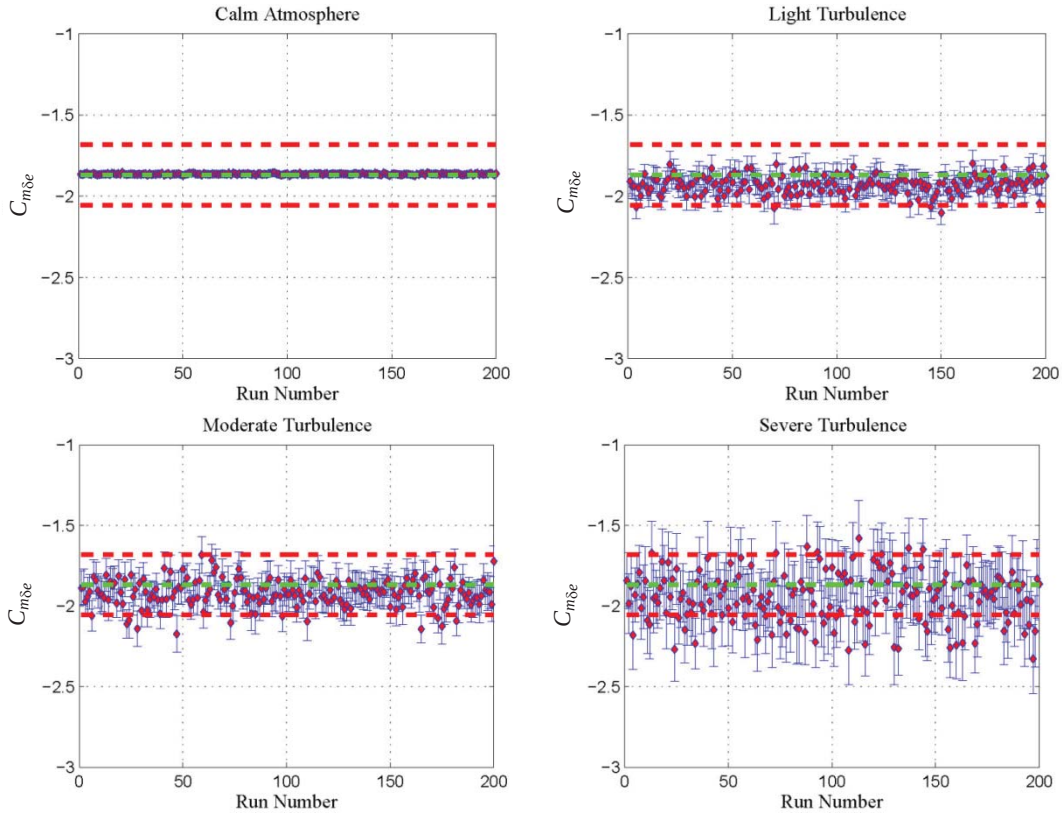

Figure D.18.—Test condition 3—Effect on $C_{m_{\delta e}}$

D.3.1.5.5 Test Condition 4

Based on the findings in Sections D.3.1.2.2, additional turbulence coefficients were added to the model structure. All of the turbulence estimates for C_{L_α} except for the estimates in calm atmosphere resulted in large degradations. In fact, the degradations were so large that they were not captured by the standard plot range. A similar pattern was observed with the estimates of C_{m_α}. This is not representative of actual flight data. The estimates for $C_{m_{\delta e}}$ resulted in greater scatter and an overall bias as turbulence intensity increased. The overall biasing effect is not representative of actual flight data. Similar patterns were observed with the remaining coefficients results are not shown.

D.3.1.6 Task 1 Conclusions

Several practical issues related to real-time parameter estimation for a linear longitudinal dynamics model in atmospheric turbulence using indirect turbulence measurements were examined and discussed. The frequency response of the airflow vanes, wing response to atmospheric turbulence, and the structural response of the air data boom were identified as sources of colored noise. The frequency response of the airflow vanes for a wide variety of combinations of natural frequency and damping ratio did not adversely impact parameter estimation results in turbulence, except for C_{Z_q} and $C_{Z_{\delta e}}$. This was attributed to noisy explanatory variables in the atmospheric turbulence implementation and relatively low aerodynamic contributions as compared to C_{Z_α}. Airflow vane dynamics do not substantially contribute to the scatter in the estimates, because all of the added dynamics are outside the range of frequencies analyzed. The structural modes of the boom lead to similar conclusions, because the natural frequencies of the boom structural modes are outside the range of frequencies used for dynamic modeling. A major source of colored noise was identified as the frequency-dependent upwash and time delay induced by the wing-bound vortex system and the longitudinal separation between the AOA measurement and the wing. It was also surmised that the frequency-dependent sidewash was a major source of colored noise. The frequency-dependent upwash and time delay appear to be significant contributors to biasing and increased scatter and uncertainty for parameter estimates in atmospheric turbulence.

Practical issues were examined using data from a Twin Otter DHC-6 longitudinal linear simulation, with realistic noise sequences added to the computed aircraft responses. This allowed a clear view of the effect of each source of colored noise to the modeling problem, because the true values of the model parameters were known. This approach was used initially to show that real-time parameter estimation can be done accurately in all atmospheric turbulence conditions if the AOA measurement is accurate. Flight test data from the GRC DHC-6 Twin Otter aircraft was used to validate the effect of the identified colored noise sources.

Based on these findings, several practical recommendations for flight testing in atmospheric turbulence are suggested, as well as areas for future study. First, mount the air data boom at the nose of the aircraft to minimize the effect of the wing-bound and wing-tip vortices. Second, if the air data boom is mounted on the nose of the aircraft, an upwash and time delay calibration as a function of frequency is required.

The following Task 2 and Task 3 results were carried out assuming that these precautions and calibrations had been taken care of. This assumed that the frequency response was adequate (good assumption based on the results of this section for a well calibrated, stiff, nose mounted sensor). This left the sensor's static performance to be evaluated in Task 2 and Task 3. This eliminated the need to update the D-Six Twin Otter simulation from previous studies. In other words, if these precautions are taken, the RT-PID estimates will behave similarly inside and outside of atmospheric turbulence.

D.3.2 Task 2

Through initial testing it was found that the Twin Otter at a typical cruise condition was not capable of controlled flight in severe turbulence with the virtual pilot used for this study. During runs in severe turbulence, the aircraft would consistently enter a wing stall. The data from stalled runs was not

considered useful, because stalled flight does not produce reliable data. As a result, all severe turbulence test conditions have been omitted from Task 2 analysis. Additionally, non-ice test conditions were run, but in the context of RT-PID, were considered outside of the scope and omitted from the analysis. Both ice and no ice runs were considered when evaluating D-ICES performance.

The purpose of Task 2 was to modify, test, and validate the use of RT-PID and D-ICES algorithms with atmospheric turbulence as an input for various levels of atmospheric turbulence, and to identify an acceptable error in the wind measurement during turbulence for RT-PID and D-ICES algorithms. Wind measurement error was varied from 0.0 to 1.0 kt. Eighty test runs were conducted with and without ice, turbulence, and wind measurement errors.

D.3.2.1 D-ICES Study Results

It was found that the application of turbulence and sensor noise on D-ICES had a minimal impact on performance without filtering. With the filtering scheme of state variables described in Section D.3.2.1.1, D-ICES performance allowed accurate detection of possible icing situations in the presence of turbulence and sensor noise. D-ICES used a Theil inequality coefficient, comparing the a-priori elevator deflection for a clean aircraft to that of the current flight condition, to statistically estimate the aircraft's current state. The estimated clean elevator deflections were calculated using a flight model inversion technique to find a corresponding control deflection for the given flight condition. The Theil inequality coefficient provided a measure of how well the actual elevator deflection matched the calculated elevator deflection, where a value of 0 indicated a total match, and 1 indicated a total mismatch. If the coefficient exceeds a threshold of 0.18 with a 3 sec delay to latch true, D-ICES activates the IVHM ID mode.

As a result, a metric for success with sensor noise and turbulence is determined by their effect on creating false positive or false negative mode switches. A false positive condition would be one where D-ICES latches the ICEPro ID mode in a non-iced flight condition. While the impact of an occasional false positive is a human factors exercise, the impact of a false negative where the pilot is told the aircraft is clean while accreting ice would have serious implications.

As shown in Figure D.19 D-ICES allows one false positive indication without filtering. Adding sensor noise to selected parameters used in the ICEPro logic, as discussed in Section D.2 causes the Theil inequality coefficient to increase, growing larger as the severity of the sensor noise increases. When the largest sensor noise was used the Theil inequality coefficient exceeded the ID mode threshold, which would cause an IVHM mode switch to ID mode in normal operation.

Looking at the iced aircraft results without filtering in Figure D.20, D-ICES fails to indicate iced conditions in severe turbulence. This system failure is due to the severity of the turbulence as the aircraft stalls and full elevator deflection has been reached by the virtual pilot. The virtual pilot, described in Equation (D.1), was unable to maintain airspeed or a level attitude. This is seen in Figure D.21. Due to the lack of aircraft control and severity of the turbulence in the severe turbulence scenarios these conditions will not be evaluated. As discussed in Section D.2.2, low virtual pilot gains were used for all conditions which worked well without turbulence, but were less than optimal in turbulence. The low virtual pilot gains most likely contributed to the aircraft stalling in severe turbulence. For Phase I tests, a fixed throttle setting was used. However, during Phase II testing, aircraft configuration changes required the throttles to be actively controlled. The deactivation of the throttles during Phase I was done to eliminate the excessive and frequent throttle movements during flight in turbulence where the control logic was attempting to hold velocity in dynamic conditions.

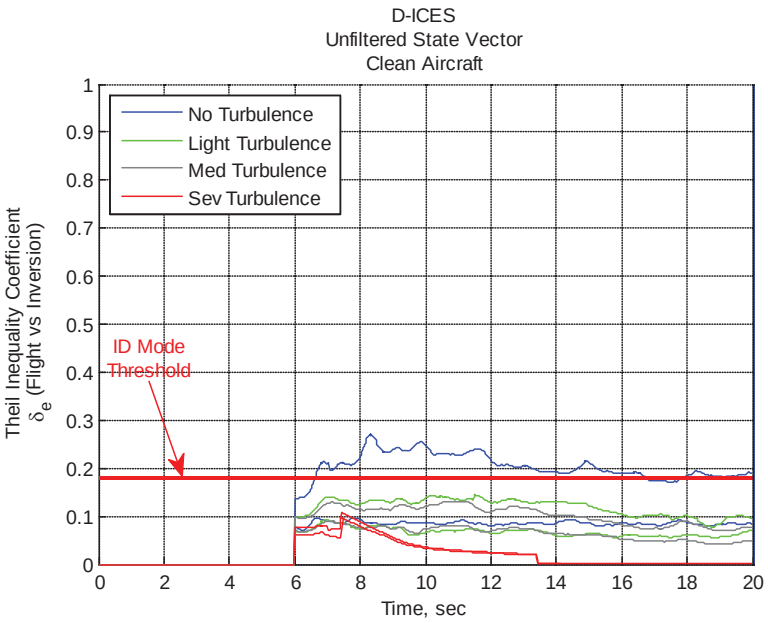

Figure D.19.—Unfiltered D-ICES Performance with Clean Aircraft

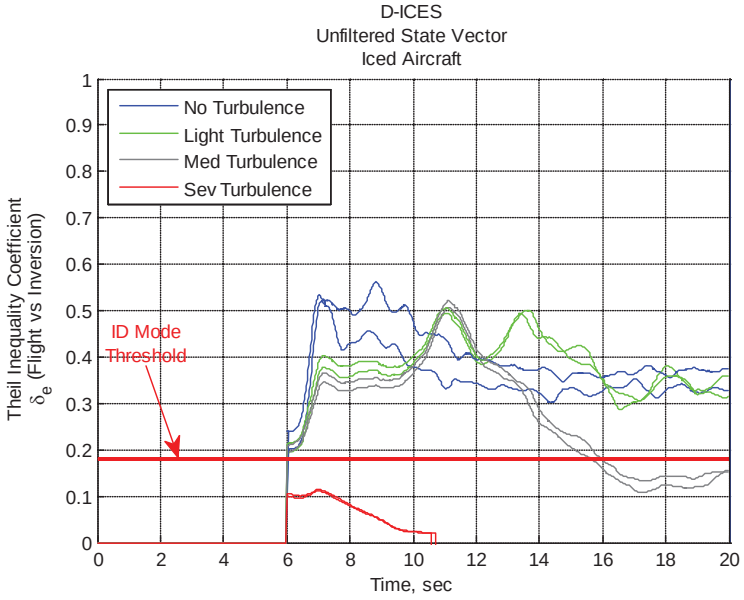

Figure D.20.—Unfiltered D-ICES Performance with Iced Aircraft

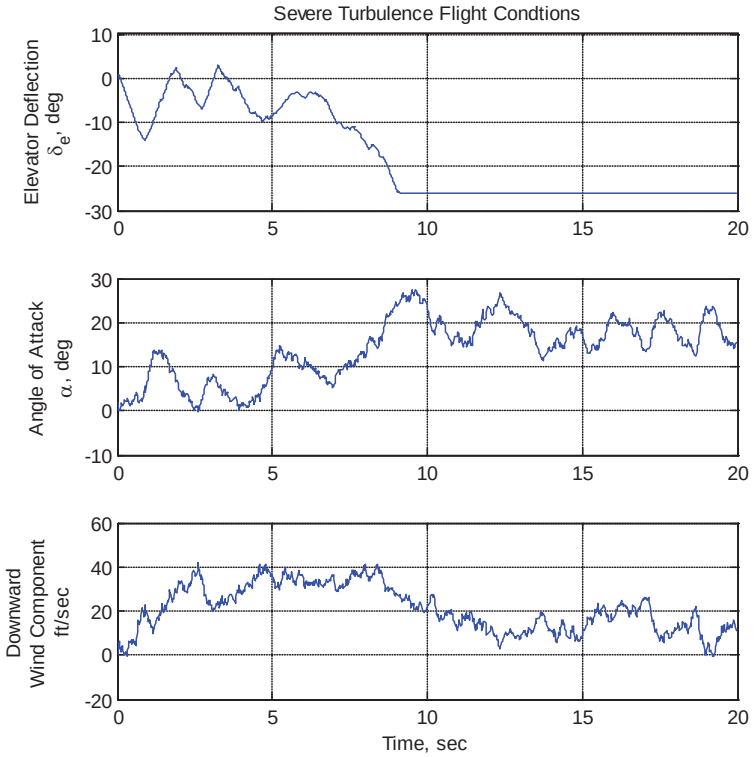

Figure D.21.—Severe Turbulence Flight Conditions

D.3.2.1.1 Results of 80 Runs With Fixed Random Seed

The flight model inversion process in D-ICES is dependent on an input state vector derived from the current flight conditions. This state vector includes the following eight elements:

- Angle of attack
- Angle of sideslip
- Roll rate
- Pitch rate
- Yaw rate
- Elevator deflection
- Aileron deflections
- Rudder deflection

Since D-ICES was only used in initial mode switching, it was proposed that filtering these inputs for the flight model inversion calculation could be done with a minimal delay on system mode switching. A second order low pass filter was chosen with a cut-off frequency of 2.5 Hz.

The four turbulence scenarios were tested, no turbulence, light turbulence, medium turbulence and severe turbulence. As previously explained, the severe turbulence results were omitted from the analysis. In each turbulence scenario, sensor noise was added, set to either a nominal condition or off. Finally, a fixed random seed, or a reusable series of random numbers, was used to generate turbulence to allow direct comparison between the runs.

Figure D.22 shows the filtered conditions for the no-ice or clean aircraft with a fixed random noise seed. Here the noise influence shown in Figure D.19 resulting in a false positive has been addressed. In addition the effect of atmospheric turbulence on the D-ICES algorithm is minimal.

In the iced aircraft scenario, shown in Figure D.23, there were no false negatives with D-ICES. The sensor noise effects have been addressed as the scenarios with and without noise are almost over-plots. There is a banding effect due to the level of turbulence (i.e., all of the results for a common level of turbulence grouped tightly together but at different Theil inequality coefficient values); however, all conditions are well above the selected ID Mode switch threshold and result in mode switching at similar times.

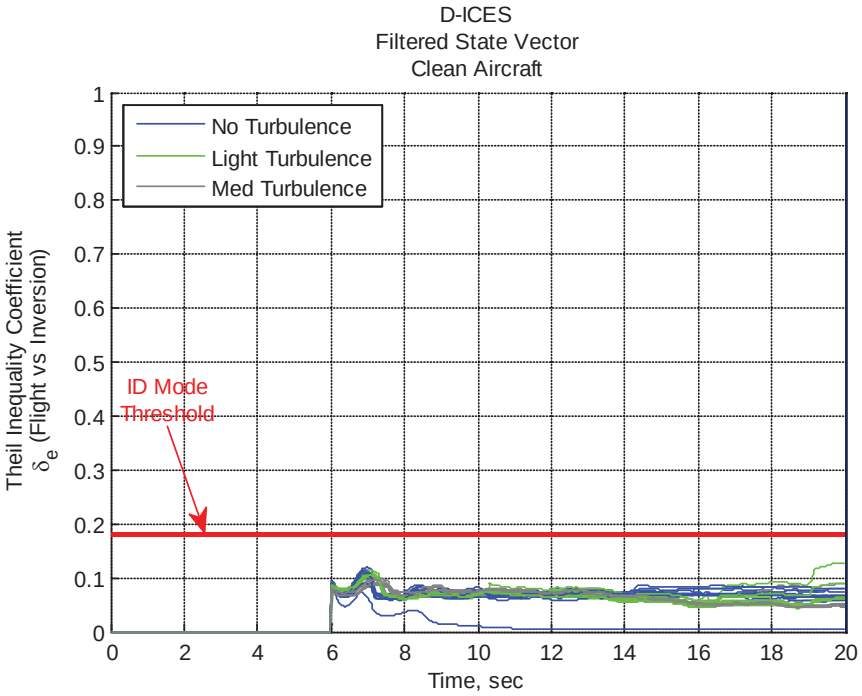

Figure D.22.—Filtered Clean Aircraft with Fixed Random Seed

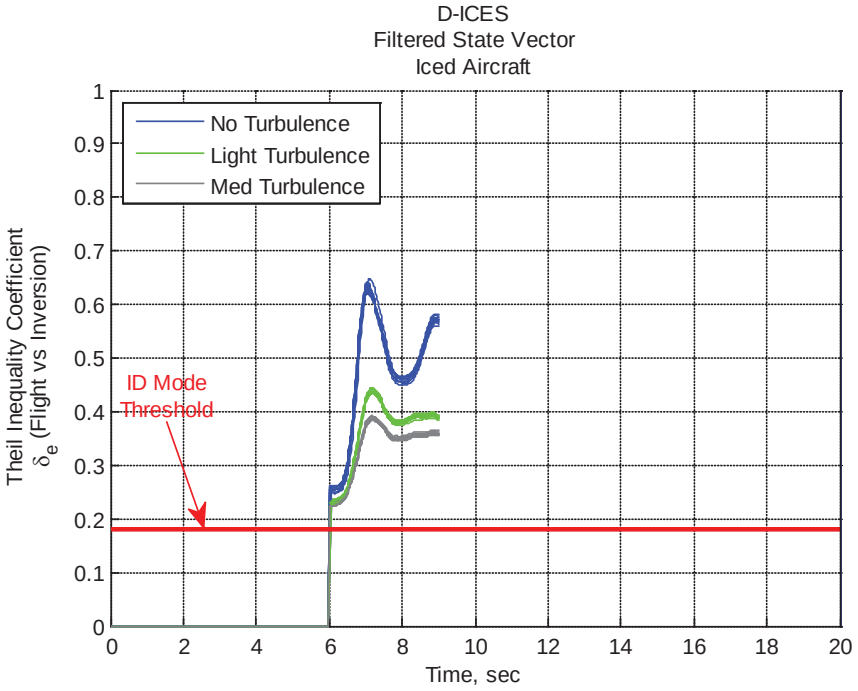

Figure D.23.—Filtered Iced Aircraft with Fixed Random Seed

D.3.2.1.2 Results of 60 Runs Random Seed

A total of 60 scenarios were tested (the 20 severe turbulence cases were dropped, as mentioned earlier), again at three turbulence levels with one condition without sensor noise and nine additional scenarios with sensor noise. In addition, the seed for the random number generation was selected randomly creating a unique set of random number for every run.

In Figure D.24, the clean aircraft conditions continue to exhibit a very tight banding with only three turbulence conditions potentially exhibiting a false positive. Further examination revealed that in the immediate trim AOA region, small changes in AOA produced very little variation in pitching moment due to a specific elevator deflection. If the AOA went to higher values where there was a variation with AOA, the Theil inequality coefficient remained well below the threshold value. It was surmised that the D-ICES inversion process had some troubles in determining the correct elevator deflection near trim, in the presence of light turbulence with these pitch due to elevator characteristics. A real pilot would probably not chase the variations in speed and flight path in the same manner as the virtual pilot did in these runs, and the results could differ. Looking at only the initial 6 sec after buffer fill (t = 6 to t = 12) provides a snapshot of the typical D-ICES operation.

Figure D.25 shows 60 separate runs in D-ICES performance under three turbulence conditions. Under light and medium turbulence D-ICES successfully detected the presence of icing conditions without degradation or delaying IVHM mode shifting.

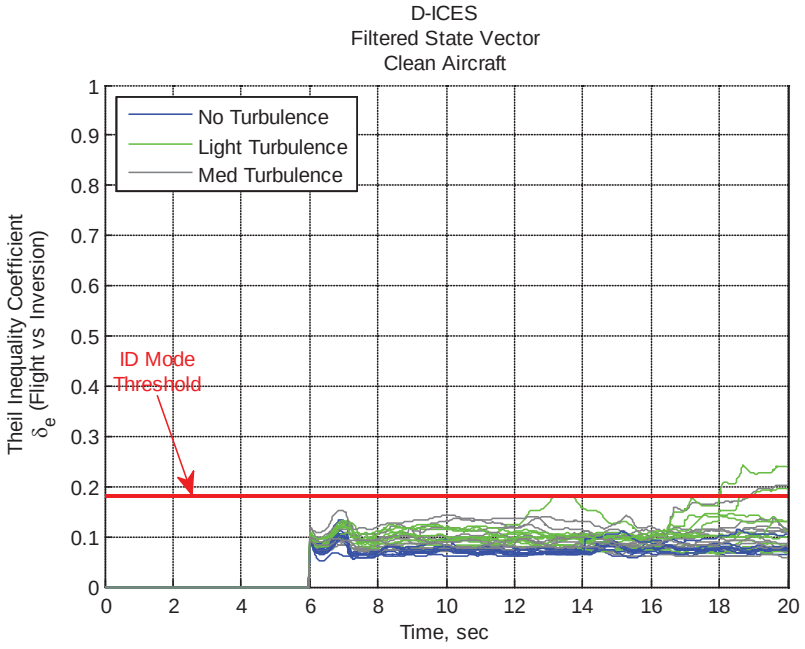

Figure D.24.—Filtered Clean Aircraft with Random Seed

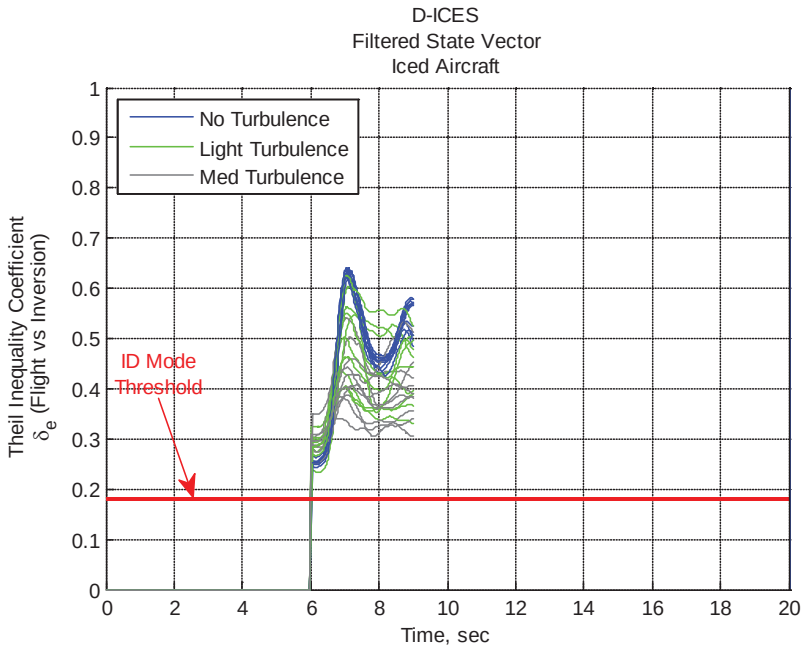

Figure D.25.—Filtered Iced Aircraft with Random Seed

D.3.2.2 RT-PID Study Results

It was found that the application of turbulence and sensor noise on RT-PID had a significant impact on performance. As previously mentioned, non-ice test conditions were run, but in the context of RT-PID were considered outside of the scope and omitted from the analysis. Therefore, only the 40 iced runs will be reported. Results from the 40 iced runs with fixed turbulence seed are depicted in Figure D.26. The error in flow angles was varied from 0.0° to 1.0° in 0.1° increments. All other errors were fixed using the probe specifications in Table D.1.

The results of Figure D.27 illustrate the effect of flow angle error on the coefficient $C_{m\alpha}$. As expected, increased flow angle error results in increasing error in the estimate and increased error bars throughout each turbulence level. The severe turbulence cases are discarded from the analysis since the majority of the flight resulted in a stalled condition.

Next, the MOS message criterion was applied with white Gaussian measurement noise. The following results for $C_{m_{\delta e}}$, representative of the pitch degrade message, are depicted in Figure D.27 with fixed turbulence seed. As the turbulence level increases so does the error in the estimate and the error bounds.

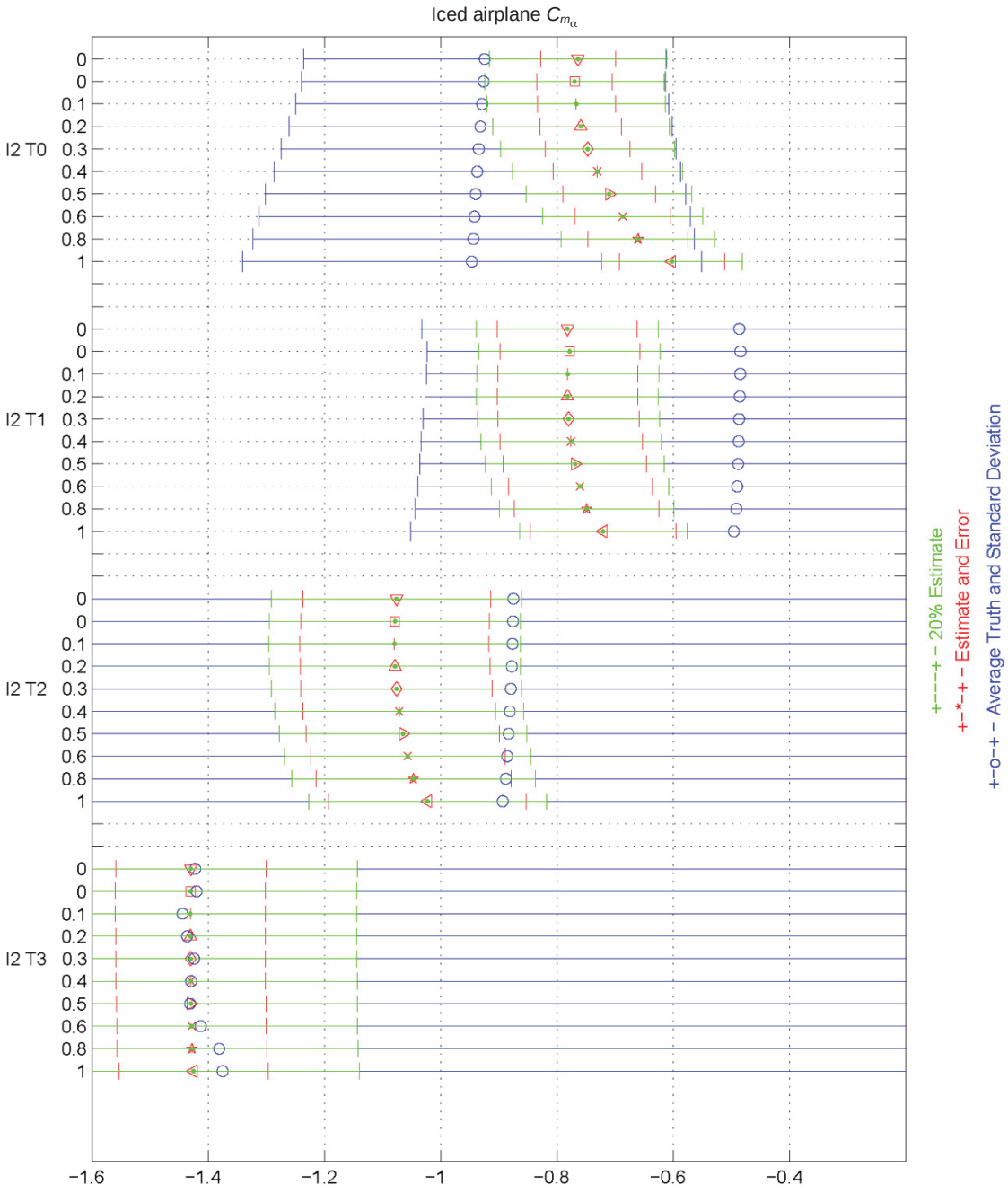

Figure D.26.—Effect of flow angle error on C_{m_α}

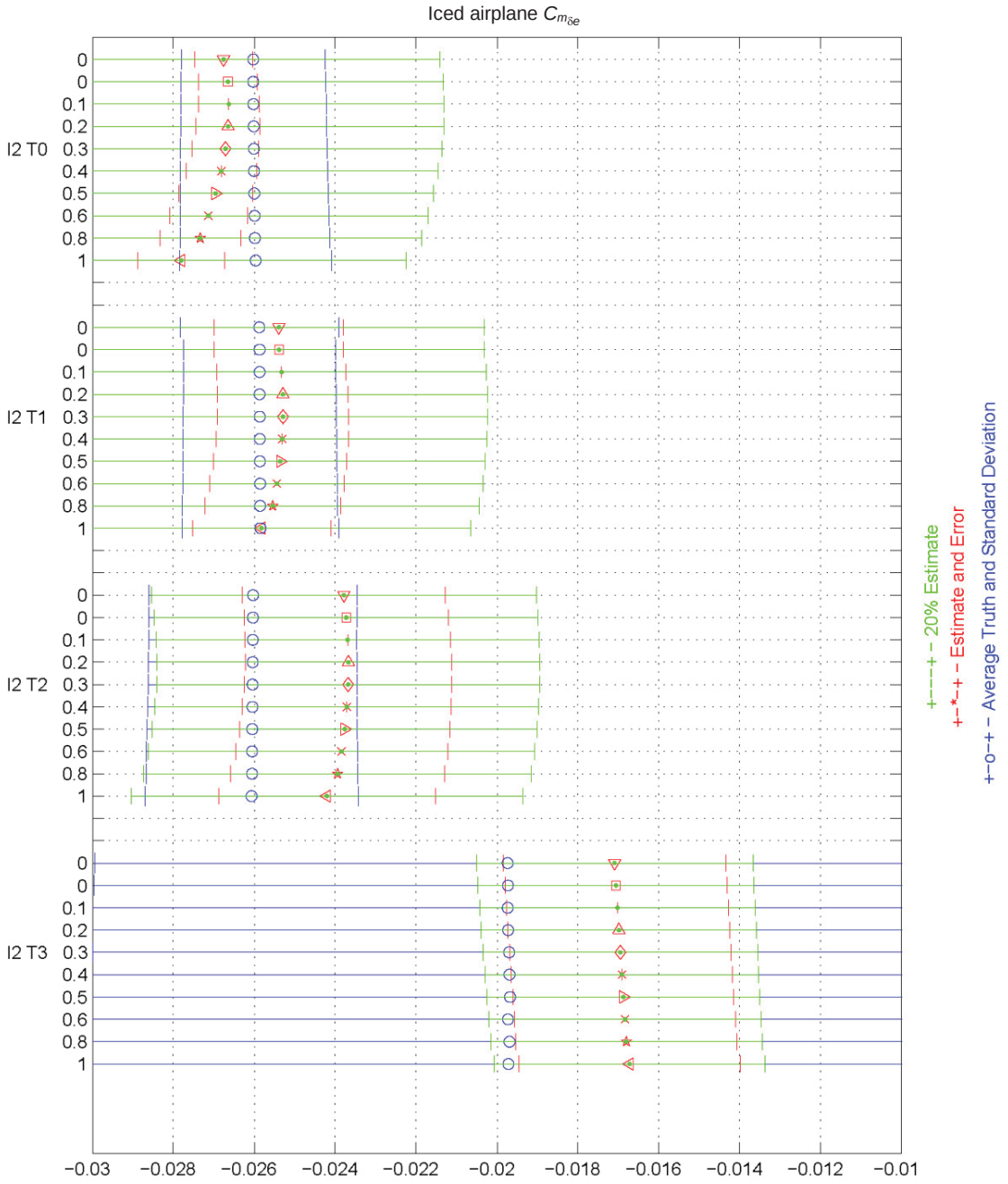

Figure D.27.—Effect of flow angle error on $C_{m_{\delta e}}$

D.3.2.3 Task 2 Measures of Success (MOS)

The MOS message criterion is summarized below for convenience (Appendix E).

1) Message accuracy

   Message error will be determined by the error bounds and accuracy of its associated stability and control coefficient for all ICEPro messages. Coefficients must meet or exceed the non-atmospheric turbulence error bound and accuracy in atmospheric turbulence.

In general, the MOS for message accuracy is not achieved. As seen in Figure D.27, the estimates move away from the truth and error bounds increase with each increase in turbulence level. The same

runs that were used to disqualify the MOS message criterion were used to evaluate the ISP MOS criterion summarized below for convenience (Appendix E).

2) ISP accuracy

ISP error will be determined by comparing the true ISP value with the estimated ISP value. ISP is a function of five stability and control coefficients: Longitudinal static stability, elevator control power, dihedral effect, aileron control power, and normal lift coefficient. The ISP error must meet or exceed its non-atmospheric turbulence error bound and accuracy in atmospheric turbulence.

The following results for ISP, representative of all 40 ice runs with fixed turbulence seed, are depicted in Figure D.28.

Figure D.28 depicts the ISP time history for each simulated flow angle error. The ISP value is initially set to zero at the start of each run and ramps up as ice is detected. The D-ICES threshold for determining an ice condition is an ISP value of 0.5. This is depicted by dashed red lines in each subplot. Visual inspection confirms that the ISP is different in and out of turbulence. In order to satisfy the original MOS criteria, the ISP lines in and out of turbulence must be the same. As shown in Figure D.28 this is not the case. Additionally the ISP deteriorated greatly with increased flow angle error. In general, the MOS criterions for both messages and ISP, as originally defined, were not achieved. A new MOS criterion was formulated based on the results depicted in Figure D.27 and Figure D.28. The new criterion takes into account the degradation of RT-PID estimates and error bounds in turbulence. Errors in the estimates and in the error bounds with turbulence were tolerated as long as the ICEPro messages and AOA brackets are equivalently displayed inside and outside of turbulence. The criterion is summarized below.

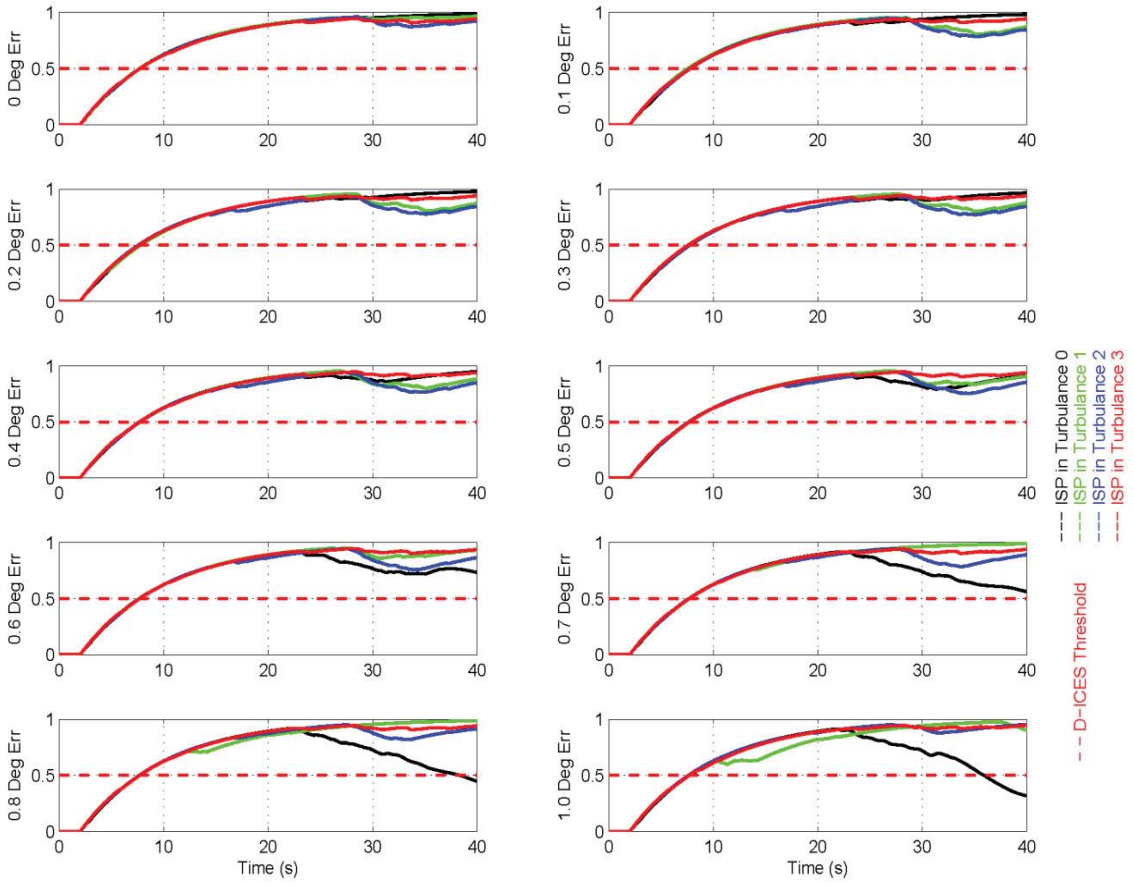

Figure D.28.—ISP for all turbulence levels and flow angle errors (α and β)

1. Compare high and low AOA brackets across turbulence levels. Angle of attack brackets are strongly dependent on AOA and flap deflection and weekly dependent on ISP.
    - Equal or conservative bracket location
        - Successful envelope protection
    - Unconservative bracket location
        - Unsuccessful envelope protection
2. Compare message state across turbulence levels as well as time to latch and time to delatch.
    - Same state annunciation
        - Successful envelope protection
    - Varying state annunciation
        - Unsuccessful envelope protection
    - Latch / delatch within 10 sec of no turbulence results
        - Successful envelope protection

The following results for message accuracy, representative of AIMMS-20 measurement errors for all turbulence levels, are depicted in Figure D.29 using the new MOS criterion. Only the results of the Roll degrade message are plotted since the remaining messages did not result in false positives or false negatives and were considered successful. In theory, the same messages are expected for all turbulence levels since the aircraft is flown about the same reference condition. In Figure D.29, this is represented by the average AOA and angle of sideslip during each run. In practice, for zero, light, and moderate turbulence the average flow angles are similar. In severe turbulence, the average flow angles are significantly different due to wing stall, but do not affect the message accuracy. As stated previously the severe turbulence runs are omitted from the analyses and all runs used a fixed turbulence seed for comparison purposes.

In the zero turbulence case, the roll degrade message results in a false positive warning message. This is explained by the aileron control power estimate subplot. The estimate of the aileron control power quickly diverges from the truth. This difference causes the false positive indication. It should be noted that although a false positive condition occurs due to poor estimates the ICEPro logics latches at the correct levels. As a side note, this condition was repeated with higher buzzing amplitudes and no false positives occurred. In each of the turbulence cases, the additional aileron inputs provided by the virtual pilot improved the RT-PID estimates so that no false positives were annunciated. In general the new MOS message criterion is considered to be successful.

Additional testing was conducted to access the new MOS AOA bracket criterion. The following results for AOA bracket accuracy, representative of AIMMS-20 measurement errors with conservative flow angle errors for all turbulence levels, are depicted in Figure D.30. A conservative flow angle error of 0.3° versus the stated 0.1° was chosen because experience has proven the difficulty of calibrating up-wash and side-wash corrections on air data probes.

As in the message MOS criterion, the same AOA bracket locations are expected for all turbulence levels since the aircraft is flown about the same reference condition. In Figure D.30, these are represented by the upper and lower bar delta plots using zero turbulence as the reference. For light and moderate turbulence the average deltas are similar. In severe turbulence, the average delta positions are significantly different due to wing stall and hence significantly affect the angle of attach bracket location and accuracy. The severe turbulence results are omitted from the analysis.

As shown in Figure D.30, after 25 sec from start-up the ISP oscillates between 0.8 and 1.0. Similarly, after 25 sec the AOA brackets oscillate about the zero turbulence AOA brackets. Additional filtering was implemented to smooth the AOA brackets in turbulence. The filtered results are shown in Figure D.31.

The results presented in Figure D.31 are filtered by a low pass fourth order Butterworth filter with a cut off frequency of 0.1 radians per second. Similar plots were generated to determine the effect of flow

angle error versus ISP. It was determined that the AOA brackets are strongly dependant on AOA and weekly dependant on ISP. Even with perfect instruments the ISP was very similar to the ISP in Figure D.31 with 0.3° flow angle error. The trend in Figure D.31 is that the AOA bracket location in turbulence oscillates around the zero turbulence case. This agrees with the analysis in Figure D.29 were the average AOA and sideslip was approximately the same for all runs except severe turbulence. Closer inspection shows that the AOA brackets are conservative and unconservative throughout the runs. Looking at the period after 30 sec, where the ISP has stabilized after start-up, the oscillations are approximately 1° for light turbulence and 2° for moderate turbulence. These small changes are not considered to be discernible by the pilot. Additionally, since the oscillations are due to the variation in AOA throughout the run and not due to the ISP, the new MOS AOA bracket criterion is considered to be successful for this task.

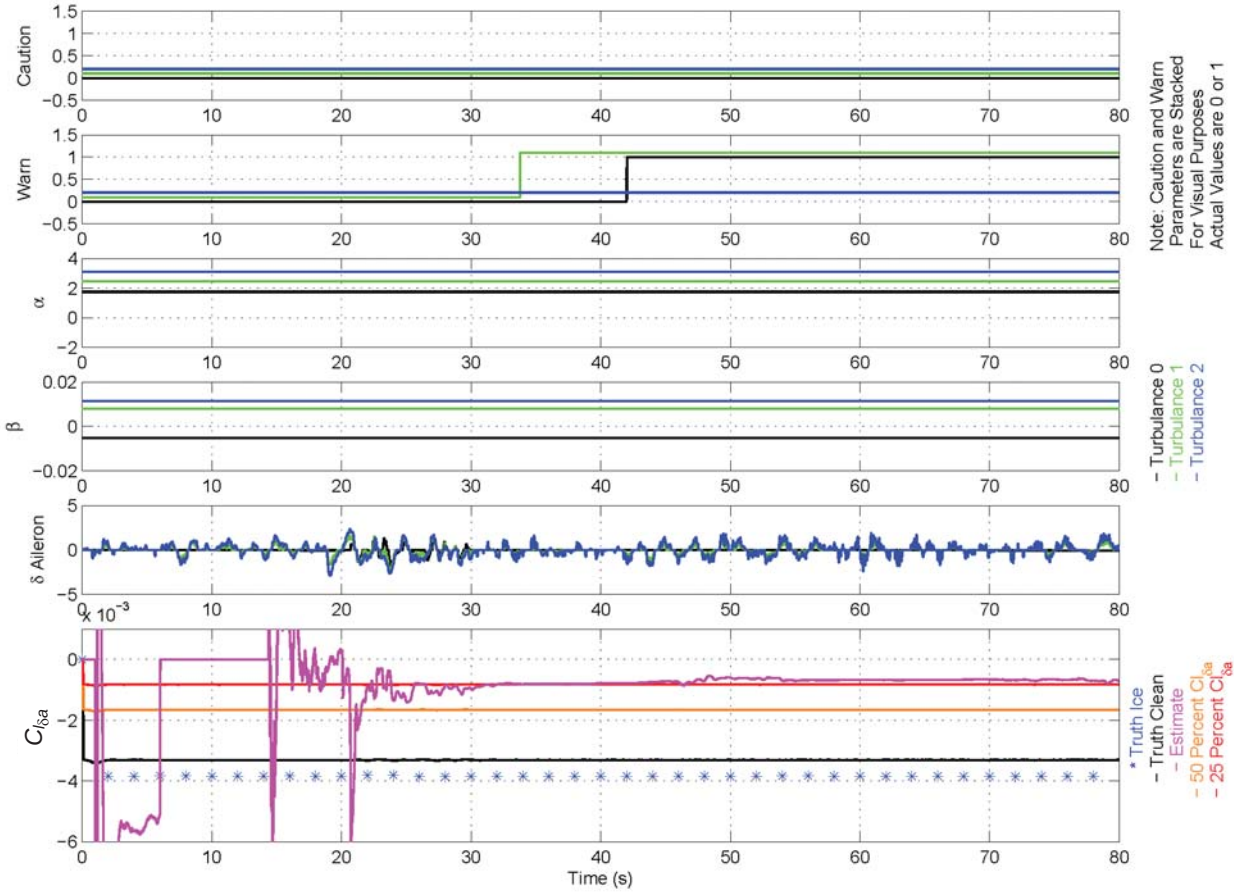

Figure D.29.—Roll degrade indication analyses

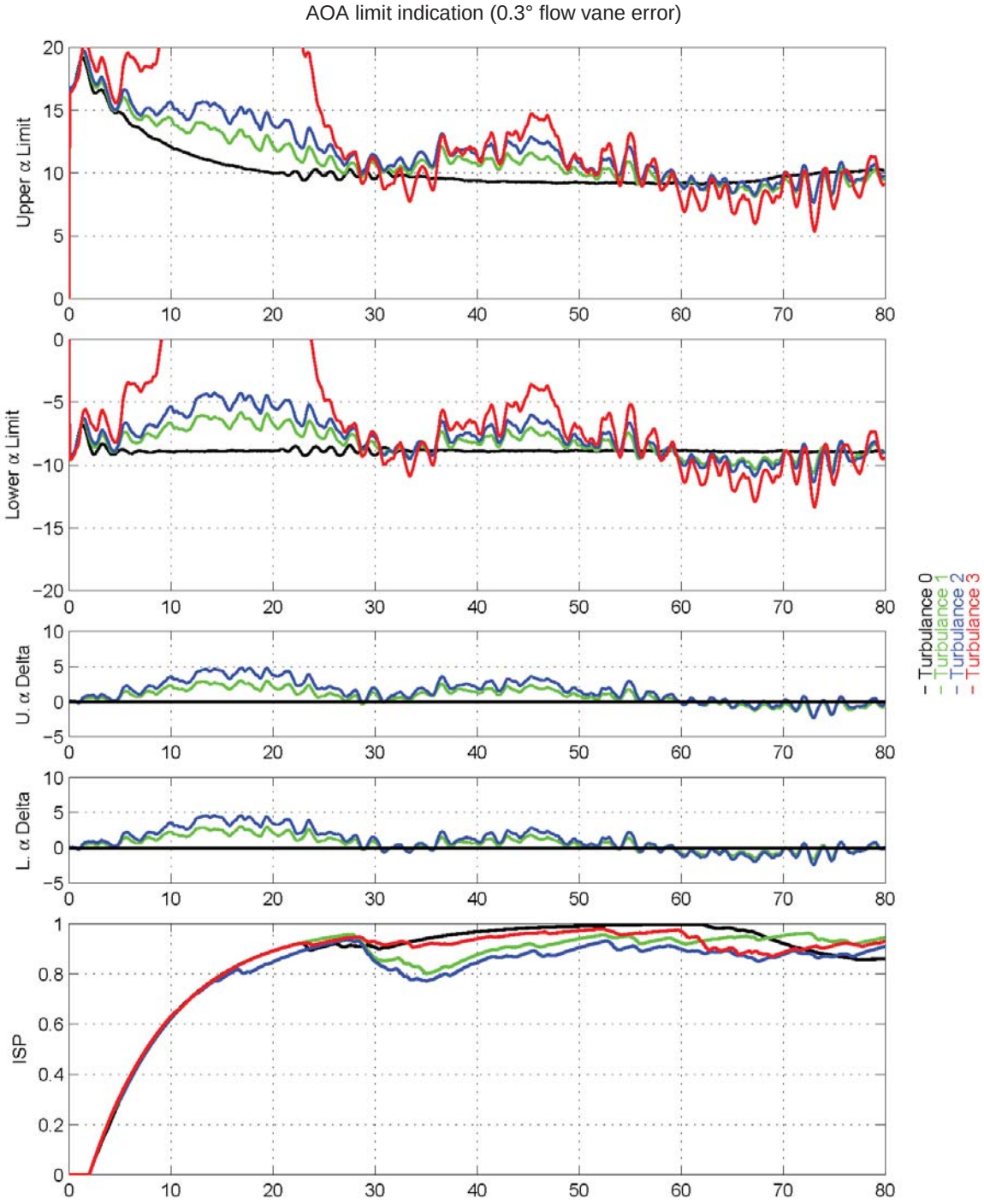

Figure D.30.—Angle of attack bracket indication analyses

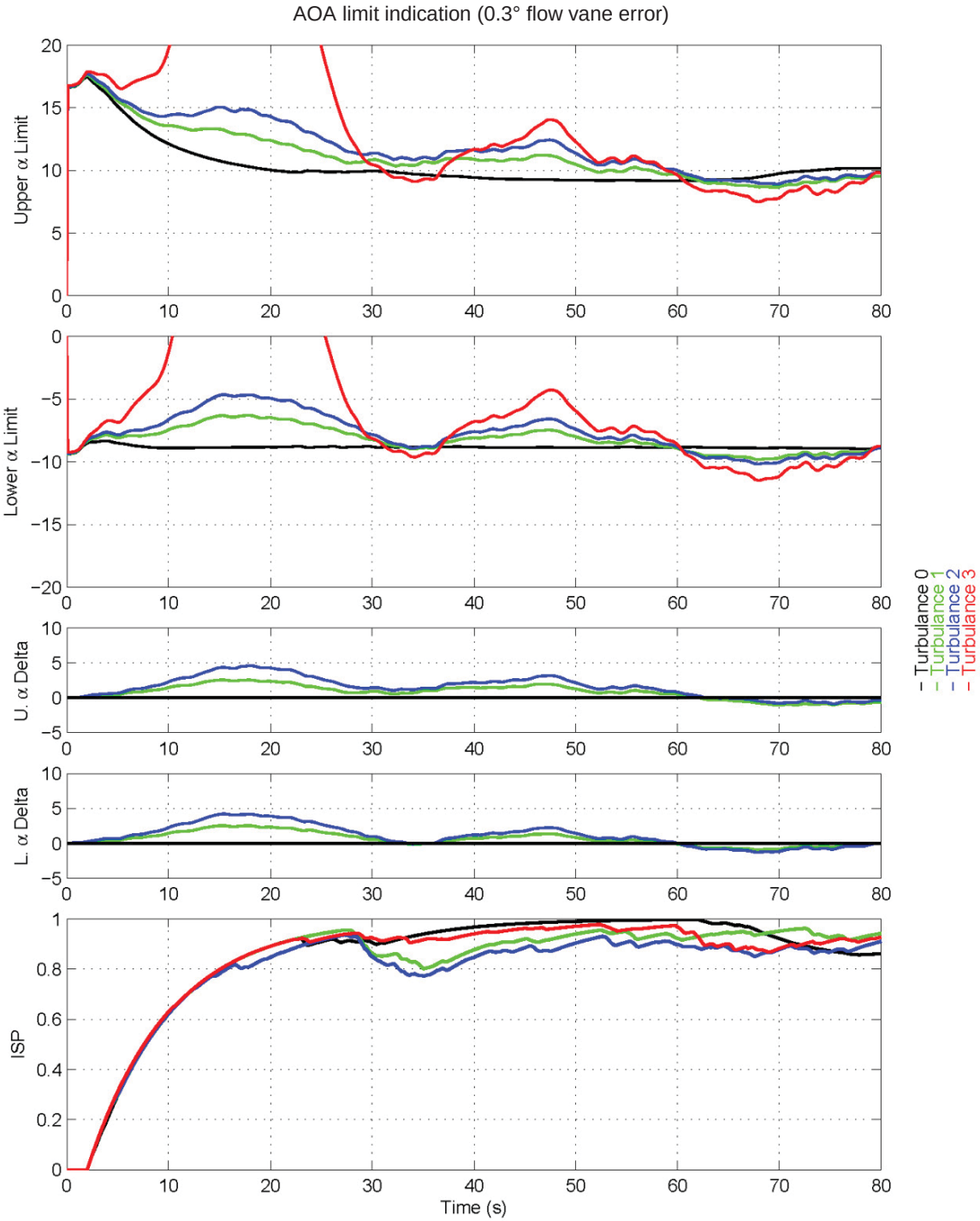

Figure D.31.—Filtered AOA bracket indication analyses

D.3.2.4 Task 2 Conclusions

RT-PID

- The original RT-PID MOS (Appendix E) for message accuracy were not achieved. A new MOS criterion was formulated due to results depicted in Figure D.27 and Figure D.28.
- A new MOS was defined were errors in the estimates and in the error bounds with turbulence are tolerated as long as the ICEPro messages and AOA brackets are equivalently displayed inside and outside of turbulence.
- The average flow angles are similar for zero, light, and moderate turbulence. In severe turbulence, the average flow angles are significantly different due to wing stall, but do not affect the message accuracy.
- With the exception of the Roll degrade message, there were no false positives or false negatives. The roll degrade message was caused during a period of low control activity. In each of the turbulence cases, the additional aileron inputs provided by the virtual pilot improved the RT-PID estimates so that no false positives were annunciated.
- In general the new MOS message criterion is considered to be successful.

D-ICES

- It was found that the application of turbulence and sensor noise on D-ICES had minimal impact on performance without filtering.
    - Only one condition was found that yielded a false positive that would have caused the system to enter ID Mode when no icing was present.
    - There was one condition where the elevator deflection Theil inequality coefficient for an iced airplane failed to exceed the threshold and two where the value originally exceeded the threshold but with time decreased until it was below the threshold.
- When the state vectors going to the D-ICES inversion routine were filtered to remove higher frequency disturbances due to turbulence and noise, D-ICES accurately detected all icing conditions in the presence of turbulence and sensor noise and thus operated correctly.
- Three potential false positive cases were found that showed the elevator Theil Coefficient built up over time to exceed the threshold when no ice was present. An examination of the data in this region led to supposition that the D-ICES inversion process had some troubles in determining the correct elevator deflection with the pitch due to elevator characteristics at those flight conditions.

Overall it was found that the objective to identify an acceptable error in the wind measurement was not required and that the performance of the AIMMS-20 probe was satisfactory for Task 2.

D.3.3 Task 3

The purpose of Task 3 was to evaluate four representative phases of flight (Appendix E) with the performance results of Task 2. Twenty four test runs were conducted with and without ice, turbulence, and wind measurement errors over four phases of flights. Turbulence was tested as calm, light, moderate, and severe. Turbulence levels are defined per MIL-F-8785C. All measurement errors were biased in a random time history with limits defined by the condition matrix and sensor specifications using the probe specifications in Table D.1 and the same conservative flow angle errors.

Whereas Task 2 focused on straight and level flight in the cruise configuration, Task 3 involved additional flight phases including, for a reference, a repeat of flaps up straight and level flight, straight and level flight flap transition, straight and level flight heading capture, and –3° flight path angle with a flap transition. This last phase is representative of the instrument approach task studied with the ICEFTD and thirty subject pilots at Embry-Riddle Aeronautical University during the summer of 2009.

Through initial testing it was found that the Twin Otter in approach configuration (20° flap) was not capable of controlled flight in moderate and severe turbulence. During some runs in moderate and all runs in severe turbulence, the aircraft entered a wing stall with the virtual pilot. The data from stalled runs was

not considered useful. As a result, all moderate and severe turbulence test conditions have been omitted from the RT-PID Task 3 analysis. The non-ice test conditions were run, but in the context of RT-PID, were considered outside of the scope and omitted from analysis. Additionally, the severe turbulence test conditions have been omitted from the D-ICES Task 3 analyses.

D.3.3.1 D-ICES Study Results

D.3.3.1.1 Results of 24 Runs Fixed Seed

The first phase matched the Task 2 conditions. The aircraft was level at 2500 ft, 110 kt with the flaps retracted. As expected, results in Figure D.32 match Figure D.22 and Figure D.23 in Task 2.

In the second phase of flight, the aircraft was slowed from an initial velocity of 110 to 80 kt and the flaps were then extended from 0° to 20°. D-ICES experienced no false positives during this scenario as seen in Figure D.33. The clean aircraft tests experienced little change due to the dynamic flight conditions.

The next phase of flight examined a heading change from 090° to 045°. Here a false negative was seen for the iced airplane with no turbulence, as shown in Figure D.34. The value of the Theil inequality coefficient for elevator deflection is a measure of how well the actual elevator time history matches the predicted time history for an uniced airplane. For an uniced airplane, the elevator deflection time history should be virtually identical to the D-ICES predicted time history. This will produce very low values of the *deU* Theil inequality coefficient. A sample of the elevator and corresponding Theil inequality coefficients for the uniced airplane with light turbulence is shown in Figure D.35. In the lower plot, INV_PitchCmd is the predicted elevator deflection, while δ_e is the actual deflection.

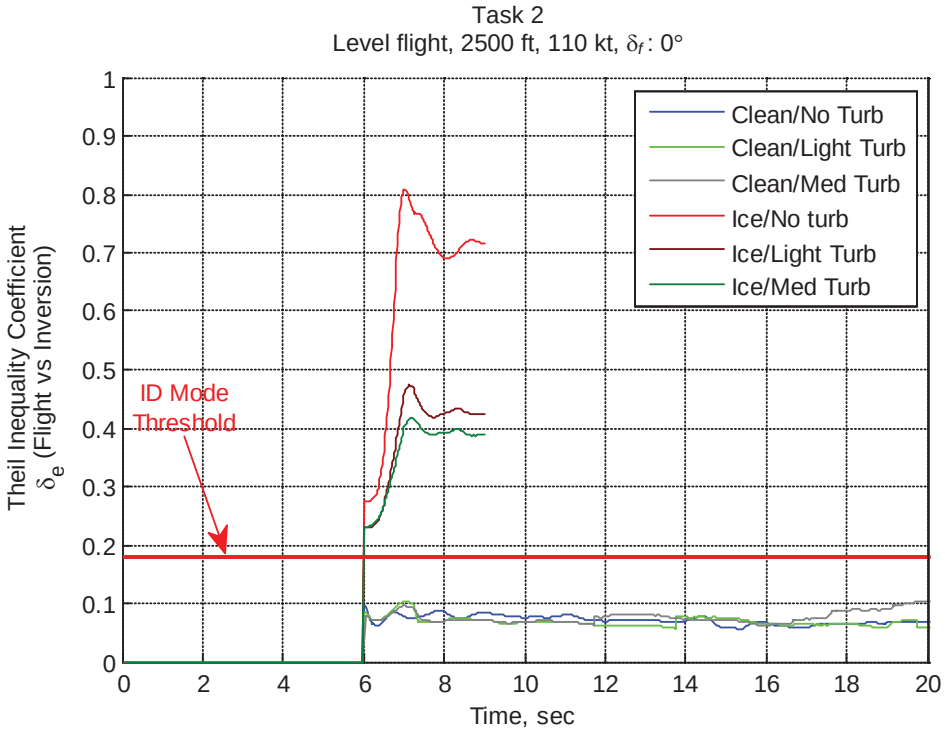

Figure D.32.—D-ICES Level Flight Scenario

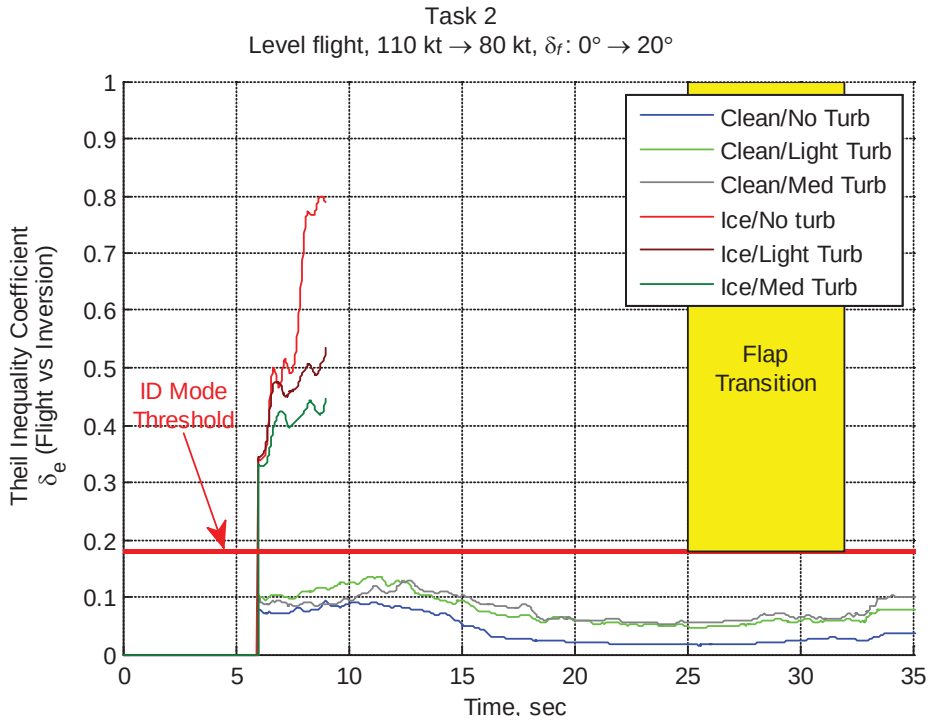

Figure D.33.—D-ICES Flap Transition Scenario

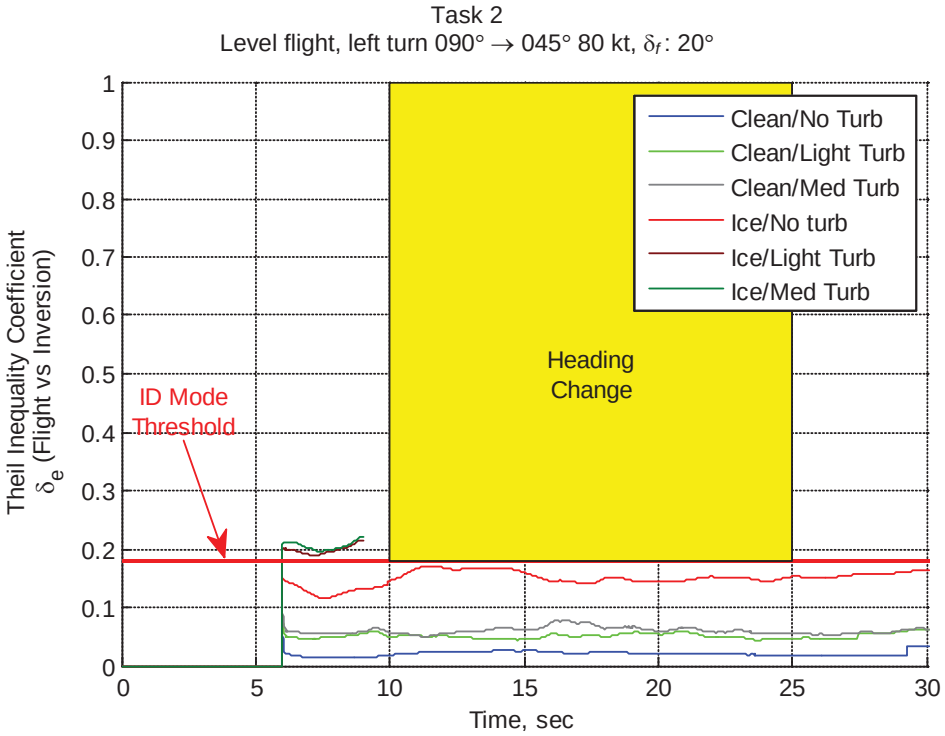

Figure D.34.—D-ICES Heading Change Scenario

For an iced airplane, there should be some differences between the expected (uniced) elevator deflection and the actual deflection. The closer the iced and uniced $C_{m_{\delta e}}$ values are, the less this will be. In Figure D.36, one can see that the actual and predicted elevator deflection were starting to separate

resulting in the larger Theil inequality coefficient values. However, because the iced $C_{m_{\delta e}}$ was not very different from the uniced values at this flight condition, the differences without turbulence were not enough to exceed the threshold. With the addition of turbulence, the elevator deflection separation became greater and resulted in Theil inequality coefficient values that exceeded the threshold. This is probably because the turbulence oscillations caused changes in alphas where there was greater difference between the iced and uniced $C_{m_{\delta e}}$'s.

In the fourth phase of flight, the aircraft was flown down a 3° glide slope from 3000 ft at 75 kt. As the descent was established, the airspeed was reduced from 75 to 70 kt and flaps were then extended to 30°. While there were no false indications, Figure D.37 shows that the D-ICES results remained close to the singular condition seen in the level turning flight case condition. However, the Theil inequality coefficient values are still sufficient to exceed the threshold for transitioning to ID mode for all of the iced conditions.

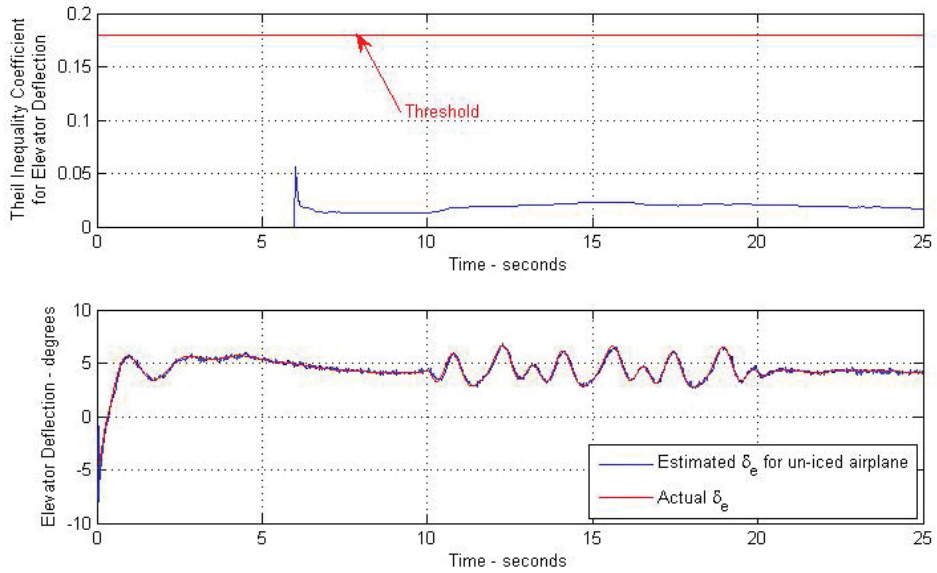

Figure D.35.—Uniced Elevator Deflection Theil inequality Coefficient Analysis

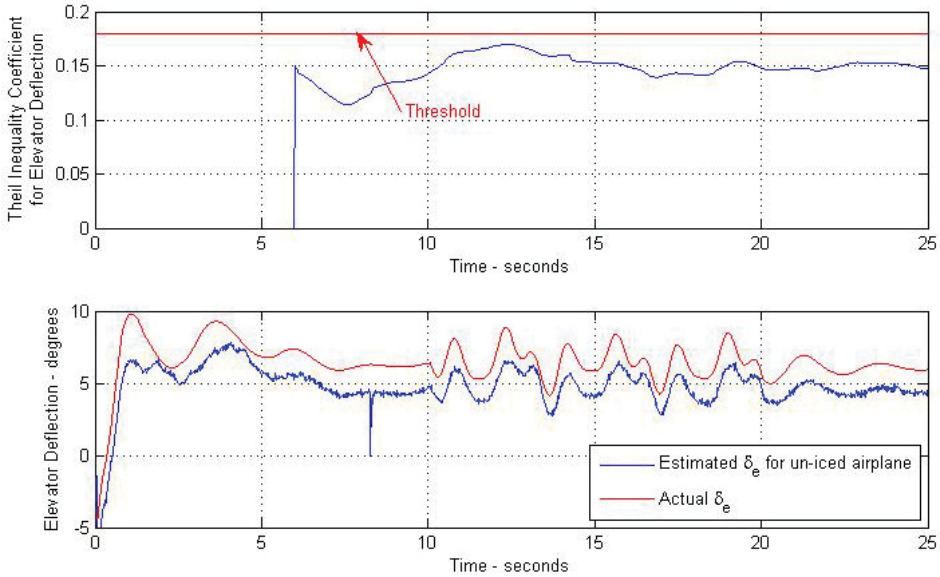

Figure D.36.—Iced Elevator Deflection Theil inequality Coefficient Analysis

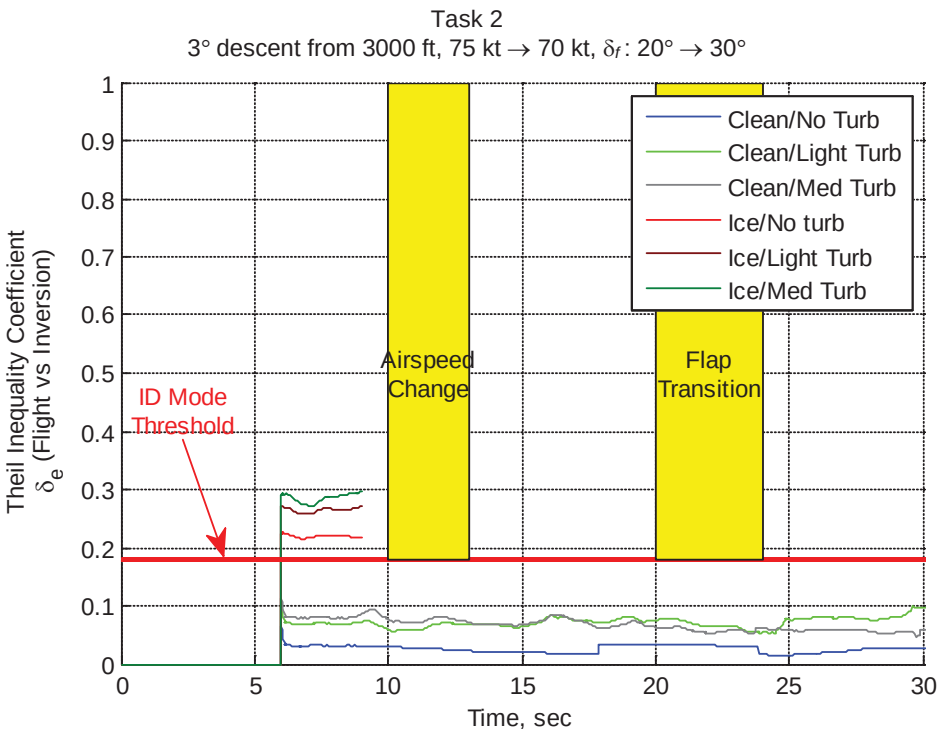

Figure D.37.—D-ICES Descent with Flap Change Scenario

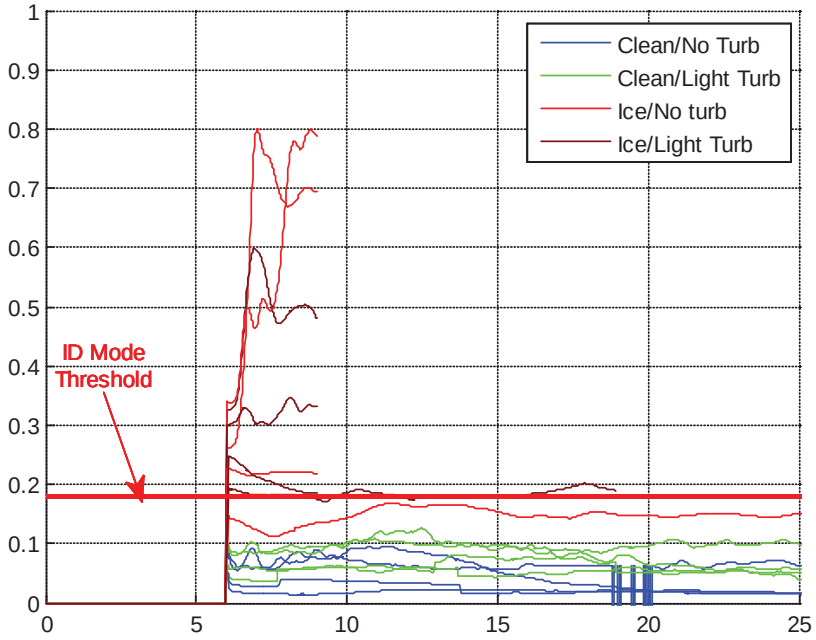

Figure D.38.—D-ICES Task 2 with Random Seed

D.3.3.1.2 Results of 24 Runs Random Seed

Task 3 was rerun using a random seed. Figure D.38, summarizes the results with all four scenarios plotted. Due to occasional low speed stall issues with medium turbulence with the random seed, these conditions were excluded. As expected, the condition that caused the iced aircraft with no turbulence to exhibit a false positive during the heading capture scenario still produced similar results here. Also, with

the random seed, the same scenario light turbulence condition was delayed by 10 sec before latching into ID Mode.

D.3.3.2 RT-PID Study Results

In general, the original MOS criterion for both messages and ISP are not achieved in Task 3 and results are similar to Figure D.27 and Figure D.28 in Task 2. As in Task 2 the new MOS criterion based on AOA brackets and messaging was applied to each flight phase. The results for this task are broken up by respective flight phase.

D.3.3.2.1 Phase 1—Flaps Up Straight and Level Flight

As expected from Task 2 results, Phase 1 runs had no pitch degrade, climb limit, or flap limit messages for zero, light, and moderate turbulence levels.

As shown in Figure D.39, the light turbulence roll degrade message appears before the zero turbulence roll degrade message. Since this is within the 10 sec defined in the MOS this is considered successful. Like Figure D.29 in Task 2, Figure D.39 shows false positives for light and no turbulence cases. This condition was repeated with higher buzzing amplitudes and no false positives occurred. The MOS criterion for AOA bracket was applied to Phase 1 with similar results as shown in Task 2 Figure D.31 and considered to be successful.

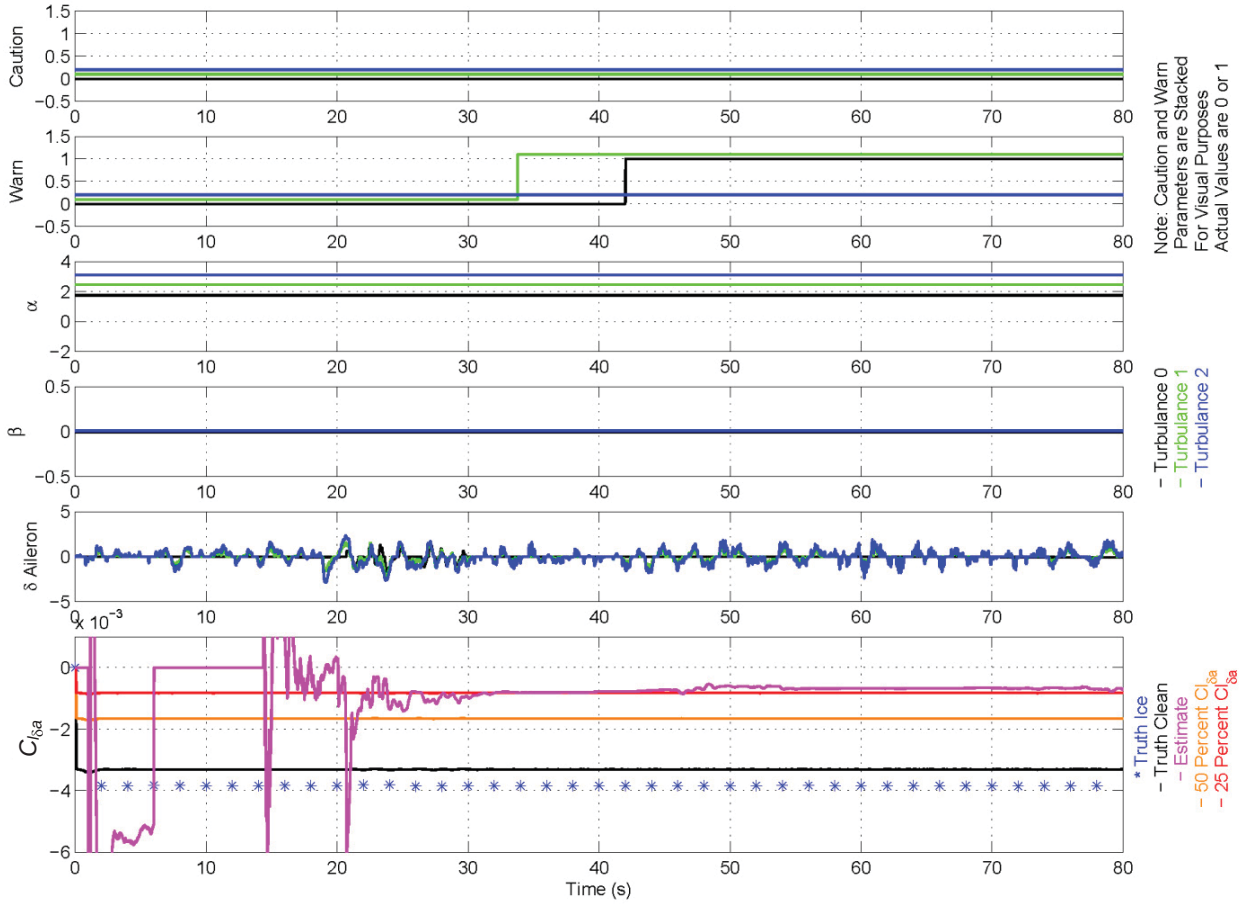

Figure D.39.—Phase 1 Roll degrade indication analyses

D.3.3.2.2 Phase 2—Straight and Level Flight Flap Transition

Phase 2 runs had no pitch degrade, yaw degrade, climb limit, or flap limit messages for zero, light, and moderate turbulence levels. As shown in Figure D.40 the roll degrade message performance in turbulence was better than outside of turbulence. In light and moderate turbulence the system did not annunciate any caution or warning messages. The increase in virtual pilot activity in turbulence during the flap transition provided improved RT-PID performance to that shown in Figure D.40. In Figure D.40 the bottom plot shows poor RT-PID performance in zero turbulence with respect to the truth values due to lack of information content.

As in Task 2, the same AOA bracket locations are expected for all turbulence levels since the aircraft is flown about the same reference condition. In Figure D.41, these are represented by the upper and lower bar delta plots using calm atmosphere as a reference. After approximately 35 sec the flap transition from zero to 20° flap is complete. Incidentally it takes approximately the same amount of time for the ISP to stabilize from start-up as shown at the bottom of Figure D.41. It should be noted that the AOA brackets exhibit similar behavior to that found in Task 2 from 35 to 60 sec and therefore considered to be successful. There are no pitch degrade messages generated during this time because the current ICEPro logic for pitch degrade messaging is based on the elevator effectiveness, $C_{m_{\delta e}}$, which is well within the thresholds such that no messages are generated. Data after 60 sec should be discarded because the virtual pilot is unable to adapt near the tail stall boundary and enters into a pilot coupling event between repeated incipient tail stalls and wing stalls causing the large oscillations shown. Along these lines it should be noted that the virtual pilot gains were set as low as practical while obtain reasonable performance without excessive control activity. A human pilot who is familiar with the aircraft and its flying characteristics may be better suited to control these situations. It is recommended that additional piloted runs be conducted to verify this conclusion by the virtual pilot.

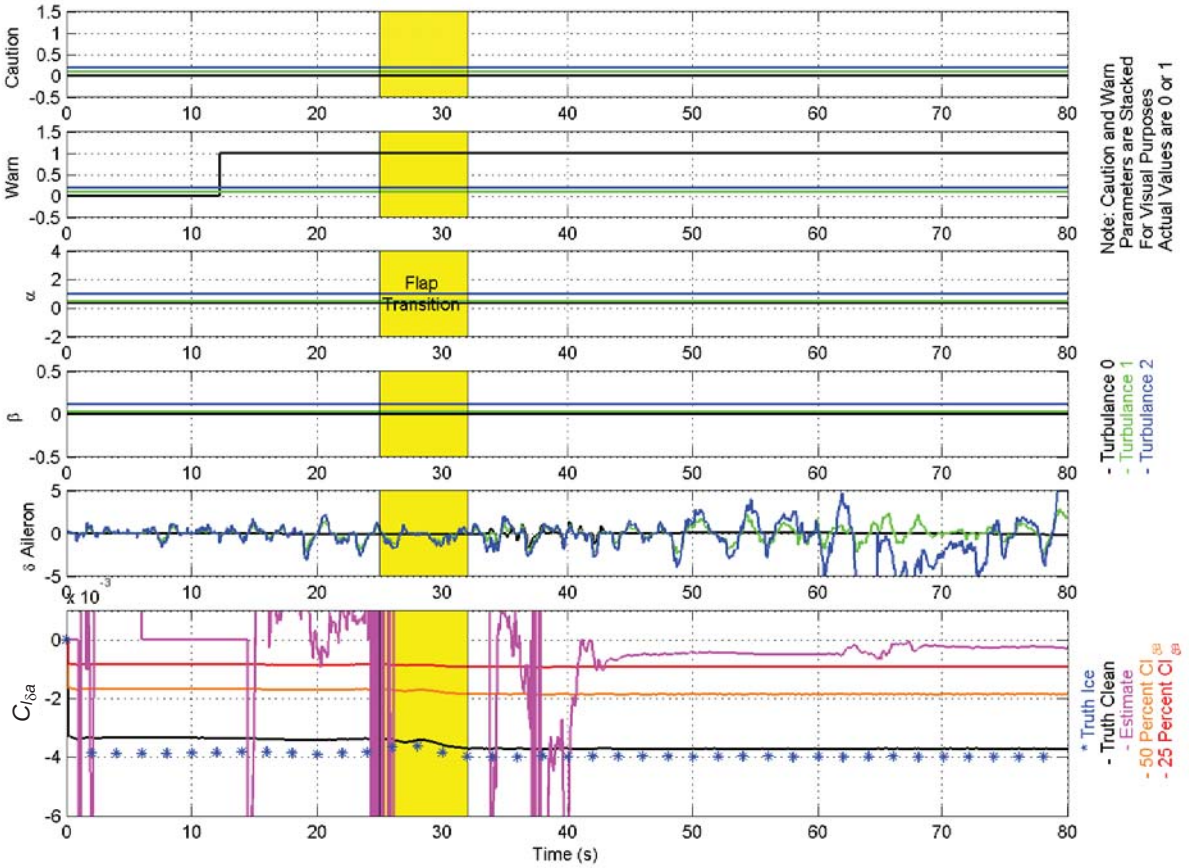

Figure D.40.—Phase 2 Roll degrade indication analyses

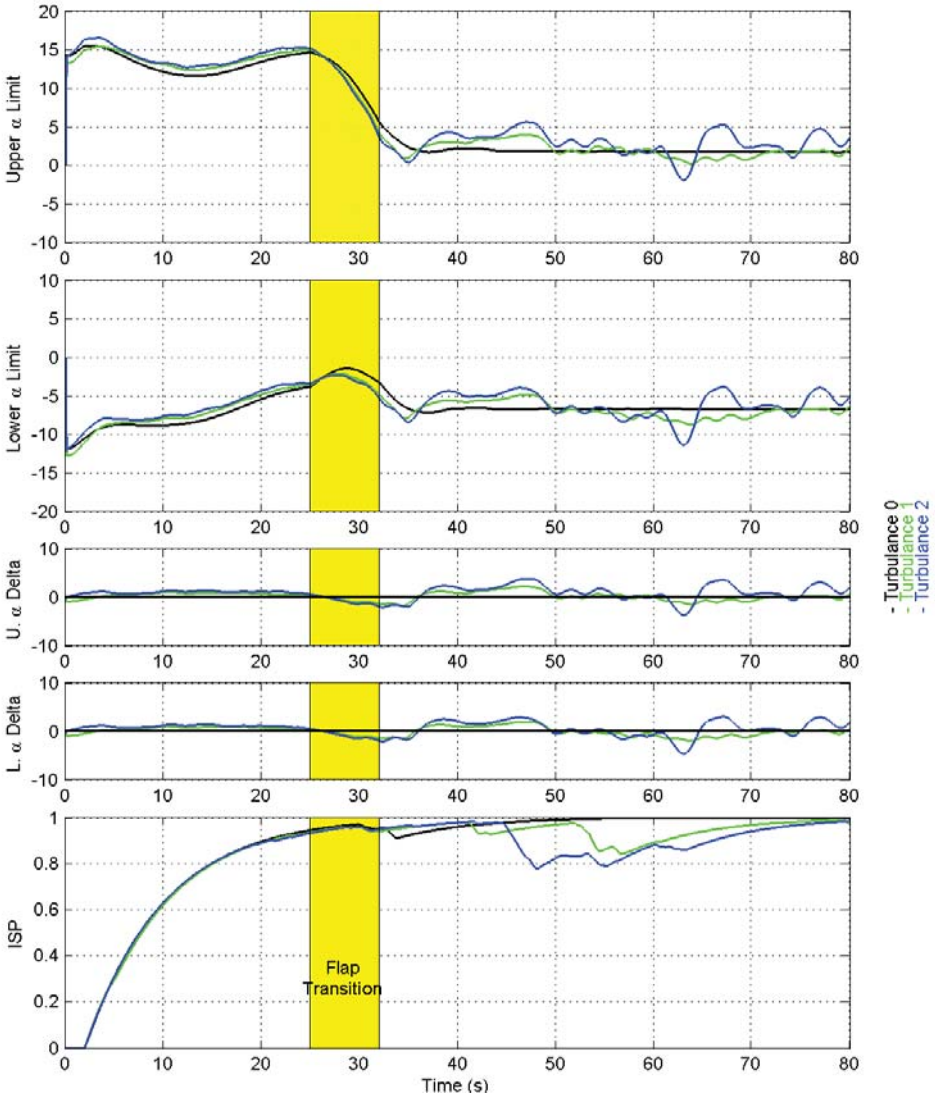

Figure D.41.—Phase 2 AOA bracket analyses

D.3.3.2.3 Phase 3—Straight and Level Flight Heading Capture

Phase 3 runs had no pitch degrade, climb limit, or flap limit messages for zero, light and moderate turbulence levels. As shown in Figure D.42 the roll degrade message performance in turbulence was better than out of turbulence. In light turbulence the system annunciates a caution message and in moderate turbulence the system did not annunciate any caution or warning messages. The increase in virtual pilot activity during the heading capture due to turbulence provided improved RT-PID performance. In Figure D.42 the bottom plot shows poor RT-PID performance in zero turbulence with respect to the truth values due to lack of information content.

Figure D.43 shows a typical run for Phase 3, heading capture. Ice did not greatly affect the rudder effectiveness for this airplane, so it was anticipated that there would be few, if any yaw degrade messages as is shown to be the case in Figure D.43 no messages were generated for any of the heading capture conditions investigated.

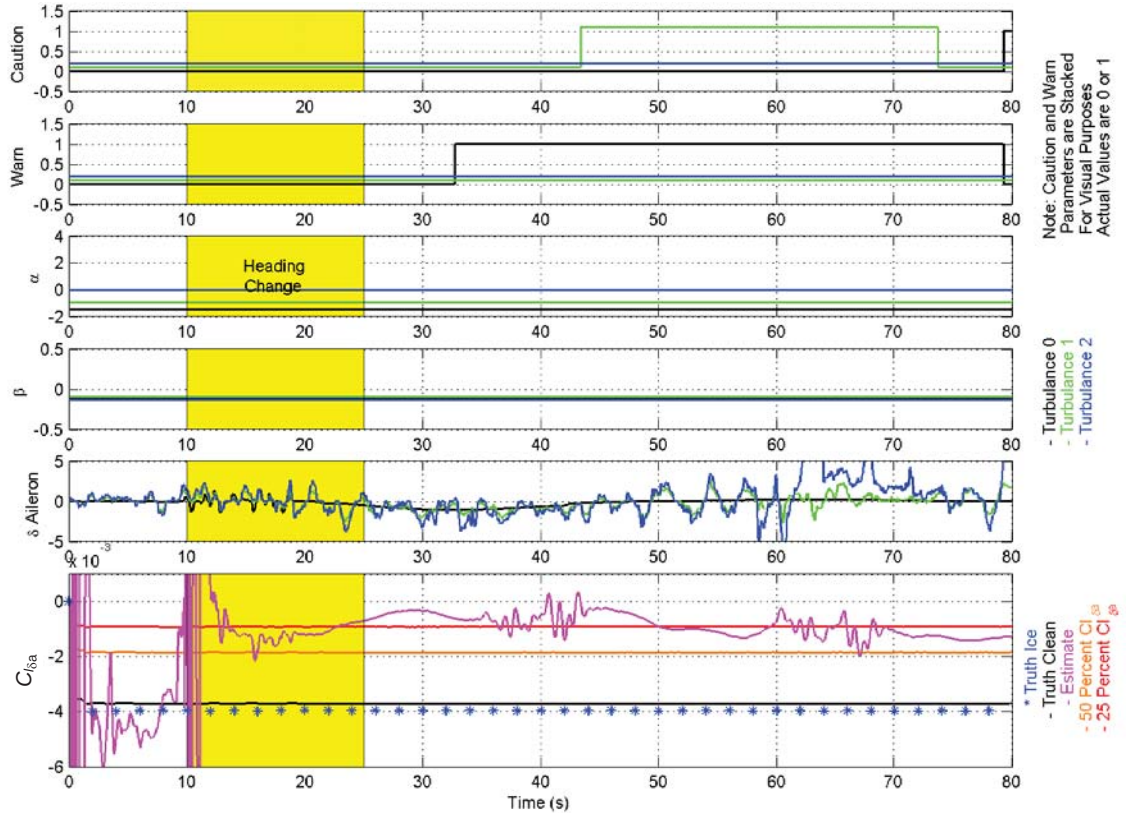

Figure D.42.—Phase 3 Roll degrade indication analyses

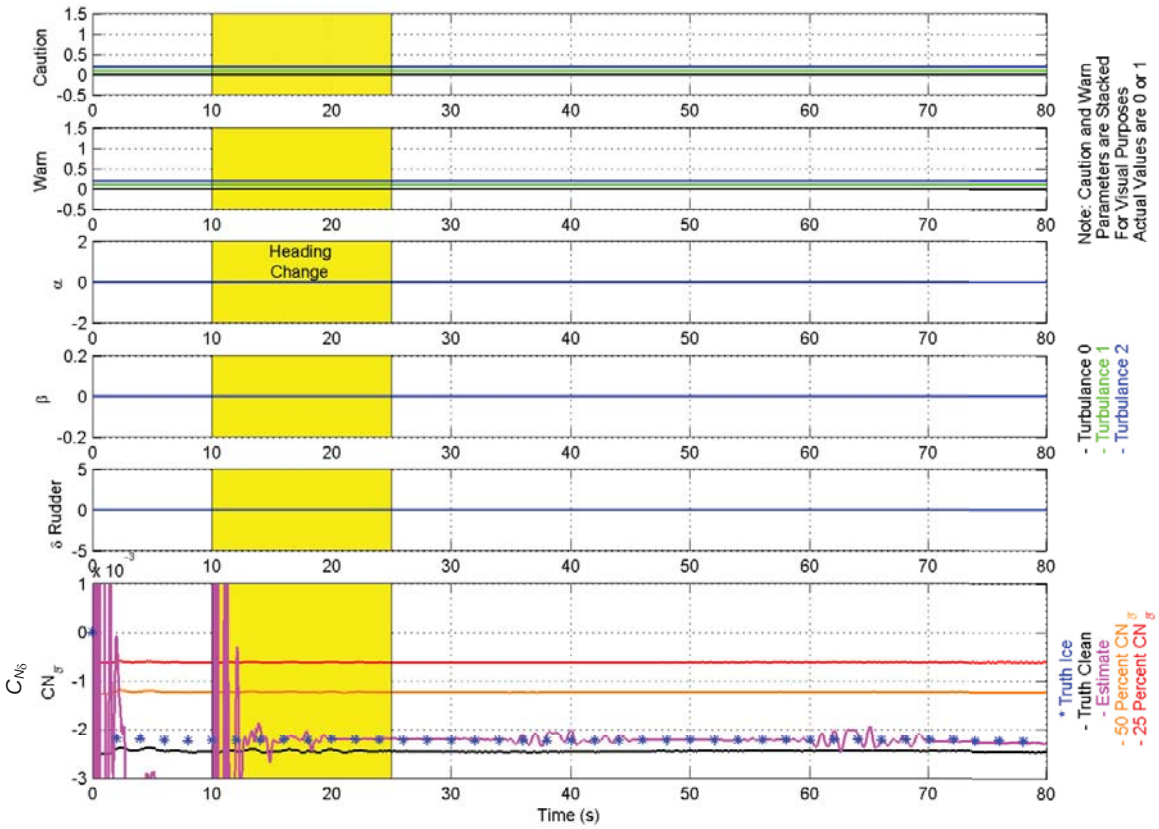

Figure D.43.—Phase 3 Yaw degrade indication analyses

The MOS criterion for AOA bracket was applied to Phase 3 with similar results as shown in Task 2, Figure D.31 and Task 3, Figure D.41 and considered to be successful. Similar to Task 3 Figure D.41 the last 20 sec should be discarded because the virtual pilot is unable to adapt near the tail stall boundary and enters into a pilot coupling event between repeated incipient tail stalls and wing stalls causing large oscillations.

D.3.3.2.4 Phase 4—Descending Flight Flap Transition—3° Glide Slope

Phase 4 runs had no pitch degrade or yaw degrade messages for zero, light or moderate turbulence levels. As shown in Figure D.44 the roll degrade message performance in turbulence was better that out of turbulence. The increase in virtual pilot activity during the heading capture due to turbulence provided improved RT-PID performance. In Figure D.44 the bottom plot shows poor RT-PID performance in zero turbulence with respect to the truth values due to lack of information content.

As shown in Figure D.44 the zero turbulence roll degrade caution and warning messages annunciate before the light turbulence messages. This is considered to be conservative and successful based on MOS criterion. The toggle in the warning message in moderate turbulence is discarded because as before the virtual pilot is unable to adapt near the tail stall boundary and enters into a pilot coupling event between repeated incipient tail stalls and wing stalls. Because the elevator effectiveness during this maneuver stays within the thresholds for caution and warning messages, no pitch degrade messages are generated.

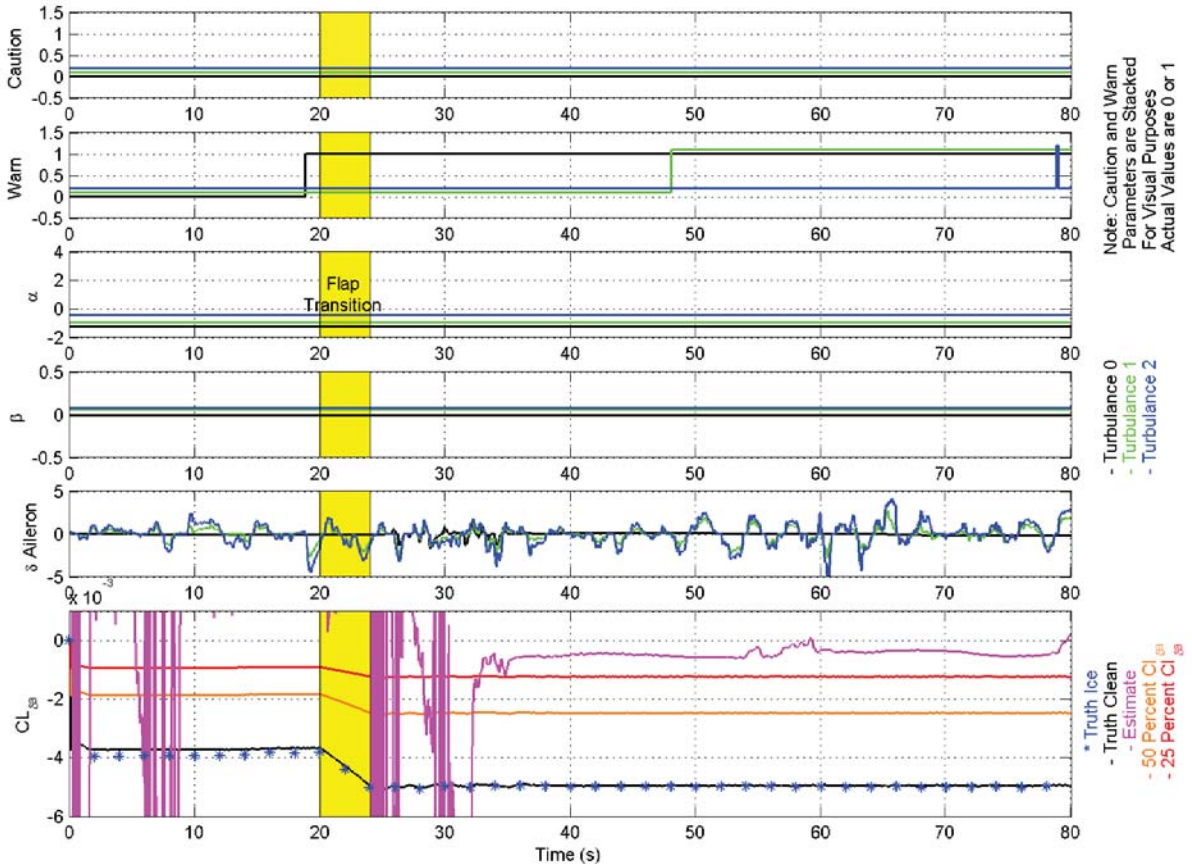

Figure D.44.—Phase 4 Roll degrade indication analyses

As shown in Figure D.45 the zero turbulence climb limit warning message annunciated at the same time as in light turbulence. This is considered to be successful based on the MOS criterion. In moderate turbulence the warning message came on for approximately 7 sec. The ICEPro message logic requires messages to persist for 10 sec before they can unlatch, however, when a stall is detected by ICEPro, it declutters the PFD by removing all other messaging for 20 sec to allow the pilot to regain normal flight. After that time, ICEPro returns to normal messaging. In the situation shown in Figure D.45, a stall condition occurred which terminated the messaging.

As shown in Figure D.46 the zero turbulence flap limit warning message annunciates at the same time as in light turbulence. This is considered to be successful based on the MOS criterion. As in the climb limit message, in the moderate turbulence case the warning message came on for approximately 7 sec. The ICEPro message logic requires messages to persist for 10 sec before they can unlatch. The stall condition resulted in decluttering the PFD and removed the message after 7 sec, as discussed above.

The MOS criterion for AOA bracket was applied to Phase 4 and shown in Figure D.47. After approximately 30 sec the flap transition from 20 to 30° flap is complete. Incidentally it takes approximately the same amount of time for the ISP to stabilize from start-up as show at the bottom of Figure D.47. It is believed that the increased oscillations in Phase 4 AOA brackets over previous phases is because of the narrow envelope between wing stall and tail stall at flaps 30°. The inability to adapt by the virtual pilot in this reduced stability regime causes larger oscillations. Applying the MOS criterion would be unsuccessful in this phase since a pilot is able to discern the unconservative variation in the AOA brackets. It is recommended that additional piloted runs be conducted to verify this conclusion by the virtual pilot.

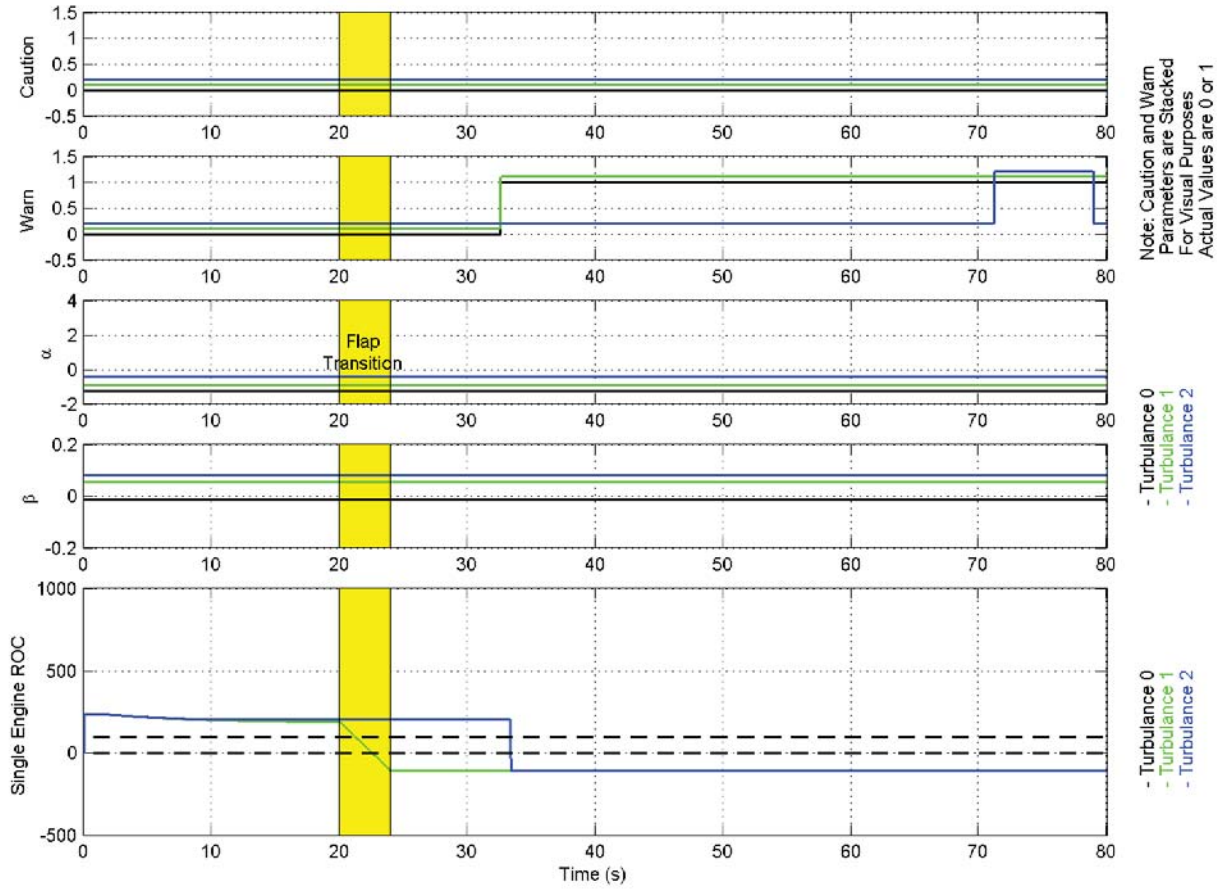

Figure D.45.—Phase 4 Climb Limit indication analyses

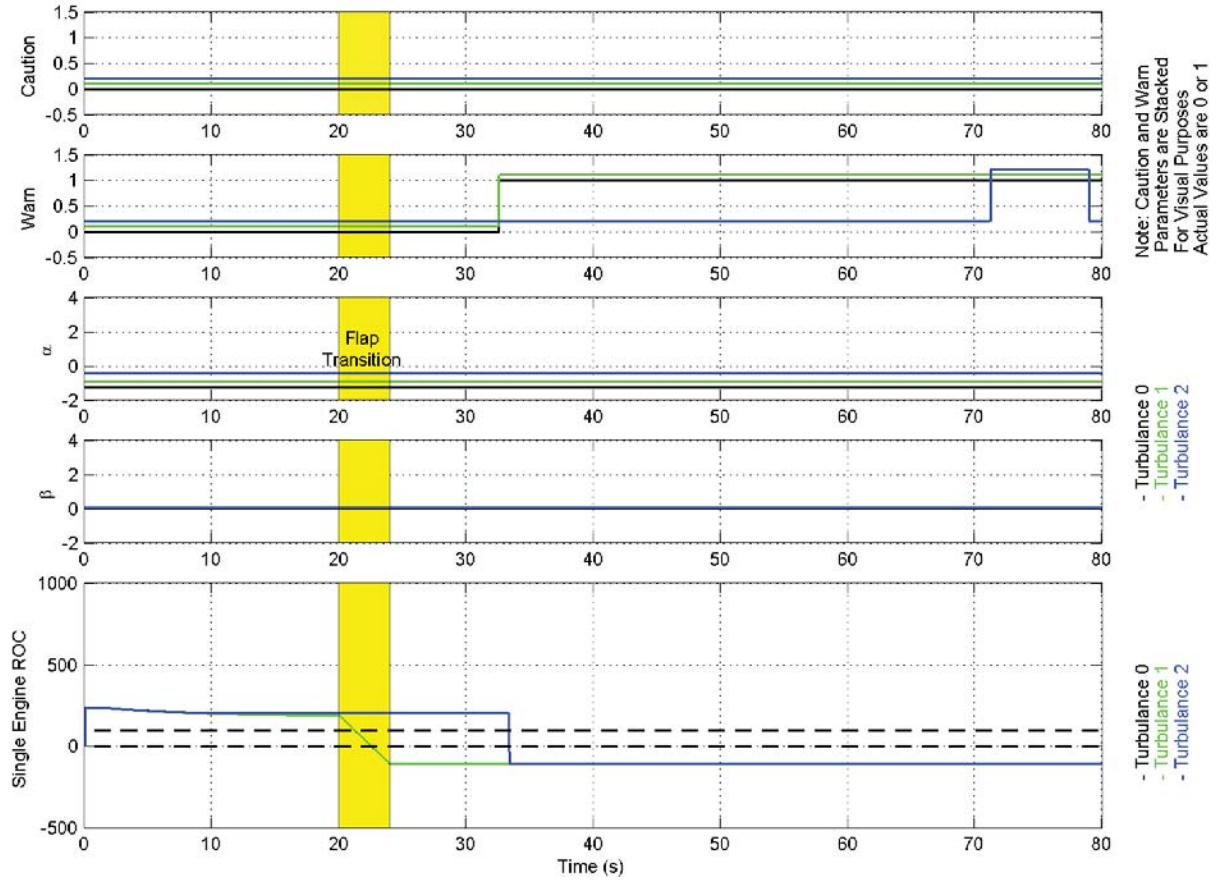

Figure D.46.—Phase 4 Flap Limit indication analyses

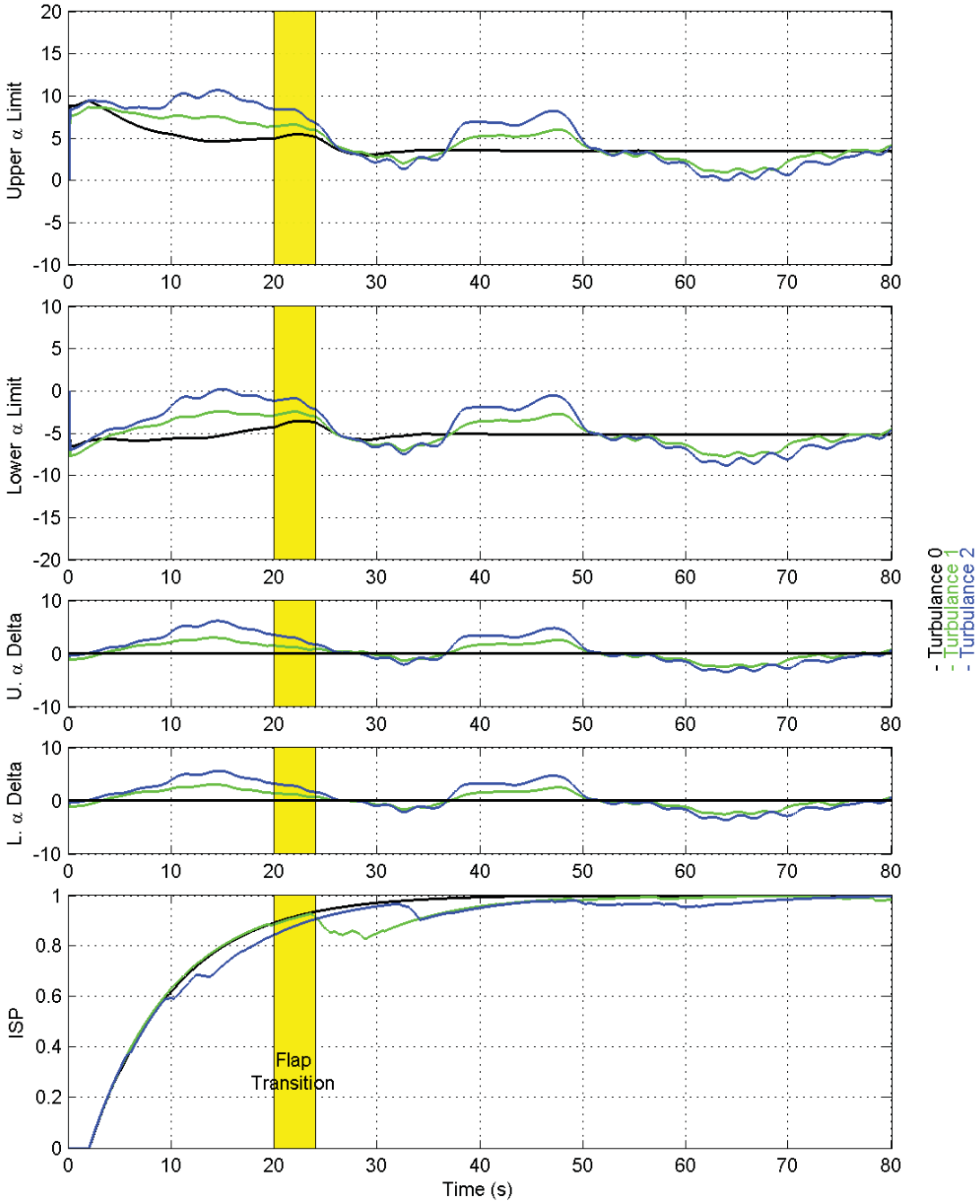

Figure D.47.—Phase 4 AOA bracket analyses

D.3.3.3 Task 3 Conclusions

D-ICES

- The first scenario was a repeat of Task 2 conditions and the results were similar.
- For the level flight flap extension scenario, the aircraft was slowed from an initial velocity of 110 to 80 kt and the flaps were then extended from 0° to 20°. D-ICES experienced no false positives during this scenario as seen in Figure D.33
- The next scenario examined was a heading change from 090° to 045°. Here a false negative was seen for the iced airplane with no turbulence but correctly predicted positives for the low and mid

turbulence levels. The false positive was believed to be due to a singular condition where there was little difference between the iced and clean airplane's control effectiveness at the chosen flight condition.
- For the 3° glide slope descent scenario there were no false indications, even though the results remained close to a singular condition seen in the level turning flight case. However, the Theil inequality coefficient values are still sufficient to exceed the threshold for transitioning to ID mode for all of the iced conditions.
- In most cases, D-ICES performed as designed in the presence of turbulence and noise. However, the exceptions noted above, especially the false negatives, do indicate that some further development of the system is warranted. One possible area to examine would be utilizing other terms related to the Theil inequality coefficient, namely the bias, variance and co-variance terms in some way to develop a more robust detection scheme.

RT-PID

- Phase 1 runs had no pitch degrade, climb limit, or flap limit messages for zero, light, and moderate turbulence levels. The MOS criterion for AOA bracket was applied to Phase 1 and considered to be successful.
- Phase 2 runs had no pitch degrade, yaw degrade, climb limit, or flap limit messages for zero, light, and moderate turbulence levels. The MOS criterion for AOA bracket was applied to Phase 2 and therefore considered to be successful.
- Phase 3 runs had no pitch degrade, climb limit, or flap limit messages for zero, light, and moderate turbulence levels. The MOS criterion for AOA bracket was applied to Phase 3 and considered to be successful.
- Phase 4 runs had no pitch degrade or yaw degrade messages for zero, light, and moderate turbulence levels. As shown in Figure D.46 the calm atmosphere flap limit warning message annunciates at the same time as in light turbulence. This is considered to be successful based on the MOS criterion. The MOS criterion for AOA bracket was applied to Phase 4: Applying the MOS criterion would be unsuccessful in this phase since a pilot is able to discern the unconservative variation in the AOA brackets.
- It is recommended that additional piloted runs be conducted to verify this conclusion by the virtual pilot.

In general, it was found that the performance of the AIMMS-20 probe was satisfactory for Task 3.

D.4 Conclusions and Recommendations

Summaries are provided of the results of each task. For Task 2 and Task 3 the summaries are divided into D-ICES and RT-PID.

D.4.1 Summary of Results

Task 1

Several practical issues related to real-time parameter estimation for a linear longitudinal dynamics model in atmospheric turbulence using indirect turbulence measurements were examined and discussed. The frequency response of the airflow vanes, wing response to atmospheric turbulence, and the structural response of the air data boom were identified as sources of colored noise. The frequency response of the airflow vanes for a wide variety of combinations of natural frequency and damping ratio did not adversely impact parameter estimation results in turbulence, except for C_{Z_q} and $C_{Z_{\delta e}}$. This was attributed to noisy explanatory variables in the atmospheric turbulence implementation and relatively low aerodynamic contributions as compared to C_{Z_α}. Airflow vane dynamics do not substantially contribute to the scatter in the estimates, because all of the added dynamics are outside the range of frequencies analyzed. The

structural modes of the boom lead to similar conclusions, because the natural frequencies of the boom structural modes are outside the range of frequencies used for dynamic modeling. A major source of colored noise was identified as the frequency-dependent upwash and time delay induced by the wing-bound vortex system and the longitudinal separation between the AOA measurement and the wing. It was also surmised that the frequency-dependent sidewash was a major source of colored noise. The frequency-dependent upwash and time delay appear to be significant contributors to biasing and increased scatter and uncertainty for parameter estimates in atmospheric turbulence.

Practical issues were examined using data from a Twin Otter DHC-6 longitudinal linear simulation, with realistic noise sequences added to the computed aircraft responses. This allowed a clear view of the effect of each source of colored noise to the modeling problem, because the true values of the model parameters were known. This approach was used initially to show that real-time parameter estimation can be done accurately in all atmospheric turbulence conditions if the AOA measurement is accurate. Flight test data from the GRC DHC-6 Twin Otter aircraft was used to validate the effect of the identified colored noise sources.

Based on these findings, several practical recommendations for flight testing in atmospheric turbulence are suggested, as well as areas for future study. First, mount the air data boom at the nose of the aircraft to minimize the effect of the wing-bound and wing-tip vortices. Second, if the air data boom is mounted on the nose of the aircraft, an upwash and time delay calibration as a function of frequency is required.

Task 2

D-ICES

- It was found that the application of turbulence and sensor noise on D-ICES generally had a minimal impact on performance without filtering.
    - Only one condition was found that yielded a false positive that would have caused the system to enter ID Mode when no icing was present.
    - There was one condition where the elevator deflection Theil inequality coefficient for an iced airplane failed to exceed the threshold and two where the value originally exceeded the threshold but with time decreased until it was below the threshold.
- When the state vectors going to the D-ICES inversion routine were filtered to remove higher frequency disturbances due to turbulence and noise, D-ICES accurately detected all icing conditions in the presence of turbulence and sensor noise and thus operated correctly.
- Three potential false positive cases were found that showed the elevator Theil Coefficient built up over time to exceed the threshold when no ice was present. An examination of the data in this region led to supposition that the D-ICES inversion process had some troubles in determining the correct elevator deflection with the pitch due to elevator characteristics at those flight conditions.

RT-PID

- In general, the (Old) RT-PID MOS for message accuracy was not achieved. A new MOS criterion was formulated due to results depicted in Figure D.27 and Figure D.28.
- Errors in the estimates and in the error bounds with turbulence are tolerated as long as the ICEPro messages and AOA brackets are equivalently displayed inside and outside of turbulence (New MOS).
- In practice, for zero, light, and moderate turbulence the average flow angles are similar. In severe turbulence, the average flow angles are significantly different due to wing stall, but do not affect the message accuracy.
- With the exception of the Roll degrade message, there were no false positives or false negatives.
- In each of the turbulence cases, the additional aileron inputs provided by the virtual pilot improved the RT-PID estimates so that no false positives were annunciated.

- In general the new MOS message criterion is considered to be successful.

Overall it was found that the objective to identify an acceptable error in the wind measurement was not required and that the performance of the AIMMS-20 probe was satisfactory for Task 2.

Task 3

D-ICES

- For the level flight flap extension scenario, the aircraft was slowed from an initial velocity of 110 to 80 kt and the flaps were then extended from 0° to 20°. D-ICES experienced no false positives during this scenario as seen in Figure D.33.
- The next scenario examined was a heading change from 090° to 045°. Here a false negative was seen for the iced airplane with no turbulence but correctly predicted positives for the low and mid turbulence levels. The false positive was believed to be due to a singular condition where there was little difference between the iced and clean airplane's control effectiveness at the chosen flight condition.
- For the 3° glide slope descent scenario there were no false indications, even though the results remained close to a singular condition seen in the level turning flight case. However, the Theil inequality coefficient values are still sufficient to exceed the threshold for transitioning to ID mode for all of the iced conditions.

RT-PID

- Phase 1 runs had no pitch degrade, climb limit, or flap limit messages for zero, light, and moderate turbulence levels. The MOS criterion for AOA bracket was applied to Phase 1 and considered to be successful.
- Phase 2 runs had no pitch degrade, yaw degrade, climb limit, or flap limit messages for zero, light, and moderate turbulence levels. The MOS criterion for AOA bracket was applied to Phase 2 and therefore considered to be successful.
- Phase 3 runs had no pitch degrade, climb limit, or flap limit messages for zero, light, and moderate turbulence levels. The MOS criterion for AOA bracket was applied to Phase 3 and considered to be successful.
- Phase 4 runs had no pitch degrade or yaw degrade messages for zero, light or moderate turbulence levels. As shown in Figure D.46 the calm atmosphere flap limit warning message annunciates at the same time as in light turbulence. This is considered to be successful based on the MOS criterion. The MOS criterion for AOA bracket was applied to Phase 4: Applying the MOS criterion would be unsuccessful in this phase since a pilot is able to discern the unconservative variation in the AOA brackets.
- It is recommended that additional piloted runs be conducted to verify this conclusion by the virtual pilot.

In general, it was found that the performance of the AIMMS-20 probe was satisfactory for Tasks 2 and 3. Acceptable error is therefore defined by current specification of AIMMS-20 probe. As long as booms are not used and the calibration for wing response to turbulence has been taken care of the system will work.

D.4.2 Additional Questions Raised by Research

1. What is the calibration accuracy required of the wing response to turbulence for RT-PID estimates to be within ± 10 percent?
2. What is the boom stiffness required for RT-PID estimates to be within ± 10 percent
3. How can the other terms related to the Theil inequality coefficient, namely the bias, variance and co-variance terms be used to develop a more robust detection scheme.

D.4.3 Recommended Future Studies

1. Execute Task 4. This task evaluates the effectiveness of manual pilot inputs alone for making high confidence vehicle state estimates when performing typical maneuvering flight tasks under varying levels of atmospheric turbulence.
2. Flight test to validate RT-PID findings based on colored AOA regressor findings.
3. Flight test to validate ICEPro.

D.5 References

1. Lawless, Al, "Inertial-Based Instrumentation for Performance Flight Testing," *SFTE Symposium XX Proceedings*, 2008.
2. Olson, Wayne, "Aircraft Performance Flight Testing," AFFTC-TIH-99-01.
3. Advisory Group for Aeronautical Research and Development, "Flying Qualities Flight Testing of Digital Flight Control Systems," *Flight Test Techniques Series – RTO AG-300*, Volume 21, pp. 58-60, Dec, 2001.
4. Mathworks, "Dryden Wind Turbulence Model (Discrete)" [http://www.mathworks.com/help/toolbox/aeroblks/drydenwindturbulencemodeldiscrete.html. Accessed 1/20/12.]
5. Maine, R. E. and Iliff, K. W., "Formulation and Implementation of a Practical Algorithm for Parameter Estimation with Process and Measurement Noise," SIAM Journal of Applied Mathematics, Vol. 41, No. 3, 1981, pp. 558-579.
6. Maine, R.E. and Iliff, K.W., "Identification of Dynamic Systems," AGARD AG-300 Vol. 2, Jan. 1985.
7. Crawford, T.L., and R. J. Dobosy, 1992: A sensitive fast-response probe to measure turbulence and heat flux from any airplane. J. Boundary Layer Meteorology, 59, 257–278.
8. Kalogiros, John A., Qing Wang, 2002: Aerodynamic Effects on Wind Turbulence Measurements with Research Aircraft. J. Atmos. Oceanic Technol., 19, 1567–1576.
9. Kalogiros, J. A., and Q. Wang, 2002: Calibration of a radome-differential GPS system on a Twin Otter research aircraft for turbulence measurements. J. Atmos. Oceanic Technol., 19, 159–171.
10. Lenschow, D.H., 1971: Vanes for sensing incidence angles of the air from an aircraft. Journal of Applied Meteorology 1989-2005 (After 2005 - Journal of Applied Meteorology and Climatology), **10**, pp. 1339–1343.
11. Sakamoto, G.M., "Aerodynamic Characteristics of a Vane Flow Angularity Sensor System Capable of Measuring Flight Path Accelerations for the Mach Number Range from 0.40 to 2.54," NASA TN-D8242, 1976.
12. Foster, G.W, "The Identification of Aircraft Stability and Control Parameters in Turbulence," Ph.D Thesis, Cranfield Institute of Technology, 1982.
13. Iliff, K.W., Maine, R.E., and Montgomery, T.D., "Important Factors in the Maximum Likelihood Analysis of Flight Test Maneuvers," NASA TM-1459, 1979.
14. Klein, V and Morelli, E.A., Aircraft System Identification Theory and Practice, AIAA Education Series, Reston, VA, 2006.
15. Morelli, E.A., "Practical Aspects of the Equation-Error Method for Aircraft Parameter Estimation," AIAA-2006-6144.
16. Steers, S.T. and Iliff, K.W., "Effects of Time-Shifted Data on Flight-Determined Stability and Control Derivatives," NASA TN D-7830, 1975.

Appendix E.—ICEPro Atmospheric Turbulence Test Plan

VSST – 1 Year Extension

Borja Martos
Aviation Systems and Flight Research
University of Tennessee Space Institute
MAY 2011

E.1 Abstract

The effects of atmospheric turbulence on the RT-PID and D-ICES algorithms are studied by modeling representative atmospheric turbulence. Atmospheric turbulence is measured directly as an input to both methods. The performance of these algorithms is evaluated using reasonable assumptions for measurements from currently-available turbulence sensors in operational flight. Methods for improving the performance of these algorithms in these conditions are implemented and studied.

E.2 Introduction

E.2.1 Background

A team comprised of personnel from The University of Tennessee Space Institute (UTSI), Tullahoma, Tennessee, Bihrle Applied Research Inc (BAR), Hampton, Virginia, NASA Glenn Research Center (GRC), Cleveland, Ohio, and NASA Langley Research Center (LaRC), Hampton, Virginia, has successfully developed a prototype Ice Contamination Envelope Protection System (ICEPro). The ICEPro system facilitates flight envelope protection by making continuous real time vehicle state assessments, which are synthesized into flyable pilot cueing along with visual and aural alerts during in-flight icing conditions. Detection of degraded aircraft stability and control and performance due to icing is carried out by a dynamic inversion control evaluation system (D-ICES) that compares expected aircraft behavior from *a-priori* knowledge base with current measures of those behaviors. When differences reach defined thresholds, real time parameter identification (RT-PID) methods are invoked to estimate current state parameters, which continuously support pilot cueing and alerts. The development effort included simulation-based design, testing, and verification. A pilot in-the-loop study was conducted to gather pilot performance data and opinions of the utility of ICEPro during simulated icing encounters. Results of the study indicated that the system performed as expected and pilot performance benefited from the envelope protection cues. However, the simulation could not duplicate all of the real-world conditions that could have first-order effects on system performance, such as those due to real atmospheric turbulence. Therefore, in order to assess system performance under these conditions and minimize the technical risk of an eventual flight-test validation program, the effects of atmospheric turbulence on ICEPro are studied.

E.2.2 Participating Organizations

The following organizations will provide simulator flight test support and facilities.

UTSI: Is one of the primary organizations and facilities for simulator flight testing and algorithm development of the ICEPro system. The basis for the simulator flight tests will be a COTS desktop simulator running BAR's D-six software and representative flight controls, visuals, and virtual aircraft instruments.

BAR: Is one of the primary organizations for algorithm and software development of the ICEPro system. The basis for algorithm and software development will be a COTS desktop simulator running BAR's D-Six software and representative flight controls, visuals, and virtual aircraft instruments.

GRC: Will provide technical monitoring and serve as the NASA focal point for this grant.

LaRC: Will provide technical assistant with real-time parameter identification algorithms.

E.2.3 Overview of Test Concepts

Simulator Flight Test

The ICEPro systems software will be tested in Birhle's D-six software environment. Software will be tested both at UTSI and BAR. In support of these tests, BAR will provide the following:

1. Update the ICEPro software so that desktop simulations at BAR and UTSI match the ICEFTD.

2. Update the ICEPro system logic diagram.
3. Synchronize system software between UTSI and BAR as software changes are made.
4. Author release notes documents with each software revision and update the system logic diagram were appropriate.

E.2.4 Outline of Document

The remainder of this document is divided into two parts. Section E.3 contains the simulator flight test plan and Section E.4 contains the simulator flight test tasks.

E.3 Simulator Flight Tests

E.3.1 Test Objectives

The primary objectives of the simulator flight tests are to assess the performance of RT-PID and D-ICES algorithms in the presence of atmospheric turbulence and determine methods for improving algorithm performance in these conditions. The simulations will be based on events that cannot be repeatedly duplicated during flight testing and benefit from a controlled environment.

The secondary objective is to access the performance of RT-PID and D-ICES algorithms in the absence of an onboard excitation system (OBES) with and without atmospheric turbulence.

E.3.2 Test Guidelines

E.3.2.1 Primary Objectives

E.3.2.1.1 Performance Testing in Turbulence

The performance of the RT-PID and D-ICES algorithms will be assessed by flying a low gain and a high gain pilot-in-the-loop task in the presence of atmospheric turbulence. The low gain task is straight and level unaccelerated flight with the flaps retracted. The high gain task is the final segment of an instrument approach. This represents a descent from the final approach fix to the inner marker and requires tight control of the glide slope and localizer. Both tasks will be performed under Visual Meteorological Conditions (VMC) conditions. Prior to these tasks, a UTSI pilot will train to ensure proficiency in basic instrument flying skills and can perform a precision approach within Airline Transport Pilot (ATP) standards.

E.3.2.1.2 Development of Algorithms for Atmospheric Turbulence

To develop RT-PID and D-ICES algorithms in the presence of atmospheric turbulence this study will utilize the previous pilot in-the-loop test scenario. A copy of this scenario is found in Figure E.1. However, to coordinate testing and algorithm and software development between UTSI and BAR, the test scenario will be broken up into a series of segments or phases of flight. These will consist of straight and level unaccelerated flight, flap transition, heading capture, descent, and glide slope and localizer tracking. The use of autopilots will provide a standardized pilot performance model for batch testing at UTSI and BAR.

E.3.2.2 Secondary Objectives

E.3.2.2.1 Preliminary Feasibility Study Without OBES

Finally, the updated RT-PID and D-ICES algorithms will be assessed in the in the presence of atmospheric turbulence, with a pilot-in-the-loop, with and without an on board excitation system. The algorithms will be assessed by the same pilot-in-the-loop low gain and high gain tasks as in the initial task. Additionally, a UTSI pilot will be under the same training and flying standards as previously mentioned.

E.3.3 Performance Parameters to be Measured

All flight data will be recorded at 50 Hz. The following parameters will be recorded and calculated.

1. OBES frequency and duration
2. ISP value
3. Error in ISP parameters
   a. $C_{m\alpha}$ Longitudinal Static Stability
   b. $C_{m\delta e}$ Elevator Control Power
   c. $C_{l\beta}$ Dihedral Effect
   d. $C_{l\delta a}$ Aileron Control Power
   e. $C_{N\alpha}$ Normal Lift Coefficient
4. Error in Message parameters
5. Glide slope and localizer performance
6. Airspeed performance
7. Number of AOA exceedances
   a. Stick shaker and stick pusher firings
   b. STALL message postings
   c. Tail stall events

E.3.4 Measures of Success (MOS)

To ensure that test objectives are attained, MOS's have been formulated. A MOS is defined as a comparative requirement which must be satisfied by the results of testing. The overall measure of success for the primary and secondary objectives will be that the error bounds and accuracy in RT-PID and Theil inequality coefficients in D-ICES algorithms meets or exceeds its non-atmospheric turbulence performance in atmospheric turbulence. This success criterion focuses on the performance of these two algorithms and not on ICEPro's utility to mitigate a potentially hazardous icing encounter or on the pilot's performance during such encounter. It assumes that if the RT-PID and D-ICES algorithms perform equally in and out of atmospheric turbulence the ICEPro system will perform equally. The following MOS are defined for the primary objective.

RT-PID Algorithm

5. Message accuracy

   Message error will be determined by the error bounds and accuracy of its associated stability and control coefficient. For example, the red pitch degrade logic is a function of elevator control power

$$C_{m\delta e} \geq 0.25 C_{m\delta e\_\text{no ice}}$$

   The elevator control power must meet or exceed its non-atmospheric turbulence error bound and accuracy in atmospheric turbulence. This is repeated for all ICEPro messages.

6. ISP accuracy

   ISP error will be determined by comparing the true ISP value with the estimated ISP value. ISP is a function of five stability and control coefficients: Longitudinal static stability, elevator control power, dihedral effect, aileron control power, and normal lift coefficient. The true ISP value is known since the five true stability and control parameters are known to the simulation. The ISP error must meet or exceed its non-atmospheric turbulence error bound and accuracy in atmospheric turbulence.

D-ICES Algorithm

2. Control deflection accuracy

   Control deflection error is determined by comparing the estimated deflection Theil inequality coefficient with the baseline no turbulence case. The control deflection error must meet or exceed its non-atmospheric turbulence error in atmospheric turbulence.

E.3.5 Organizational Responsibilities

The organizational responsibilities for each task are stated in Section E.4. Through each task the responsible party's name is highlighted by parenthesis.

E.4 Simulator Flight Test Tasks

E.4.1 Task 1 (UTSI)

Determine whether the scatter in the turbulence estimates arise from, 1) colored noise in the regressor(s), and if so what is the source of the colored noise and in which regressor(s), 2) insufficient model structure, and if so how should the model structure be adjusted or, 3) some other means.

E.4.2 Primary Objective—Performance Testing in Turbulence

Accomplished in Task 2 by baseline turbulence

E.4.3 Primary Objective—Development of Algorithms for Atmospheric Turbulence

E.4.3.1 Task 2 (UTSI and BAR)

Modify, test, and validate the use of RT-PID and D-ICES algorithms with atmospheric turbulence as an input for various levels of atmospheric turbulence. Verify MOS during each phase of flight for varying atmospheric turbulence levels and icing conditions. UTSI and BAR will use the full 6-DOF nonlinear twin otter database.

Autopilot Task (Batch Testing)

1. Isolate the RT-PID problem from D-ICES and executive logic (UTSI)
   a. Flaps up straight and level flight for 30 sec at 110 KIAS and 2500 ft
      (1) Perfect Turbulence measurement—Optimal Inputs
         (a) Turbulence levels
            i. Baseline (no turbulence)
            ii. Light
            iii. Moderate
            iv. Severe
         (b) Ice 0 and 2
      (2) Degraded Turbulence measurement—Optimal Inputs
         (a) Turbulence levels
            i. Baseline (no turbulence)
            ii. Light
            iii. Moderate
            iv. Severe
         (b) Ice 0 and 2
         (c) Vary turbulence measurement error 0.3 to 1.5 kt in increments of 0.3 kt
2. Isolate the D-ICES problem from RT-PID and executive logic (BAR)
   a. Repeat steps outlined in 1

Software Requirements (Task 2 plus)

1. D-six Light, Moderate, and Severe Turbulence Models (BAR)
2. D-six level flight autopilot with OBES hook outside of the autopilot loop (BAR)
3. D-six software switch providing isolation of D-ICES or RT-PID algorithms (BAR)
4. Example script file that calls D-six within MATLAB, trims linear model to 110 KIAS, isolates an algorithm, selects a turbulence model, selects and icing state, runs the model for a given time, and saves one example parameter (BAR)
5. Batch script file for RT-PID and D-ICES testing (UTSI and BAR respectively)
6. Update RT-PID and D-ICES algorithms as required (UTSI and BAR respectively)

E.4.3.2 Task 3 (UTSI and BAR)

Modify, test, and validate the use of RT-PID and D-ICES algorithms with atmospheric turbulence as an input. Select an acceptable atmospheric turbulence measurement error based on findings from Task 2 and commercially available atmospheric turbulence sensors. Verify MOS during each phase of flight for varying atmospheric turbulence levels and icing conditions. UTSI and BAR will use the full 6-DOF nonlinear twin otter database.

Autopilot Task (Batch Testing)

Phases of flight—Autopilot with Optimal Inputs

1. Flaps up straight and level flight at 110 KIAS and 2500 ft—30 sec duration
2. Flaps up straight and level flight at 110 KIAS and 2500 ft followed by a constant altitude flap transition (0° to 20°) to 80 KIAS – 1 min duration
3. Heading capture at 80 KIAS, 2500 ft, and flaps 20° from 090° to 360° – 30 sec duration
4. Descent from 3000 ft at 75 KIAS and flaps 20° followed by a flap transition (30°) to 70 KIAS with localizer and glide slope tracking – 2 min duration

Ice Condition

1. Ice 0
2. Ice 2 in zero time

Turbulence Levels

1. Baseline (no turbulence)
2. Light
3. Moderate
4. Severe

Software Requirements (Task 1 plus)

1. D-six autopilots for Phases 2 to 4 (BAR)
2. Update RT-PID and D-ICES algorithms as required (UTSI and BAR respectively)

E.4.4 Secondary Objective—Preliminary Feasibility Study without OBES

E.4.4.1 Task 4 (UTSI and RR)

Research Objectives

1. Evaluate the effectiveness of manual pilot inputs alone for making high confidence vehicle state estimates when performing typical maneuvering flight tasks under varying levels of atmospheric turbulence.
   a. Determine the portion or portions of the maneuvers, which provide frequency content at the natural frequency of the short period, dutch-roll, and roll modes and thereby support the achievement of high confidence parameter estimates from RT-PID:
      (1) Without use of the OBES.

(2) With OBES.
(3) Optionally, acquire pilot workload assessment for (1) and (2)

Assumptions

1. Accomplishment of this objective assumes that the goal of system performance as stated in the primary objectives has been met.

Test Design

1. This test will be designed and executed to acquire data that will enable the researcher to compare the differences between the effect of manual only pilot control inputs and pilot inputs that are augmented by the operation of the OBES on RT-PID vehicle state estimates. This comparison will be made for four atmospheric turbulence conditions, which were previously defined under Task 1. The required data will come from maneuver time histories of pilot control inputs with and without OBES "buzzing" and from RT-PID derived confidence intervals of key stability and control coefficients in each of the aircraft's three rotational axes. The *a priori* truth versus the current estimate for each stability and control coefficient in the ISP formulation will be used to determine the accuracy in the estimate and will be reflected in the magnitude error bars for each coefficient of interest. This will form the basis for pilot alerting when the state estimate needs to be improved. A *power spectral density* analysis of control activity with and without OBES, for each part of the maneuver where a poor vehicle state estimate exists will be used to determine the amount of energy in the inputs at the desired frequency. *Coherence plots* will then be developed will facilitate the comparison between the non-OBES and OBES control input condition.

Method of Test

1. Task 4 will be divided into two subtasks.
   a. The first subtask will be an initial evaluation of normal manual pilot inputs for achieving vehicle state estimates while performing basic flight maneuvers. These maneuvers will include steady level flight, climbs and descents, changes in airspeed, turns to headings, wing flap extensions/retractions, and power transitions. These flight maneuvers are described in the following section, and will be performed with and without OBES operation. This subtask will be performed in smooth atmospheric conditions, and later, under various levels of atmospheric turbulence. The goal of this testing is to acquire data that establishes the relationship between pilot inputs alone, and pilot inputs with OBES when performing basic aircraft maneuvers, and their effect on achieving the required level of confidence in vehicle state estimation. The results of this initial testing will be used to verify system functionality, ensure readiness for more extensive data collection as described in the second subtask below, and to verify data collection, processing, and analysis methods In addition, this testing will identify and address any anomalies found with pilot cueing and messaging such nuisance alerts and toggling.
   b. The second subtask will be an extensive series data collection tests flown by a test pilot to evaluate manual *pilot control input gain* on vehicle state estimates under various conditions of atmospheric turbulence. This will involve three repeats of each maneuver after the pilot has practiced and reached a consistent level of performance. These tests will be performed both with and without OBES operation. Two means of varying pilot control activity and gain will be employed during this subtask. The first is by increasing desired maneuver performance requirements, which involves specifying high and low error tolerances during each set of repeat maneuvers. The large tolerance will result in lower gain and control activity, and the small tolerances should result in higher gain and control activity. A second means of affecting pilot gain and control activity will be to simply alert the pilot via TBD methods (voice or possibly messaging) that more aggressive inputs are required in any or all of the pitch, roll, and yaw axes until the alerting requirements no longer exist. It is also expected that some maneuvers may not

provide sufficient vehicle excitation in all the aircraft axes, e.g., level climbs and descents may not provide lateral directional excitation, and it may be necessary to combine the two methods to obtain a satisfactory state estimate. In this case, the pilot may be alerted to make inputs in the affected axes if a full state estimate is desired for that test point. As a final evaluation of manual pilot inputs, an operationally representative flight profile consisting of an instrument approach procedure as shown in Figure E.1 will be performed under each of the turbulence conditions defined in this plan. In addition to evaluating the effectiveness of manual pilot inputs on vehicle state estimation, the data derived from this subset of testing will also assess the effect of manual inputs and OBES operation on pilot workload.

c. Pilot tasks will be performed under simulated IMC conditions.

Data Requirements

1. Test data will be sampled at a minimum of 10 Hz. The sampled parameters include time histories of the following:
   a. Pressure altitude — Hp
   b. Airspeed — VIAS
   c. Angle of attack (AOA) — α
   d. Angle of sideslip (AOS) — β
   e. Heading angle — Ψ
   f. Pitch angle — θ
   g. Bank angle — φ
   h. Control and wing flap position — δe, δa, δr, δf
   i. Body rates and accelerations — p, q, r, A_X, A_Y, A_Z,
   j. Localizer and GS errors — Localizer and glide slope Theil inequality coefficient
   k. State coefficient estimates — $C_{m\alpha}$,$C_{m\delta e}$, $C_{l\beta}$, $C_{l\delta a}$, $C_{N\alpha}$, $C_{n\delta r}$ estimate, error, and truth

Pilot Performance Task Standards

1. To ensure consistency, flight standards are provided, which will cause pilot gain to be either high or low. Low gain will result from the larger error tolerance values, and high gain will result from the lower tolerance values. The appropriate standard will be specified on the test card for the maneuver event.
   a. Altitude control for level flight: ± 150 and ± 20 ft
   b. Heading control: ± 5 ° and ± 1 °
   c. Climb/descent rate: full power, idle power, power as required per test card
   d. Airspeed: ± 5 kt and ± 1 kt
   e. Roll rates: ± 10 °/sec and ± 5 °/sec
   f. Localizer course intercept angle: 45 ° and 30 °
   g. Localizer error: ± 1 dot and zero lateral deviation + 10 kt X wind
   h. Glide slope error: ± 1 dot and zero vertical deviation + 10 kt X wind

Maneuver Descriptions

1. The descriptions of each maneuver below are generalized. Detailed test cards will provide specific instructions as to how each maneuver is to be accomplished. Each evaluation will be conducted in four levels of turbulence. Icing configuration will be ICE 0 for the initial and final evaluation and ICE 02 for the instrument approach procedure as shown in Figure E.1. The 10 kt cross wind in addition to the turbulence will be applied for only the instrument approach procedure. Repeat each procedure 3 times using low gain standards, and then repeat 3 times using high gain standards. Initialization conditions will be specified for each maneuver on the test card.
2. Basic flight maneuvers
   a. Steady level flight at constant heading.

(1) Perform at 125 KIAS and 1.3 versus (90 KIAS) with PFLF
(2) Stabilize on condition with PFLF and call “mark” when stable
(3) Hold heading and altitude within specified parameters and take data for 3 min

b. Level turns to headings
(1) Perform at 125 KIAS and 1.3 versus (90 KIAS)
(2) Stabilize on condition with PFLF and call “mark” when stable
(3) Remain steady level for 15 sec. Using power as required maintaining constant airspeed and altitude while performing the following: Turn right to a heading of 090 and maintain steady level flight for 15 sec. Turn left to 045 and maintain steady flight for 15 sec. Turn left to 030 and maintain steady level flight for 1 min.

c. Constant airspeed and vertical speed climbs/descents on a steady heading
(1) Perform at 125 KIAS and 1.3 versus (90 KIAS)
(2) Stabilize on condition with PFLF and call “mark” when stable.
(3) Using power as required, maintain constant airspeed and climb at specified climb rate. Level off at 6000 ft and remain steady for 15 sec. Using power as required, begin a constant airspeed descent at the specified rate and level off at 5000 ft. Maintain steady level flight for 15 sec.

d. Constant airspeed climbing and descending turns to headings
(1) Perform at 125 KIAS and at 1.3 versus (90 KIAS)
(2) Remain steady level for 15 sec. Select maximum power and turn right to a heading of 090. Maintain constant airspeed in climb and level off at 6000 ft. Stabilize on airspeed and heading of 090 for 15 sec. Select idle power and turn left to 360. Maintain constant airspeed in the descent and level off at 5000 ft. Stabilize on airspeed and heading for 15 sec.
(3) Repeat (ii) and use power as required to establish a 300 fpm climb and descent rate

e. Wing flap transitions
(1) Initialize on heading 360, PFLF at 85 KIAS, wing flaps up. When stable, call “mark” and hold steady condition for 15 sec. Select wing flaps DOWN and use power as required to maintain airspeed and altitude while holding heading constant. After wing flaps reach DOWN, stabilize and hold the steady condition for 15 sec.
(2) Stabilize for 1 min with wing flaps full down at 85 KIAS. When stable, call “mark” and select wing flaps to UP and use power as required to maintain airspeed while keeping altitude and heading constant as the flaps retract to the fully up condition. Stabilize and hold the steady condition for 15 sec.

f. Power transitions:
(1) Initialize on a 360 heading, at 85 KIAS, wing flaps up, PFLF. When stable, call “mark” and rapidly apply full power while maintaining heading and level flight until reaching the maximum speed attainable. When stable at maximum speed, hold condition for 15 sec.
(2) Initialize on a 360 heading, at maximum level flight speed, wing flaps up, PFLF. When stable, call “mark” and rapidly reduce power to idle while maintaining heading and altitude. When approaching 90 KIAS, add power as required to maintain constant heading and airspeed. When stable at 90 KIAS, hold condition for 15 sec.

g. Operational evaluation—Instrument Approach Procedure
(1) Initialize with wing flaps up, 3000 ft, heading 360, and 125 KIAS, ICE02
(2) Conduct the approach procedure per Figure E.1 without OBES, and provide pilot alerting when state estimates need to be refreshed with additional control activity
(3) Evaluate workload using NASA TLX
(4) Repeat the procedure with OBES functioning
(5) Evaluate workload using NASA TLX

Turbulence Levels as Defined by MIL-F-8785C

1. Smooth air, no turbulence
2. Light turbulence
3. Moderate turbulence
4. Severe turbulence

Test Cards

1. Detailed test cards will be developed for each of the two sub tasks from the maneuver descriptions above. These test cards will be provided in a standard UTSI test template format and retained as part of the data package for each test session. Any deviations from initially planned test procedures will be noted on the test cards.

Software Requirements

1. D-six executive logic software switch enabling / disabling OBES functionality (BAR)
2. Alerting the pilot that control excitations are required (BAR)
   a. Update excite button functionality
   b. Apply stop light color scheme
      (1) Tie color scheme to RT-PID confidence bounds
         (a) Parameters in ISP calculation define axis color
   a. Differentiate scheme depending on which axis or axes require excitation

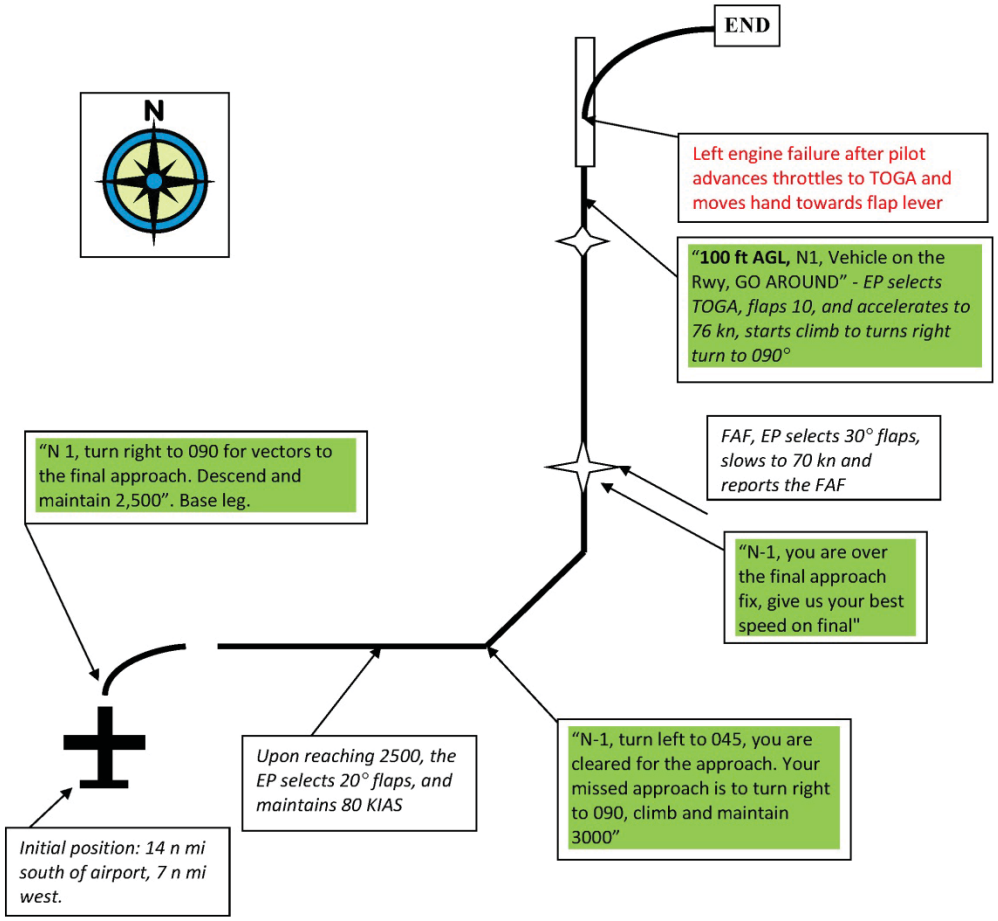

Figure E.1.—Test and evaluation profile. Total duration of test is approximately 15 min. Quotes are clearances read to the EP, italics are required EP actions per the test protocol.